Next Materials 9 (2025) 101090

Contents lists available at ScienceDirect

Next Materials

journal homepage: www.sciencedirect.com/journal/next-materials

Review article

Mechanical and physical properties of aluminum and its alloys for electrical conductors: A review

Pooya Parvizi [a,*], Milad Jalilian [b,e,**], Pedram Sorouri Mirazizi [e], Mohammad Reza Zangeneh [c,e], Alireza Mohammadi Amidi [d,e]

[a] Department of Mechanical Engineering, University of Birmingham, Edgbaston, Birmingham B15 2TT, UK
[b] Department of Physics, Faculty of Science, Lorestan University, Khorramabad, Iran
[c] Department of Energy and Mechanical Engineering, Shahid Beheshti University, Tehran, Iran
[d] Department of Electrical Engineering, Razi University, Kermanshah, Iran
[e] Pooya Power Knowledge Enterprise, Tehran, Iran

ARTICLE INFO

Keywords:
Aluminum conductors
Conductivity
Heat treatment
Alloy element
Aluminum alloy
Mechanical properties

ABSTRACT

This review paper presents a comprehensive analysis of the mechanical, physical, and thermal properties of aluminum and its alloys utilized in electrical conductors. While aluminum is primarily favored for its high electrical conductivity, lightweight nature, and corrosion resistance, its thermal properties also play a crucial role in its performance in power transmission systems. The review covers the historical evolution and classifications of aluminum conductors, including homogeneous and inhomogeneous types, and highlights key aluminum alloys: the 1xxx, 6xxx, and 8xxx series. It explores various methods for enhancing the mechanical properties of these alloys, such as alloying and grain refinement, and discusses the inherent trade-offs with electrical conductivity. Additionally, the impact of heat treatment processes and the incorporation of alloying elements like vanadium, titanium, and boron on both electrical and mechanical performance is examined. Ultimately, the findings aim to guide the selection of optimal aluminum alloy compositions and manufacturing processes, advancing the efficiency and reliability of aluminum-based conductors in the energy sector.

1. Introduction

The rapid evolution of power transmission technology has created a growing demand for efficient overhead conductors [1]. As global energy consumption increases, the need for reliable and cost-effective materials for power distribution has become paramount [2–4]. The development of conductors used in distribution and transmission lines has paralleled advancements in electrical engineering and energy management. Historically, copper was the primary material for overhead conductors; however, it has significant drawbacks such as a low strength-to-weight ratio, high cost, and considerable weight, which lead to shorter span lengths and greater reliance on transport and maintenance equipment [5]. These challenges have prompted researchers and designers to explore alternative materials to replace copper. Aluminum has emerged

Abbreviations: AAAC, All Aluminum Alloy Conductor; AAC, All Aluminum Conductor; ACAR, Aluminum Conductor Alloy Reinforced; ACCC, Aluminum Conductor Composite Core; ACSR, Aluminum Conductor Steel Reinforced; ACSS, Aluminum Conductor Steel Supported; A-H, Annealed-Heated; AHCD, Aging Heat Treatment with Cold Drawing; APT, Atom-Probe Tomography; ARB, Accumulative Roll Bonding; ASTM, American Society for Testing and Materials; CBT, Conventional Boron Treatment; CD, Cold Drawing; CDAH, Cold Drawing and Aging Heat Treatment; CTE, Coefficient of Thermal Expansion; DIN, Deutsches Institut für Normung German National Standard; EC, Electrical Conductivity; ECAP-C, Equal Channel Angular Pressing Conform; EHS, Extra High Strength; GR, Grain Refinement; HS, High Strength; HT, Heat Treatment; HTLS, High-Temperature Low-Sag; HPDC, High-Pressure Die-Cast; HPT, High-Pressure Torsion; IACS, International Annealed Copper Standard; IEC, International Electrotechnical Commission; JIS, Japanese Industrial Standards; MS, Mechanical Strength; RE, Rare Earth; RS, Rotary Swaging; RT, Room Temperature; SPD, Severe Plastic Deformation; TAL, Thermal Resistant Aluminum Alloy; TBT, Boron Treatment with Ti Assistant; TEM, Transmission Electron Microscopy; TMS, The Minerals, Metals & Materials Society; T&D, Transmission and Distribution; TS, Tensile Strength; TTTD, Time-Temperature-Transformation Diagram; UTS, Ultimate Tensile Strength; YS, Yield Strength.

* Corresponding author.
** Corresponding author at: Department of Physics, Faculty of Science, Lorestan University, Khorramabad, Iran.
E-mail addresses: PXP046@alumni.bham.ac.uk (P. Parvizi), jalilianm70@gmail.com, jalilian.mi@fs.lu.ac.ir (M. Jalilian), p.sorouri@pooyapower.com (P.S. Mirazizi), m.zangeneh@alumni.sbu.ac.ir (M.R. Zangeneh), a.mohamadi@pooyapower.com (A.M. Amidi).

https://doi.org/10.1016/j.nxmate.2025.101090
Received 14 May 2025; Received in revised form 16 August 2025; Accepted 18 August 2025
Available online 27 August 2025

as a critical substitute for copper in conductor construction. It is generally two to three times cheaper and vastly more abundant in the Earth's crust. While aluminum offers approximately 61 % of copper's EC, it weighs only about 30 % of copper's weight, resulting in aluminum conductors being roughly 50 % lighter than their copper counterparts, yet maintaining similar electrical resistance [6–11]. Moreover, aluminum is regarded as a sustainable material, often referred to as a "green metal," due to its ability to be recycled continuously without degrading its intrinsic properties [12]. The use of aluminum conductors dates back to the late 19th century, with noteworthy developments occurring in California in 1895 and the commissioning of the first stranded aluminum cable transmission line by the Connecticut Electric Light Company in 1899, which operated successfully for over five decades [13]. Today, the continuous adoption of aluminum conductors establishes them as the preferred choice among transmission line engineers. Aluminum conductors are categorized into two types: homogeneous and inhomogeneous [14]. When the same materials are utilized for both the wire and the core, the conductor is classified as homogeneous. In contrast, inhomogeneous conductors are characterized by the use of different materials for the core, which commonly includes steel or various composites. The primary aluminum alloys employed in the manufacture of these conductors are the 1xxx, 6xxx, and 8xxx series [15–19]. The most well-known homogeneous aluminum conductors are AAAC [20] and AAC [21]. Among the most prevalent inhomogeneous conductors are ACSR, ACAR, ACCC, and ACSS [22–24]. Innovations in metallurgy have led to the creation of new aluminum alloys, further enhancing performance and optimizing applications related to aluminum conductors [25]. The properties of conductor alloys can be enhanced by optimizing the base aluminum through metallic alloying elements. Specific metals promote strengthening mechanisms like solid solution formation and precipitation hardening, thereby improving mechanical properties [26]. The mechanical properties of aluminum can also benefit from GR [27]. However, these methods have limited effects on improving electrical properties [8,28]. GR can be achieved through techniques that increase nucleation sites during casting [29], and SPD methods [7,30–32]. While improvements in mechanical properties can influence EC [33], it is primarily the scattering of electrons as they encounter obstacles that affects conductivity. These obstacles include impurities within the microstructure and defects in the atomic structure of the base metal. Understanding the impact of these factors on EC is fundamentally guided by Matthiessen's Rule. This principle states that the total resistivity of a metal combines contributions from the pure metal itself and additional resistivity due to alloying elements, impurities, and structural defects [34]:

$$\rho = \rho_0 + \rho_{ss} + \rho_p + \rho_v + \rho_{dis} + \rho_{gb} \quad (1)$$

The symbol ρ_0 represents the electrical resistance of the base metal, while ρ_{ss}, ρ_p, ρ_v, ρ_{dis} and ρ_{gb} signifies the electrical resistance arising from elements in solid solution, solid precipitates, voids in the atomic structure, dislocations, and grain boundaries. This rule is crucial when designing aluminum alloys for conductors as it helps optimize the balance between MS and EC. Microstructural features can hinder electron movement, thereby reducing electrical conductivity. Therefore, understanding and controlling microstructure is crucial for optimizing both strength and conductivity in conductive alloys. In a study by Hou et al. [35], artificial aging of a 6201RE aluminum alloy resulted in the formation of finely dispersed nanoscale precipitates. These precipitates played a dual role: they enhanced the alloy's strength while simultaneously decreasing the solute concentration in the matrix and reducing lattice distortion. This effect contributed to improved electrical conductivity alongside mechanical strengthening. However, modern alloy design deliberately incorporates complex nanoscale microstructures (multicomponent solid solutions, ultrafine grains, coherent nanoprecipitates, and solute clusters) that violate the independent-scattering assumption. Indeed, APT and in-situ TEM reveal abundant nanoscale solute clustering and GP-zone precipitation in Al–Zn–Mg and Al–Mg–Si alloys, and both theory and experiment show these clusters scatter electrons much more strongly than isolated solute atoms. For example, clustering during natural or artificial aging is observed to raise resistivity beyond the value expected from additive isolated-solute scattering [36]. In summary, while Matthiessen's rule provides a useful baseline framework, nanoscale alloy engineering in modern Al systems frequently produces non-additive scattering behavior and resistivity deviations that the simple rule cannot capture, as revealed by high-resolution APT and TEM studies. While certain alloying elements can enhance mechanical properties, they may also increase electrical resistivity. Thus, engineers must manage these trade-offs to ensure that the final material properties meet the performance requirements of power transmission systems [37]. Creating alloys with an optimal chemical composition is key to addressing the challenges of enhancing these properties during design and production. The addition of specific metallic elements can influence resistance and conductivity in unique ways [38]. Understanding the behavior of impurities—such as vanadium, titanium, nickel, and manganese—in aluminum alloys is critical, as they can significantly impact both the mechanical and electrical properties of the conductors. These elements can form precipitates that affect grain structure and influence conductivity. A thorough examination of their roles will illuminate how alloy design can be optimized to minimize detrimental effects while enhancing performance [39]. These impurities can be effectively reduced by adding other metallic elements that react with them. For instance, introducing boron into molten aluminum can facilitate reactions that precipitate and remove impurities from the casting ingots, significantly lowering their impact on electrical resistance [40]. Even if the borides formed from the reaction between boron and these impurities remain, their impact on the alloy's electrical resistance is greatly diminished, reducing it to less than a tenth of its original value prior to reacting with boron [41]. Overall, achieving optimal alloy performance requires a thorough analysis of chemical composition and manufacturing processes. As global energy demands continue to rise, the evolution of conductor materials plays an essential role in enhancing the efficiency and sustainability of power transmission systems. Aluminum stands out as a vital component in this transition, providing an economically and environmentally sustainable alternative to copper.

Extensive research exists on conductive aluminum since the early 2000s, but comprehensive reviews specifically on the EC of aluminum alloys, particularly for aluminum overhead conductors, are limited, with most studies focusing on mechanical properties. It is essential to understand the relationship between factors affecting aluminum alloy wires (such as manufacturing methods and HTs) and the resulting microstructural changes that ultimately impact EC and mechanical properties [11]. While the reviewed study Zhang et al. [42] comprehensively analyzes mechanical and thermal properties of aluminum alloys, it primarily focuses on general applications rather than specialized electrical conductor requirements. The work thoroughly examines alloying effects on thermal conductivity but lacks in-depth discussion of the critical trade-off between EC and MS – a key consideration for power transmission alloys. Lunn et al. [43] review comprehensively examines past and present research on enhancing the conductivity of aluminum alloys, focusing on the fundamental principles, influential factors, traditional and emerging methods, and knowledge gaps in optimizing both conductivity and mechanical properties. This review comprehensively examines the thermal conductivity of HPDC aluminum alloys, analyzing alloying elements, secondary phases, and processing effects. While it thoroughly discusses heat transport mechanisms and microstructure-property relationships, it primarily focuses on thermal management applications (e.g., automotive/electronics cooling) rather than electrical conductor requirements. The study lacks specific insights into the EC-MS trade-off—a critical gap for power transmission materials—and omits emerging strategies like grain boundary engineering for EC optimization [12]. Although existing studies, such as the

comprehensive report by Czerwinski [44], provide valuable insights into aluminum conductors—covering their classification, markets, and metallurgical characteristics—they often adopt a broad perspective that extends beyond electrical performance (e.g., applications in electric vehicles). While such works offer a holistic overview, they lack in-depth analysis of the fundamental trade-offs between EC and MS in alloy design. This paper aims to systematically explore the impact of alloying techniques on optimizing aluminum's mechanical and electrical properties, offering insights into innovative solutions critical for future energy infrastructures. Our findings seek to inform ongoing scientific inquiries and guide industrial practices toward developing more efficient and sustainable aluminum conductor technologies. Previous reviews have fallen short in three key areas: (1) they either focus narrowly on thermal conductivity applications [42] or take too broad an industrial perspective [44], missing conductor-specific challenges; (2) they lack practical frameworks for optimizing the strength-conductivity balance that dominates overhead line design; and (3) they fail to incorporate recent breakthroughs in grain boundary engineering and nano structuring that could revolutionize conductor performance.

This study re-examines aluminum conductors by synthesizing recent advances in alloy development and processing, focusing on the potential of newer aluminum alloys enhanced with RE and strategic elements, an area less explored in existing research. Unlike other reviews, it provides an in-depth analysis of findings related to aluminum and its alloys in transmission line applications (3), delivering a comprehensive perspective for researchers. While abundant research exists on aluminum alloys, there's a gap in studies holistically integrating mechanical and electrical properties, as most literature focuses on these aspects independently. Moreover, there is particularly a lack of research specifically focusing on overhead conductors, highlighting the need for more specialized studies in this field. By addressing this gap, this research offers new insights for enhancing the efficiency and optimization of aluminum conductors in overhead power transmission line.

2. Structure of aluminum conductors

Modern overhead high-voltage power lines for T&D must exhibit significant operational flexibility while maintaining robust technical and economic performance. To meet these demands, the adoption of innovative conductor technologies and advanced conductive materials is imperative. Such advancements are crucial for ensuring adequate current-carrying capacity, minimizing transmission energy losses, and maintaining optimal cable sag levels [45]. Aluminum has played a crucial role in electrical power T&D for over 120 years. Throughout this extensive history, its use has consistently increased, making aluminum conductors the predominant choice for transmission line design engineers in modern applications [13]. Overhead conductors used in power T&D lines are typically produced with a co-axial arrangement, featuring aluminum wires. This configuration consists of a central core designed to withstand most external loads, such as those resulting from wind, ice accumulation on the outer surfaces, and overall weight. Surrounding the core, one or more layers of aluminum wire are wound alternately and spirally. This section is primarily responsible for transmitting current and ensuring EC [46]. To enhance TS and minimize elongation due to heat, strong steel wires and composites are utilized in the construction of the core. One reason for the decreased use of copper in modern conductors is its higher density and the absence of the advantageous properties mentioned earlier. Regarding the aluminum wires surrounding the core, it is essential to use aluminum alloys with high conductivity and low impurity levels. The most significant alloys employed are the 1xxx series aluminum alloy (EC grade) and the 6xxx series aluminum alloy [47]. The following sections will examine the properties and characteristics of the materials used in the construction of the core and its surrounding conductors. To facilitate a comprehensive understanding of the structure of an aluminum conductor, Fig. 1 presents an Aluminum Conductor AAC in both isometric and cross-sectional views.

2.1. Characteristics of conductive wires used in aluminum conductor

Aluminum and its alloys are divided into two main groups: heat-treatable and non-heat-treatable alloys [48,49]. For non-heat-treatable alloys, strength and hardness improvements are mainly achieved through plastic deformation methods, particularly rolling and drawing [50,51]. The strength and hardness increase proportionally with the amount of deformation applied. Among the non-heat-treatable variants, 1350 aluminum is notably popular for overhead conductors [20,52]. To render 1350 aluminum wires suitable for overhead conductors and to meet the necessary minimum levels of strength and hardness, they undergo significant deformation during an intensive wire drawing process. In conjunction with these processes, the H19 tempering operation is employed to achieve high hardness [53,54].The resulting wires from these processes are designated as 1350-H19. A significant application of these wires is in the construction of ACSR conductors. To produce low-diameter aluminum wires, an extensive drawing process is necessary. This results in more intense plastic deformation of the initial wires, consequently increasing the TS of the final product. To attain the optimal level of softness, even non-heat-treatable alloys, such as 1350 aluminum, undergo a specific hardening process followed by HT [54]. Although various degrees of softness can be attained by manipulating temperature and time, the most common method for wires used in overhead conductors is the O-temper operation. Wires subjected to this process are referred to as fully annealed or 1350-O [54,55]. One of the key conductors utilizing these wires is the ACSS conductor. Compared to 1350-H19 wire, 1350-O wire exhibits lower TS but higher ductility and conductivity. In heat-treated aluminum alloys, the strengthening and hardening processes can be achieved through a combination of plastic deformation and various HTs [56]. For aluminum alloys employed in the wire and conductive industry, deformation occurs primarily during wire drawing operations. Among the array of HTs, solution HT and aging treatment are predominantly utilized for conductive wires used in conductors. Solution HT involves multiple cycles of high temperature and controlled cooling, which significantly enhance the material's strength. This treatment can be executed in two distinct phases: either during the wire drawing process or as a separate operation after wire drawing. The subsequent HT, known as aging, occurs after the drawing process. In this phase, wires are subjected to elevated temperatures for specific durations, further increasing their strength beyond the improvements achieved in the preceding solution HT. In scenarios where designers require enhanced strength for power transmission lines, heat-treating

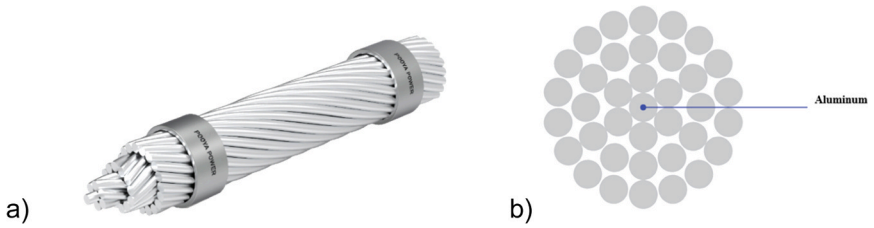

Fig. 1. Structural representation of AAC aluminum conductors. a) The isometric view b) The cross-sectional view.

aluminum, particularly the 6201 aluminum alloy, is a viable option [57]. The primary difference between the 6201-aluminum alloy and the 1350 alloy is the incorporation of chemical elements such as magnesium and silicon in the former's composition. Wires made from the 6201 alloy are significantly stronger than those produced from the 1350 alloy. The conventional HT for these alloys is the T-81 operation. Following the T-81 HT, the strength of the alloy reaches 320 MPa, which is notably higher than the approximate strength of 160 MPa for the 1350-H19 alloy. As previously indicated, Matthiessen's law states that the inclusion of chemical elements within a solid solution elevates electrical resistance, thereby diminishing conductivity. Consequently, the 6201-T81 aluminum alloy exhibits an EC of 52.5 % IACS, which is lower compared to the 61–62 % IACS EC of the 1350-H19 alloy. Achieving a desired strength and hardness in aluminum wires necessitates the application of SPD, commonly through the wire drawing process. However, empirical evidence has indicated a reduction in TS attributable to the alleviation of microstructural mechanical stresses—such as those present at grain boundaries and within the lattice—when the wires are subjected to temperatures beyond permissible thresholds during plastic deformation. Consequently, aluminum wires utilized in conventional overhead conductors must be operated within a temperature range below their defined limits, typically between 70 and 90 °C [58, 59]. The escalating demand for energy exerts maximum pressure on T&D lines [60], causing the temperature of conventional conductors to exceed the limits specified by their designers This temperature elevation, coupled with the release of mechanical stresses from aluminum wires, results in a reduction in their TS and an increase in the sag of power T&D lines. To mitigate these issues, the aluminum conductor industry has increasingly adopted HTLS conductors. This study introduces a selection of aluminum wires employed in these conductors. Among them, aluminum-zirconium alloys, known as TAL and (Z) TAL, are utilized in the fabrication of conductive wires for certain HTLS conductor models.[59]. Both TAL and (Z) TAL wires exhibit similar TS and conductivity to those of standard aluminum grade wires. The primary distinction lies in their service and operating temperature ranges compared to conventional aluminum wires. Specifically, the working temperature for TAL wires is at least 150 °C, while for (Z) TAL wires it is 210 °C, in contrast to the 90 °C working temperature for aluminum wires used in traditional conductors such as ACSR. Table 1 presents the characteristics of aluminum wires used in various types of conductors, along with a comparative analysis.

3. Aluminum and Its alloys for overhead conductor applications

Aluminum has evolved from a rare metal to a ubiquitous material that plays a vital role in modern society [61]. Including a discussion of aluminum's history in this section can provide readers and enthusiasts with a more nuanced and expansive understanding of the subject. Fig. 2 illustrates a comprehensive timeline of the discovery of aluminum.

The utilization of aluminum and its alloys in overhead transmission lines is increasingly prevalent due to their advantageous properties [62–64]. These materials offer an excellent adequate thermal conductivity, superior formability, and exceptional weldability, exceptional resistance to corrosion, good fracture toughness, impact resilience, and overall durability—has made these materials increasingly attractive to designers and engineers in the transmission line industry [65,66]. Certain aluminum alloys exhibit excellent EC, while others possess commendable mechanical properties. By employing various techniques—such as alloying with different chemical elements, performing diverse HT cycles, and applying an array of mechanical processes—the inherent properties of aluminum can be significantly enhanced. These methods can yield a synergistic balance of mechanical and electrical characteristics, ideal for the fabrication and design of both HTLS and conventional conductors. Key developments are highlighted in the following section.

3.1. A comprehensive review of research on aluminum and its alloys utilized in conductors

Zhang et al. [67] examined the impact of scandium and erbium additions on the Al-0.2Zr-based alloy wires. The study focused on assessing the electrical and mechanical properties of the Al-0.2Zr alloy following the incorporation of 0.1 wt% scandium or erbium, particularly under annealing conditions at 400°C for different durations. Their research indicated that the Vickers micro-hardness of the Al-0.2Zr sample declined from 320 MPa to 203 MPa as the annealing time extended from 0.2 to 4 h. However, introducing 0.1 wt% scandium enhanced the micro-hardness of the Al-0.2Zr-0.1Sc alloy to 603 MPa, which then slightly decreased to around 575 MPa after annealing at 400°C for a period ranging from 6 to 36 h. Similarly, adding 0.1 wt% erbium to the Al-0.2Zr alloy, forming the Al-0.2Zr-0.1Er alloy, raised the micro-hardness to 583 MPa, which subsequently decreased to 550 MPa after annealing for 2–8 h. The formation of Al_3(Zr, Sc) and Al_3(Zr, Er) precipitates during the annealing process played a crucial role in impeding dislocation movement within the microstructure, thereby enhancing the overall MS. The variations in micro-hardness of the resulting alloys over time during the annealing process are presented in Fig. 3a. Fig. 3b illustrates that the addition of scandium and erbium reduced the EC. This phenomenon is primarily attributed to electron scattering by the alloying elements within the final atomic structure. Also, the study only examined low Sc/Er additions (0.1 wt%), leaving the effects of higher concentrations unexplored. The longest annealing time was 36 h, which may not fully reveal long-term stability or coarsening effects of precipitates.

In a study conducted by Chao et al. [68], the effects of adding zirconium and scandium on the electrical and mechanical properties of several aluminum alloy wires were investigated. The study focused on alloy compositions including Al-0.16Zr, Al-0.16Sc, and Al-0.12Sc-0.04Zr, alongside pure aluminum wires (99.996 % purity), all with a diameter of 9.5 mm, manufactured through a continuous rheologic extrusion process. Mechanical testing of these samples showed that the ultimate TS s were 44.2 MPa for Al-0.16Zr, 51.76 MPa for Al-0.16Sc, and 62 MPa for Al-0.12Sc-0.04Zr. In terms of EC, pure aluminum exhibited a conductivity of 64.6 %IACS. In comparison, the conductivity values for Al-0.16Zr, Al-0.16Sc, and Al-0.12Sc-0.04Zr alloys were measured at 57.6 %IACS, 58.23 %IACS, and 56.7 %IACS, respectively. The observed enhancement in TS is primarily due to solid solution strengthening mechanisms. The formation and stability of phases such as Al_3Zr, Al_3Sc, and Al_3(Sc, Zr) contribute significantly to this effect. The larger atomic radii of zirconium and scandium compared to aluminum

Table 1
Specifications of aluminum wires used as conductors in aluminum conductors [54].

Type of aluminum	Applicable standard	Minimum conductivity (%IACS)	TS (MPa)	Allowable operating temperature (°C)	
				Continuous	Emergency
Hard drawn 1350 H19	IEC 60889	62.1	150–210	85	120
Heat-treaded 6xxx series	IEC 60104	52	319–410	85	120
Thermal resistant zirconium aluminum	IEC 62004	59.5	160–170	145	185
Super thermal resistant zirconium aluminum	IEC 62004	59.5	160–177	215	245
Fully annealed 1350	IEC 60121	63	59–97	350	350

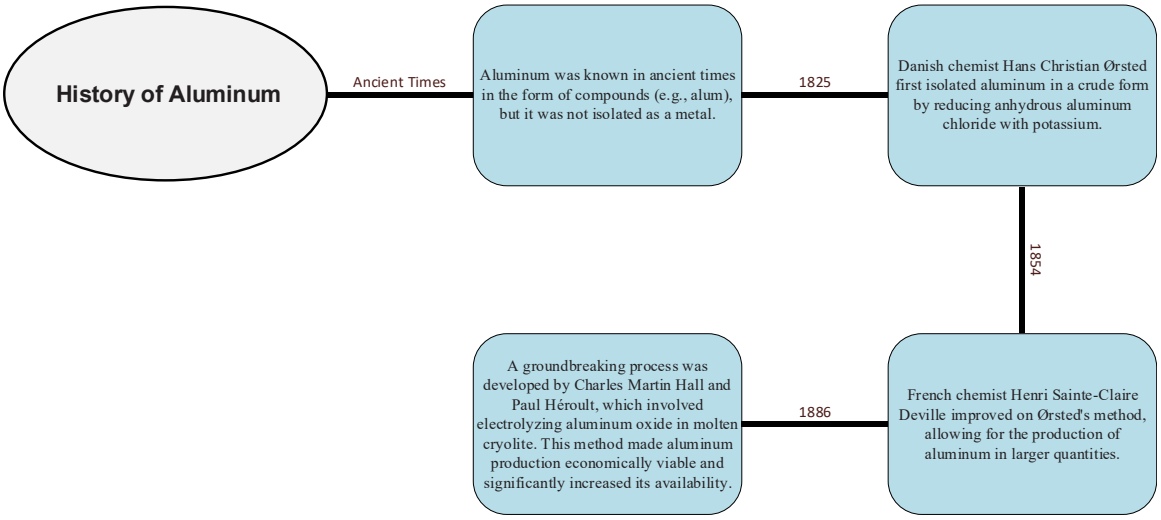

Fig. 2. Timeline of the discovery of aluminum.

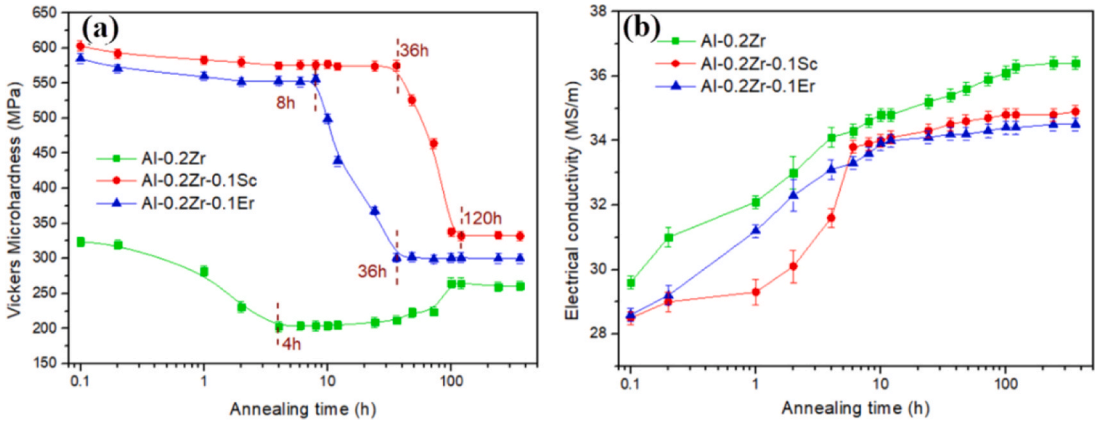

Fig. 3. Changes in a) micro-hardness (MPa) and b) the EC of Al-0.2Zr, Al-0.2Zr-0.1Sc and Al-0.2Zr-0.1Er versus the annealing time, at the same temperature conditions (400 °C) [67].

atoms result in increased lattice distortions, which in turn hinder electron flow, leading to higher electrical resistance. This phenomenon explains the reduced EC of the alloys compared to that of pure aluminum. Fig. 4 provides a comparative analysis of the EC and TS of the samples studied.

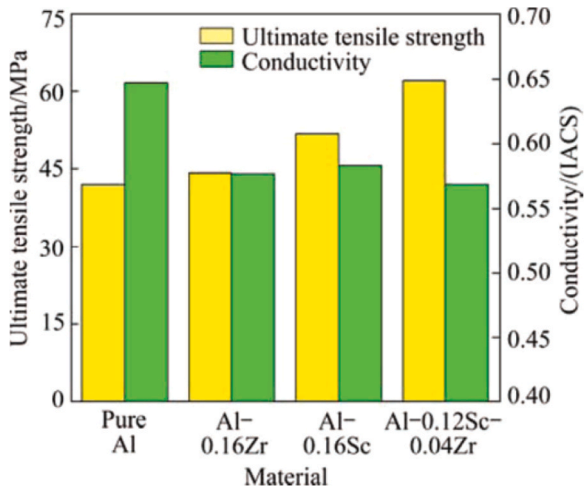

Fig. 4. Final TS and EC of various aluminum and aluminum alloy wires [68].

As previously highlighted, the Al-Mg-Si alloy is one of the most important materials in the production of aluminum conductors. A study by Xuexuan et al. [69], explored how varying ratios of magnesium to silicon affect the electrical and mechanical characteristics of Al-Mg-Si alloy wires. The findings revealed that a higher silicon content contributes positively to achieving both greater strength and improved EC. In contrast, an increased magnesium content tends to negatively impact these properties. Increased silicon content enhances the precipitation rate and the amount of the β′ precipitate phase, thereby augmenting the final TS through the solidification mechanism of the solid solution. Notably, the maximum TS achieved among the silicon-enhanced samples was 210 MPa. Additionally, a high silicon content helps to reduce lattice distortion in the final crystal structure, thereby decreasing electrical resistance and improving conductivity. Conversely, the addition of magnesium, particularly in high amounts, can lead to greater dissolution during possible HTs, which negatively affects the alloy's TS. This dissolution increases the distortion of the matrix lattice and promotes the precipitation of a magnesium-rich second phase, both of which adversely impact the final EC. Zhang et al. [70], conducted an extensive study investigating how the addition of cerium and lanthanum affects the EC of aluminum alloys. The results demonstrated that cast aluminum alloys with cerium exhibit better EC than those with lanthanum, as shown in Fig. 5a. Interestingly, after HT at 300°C for 24 h, the electrical conductivities of both types of alloys nearly equalized (Fig. 5b). This convergence is mainly due to cerium's effectiveness in purifying iron

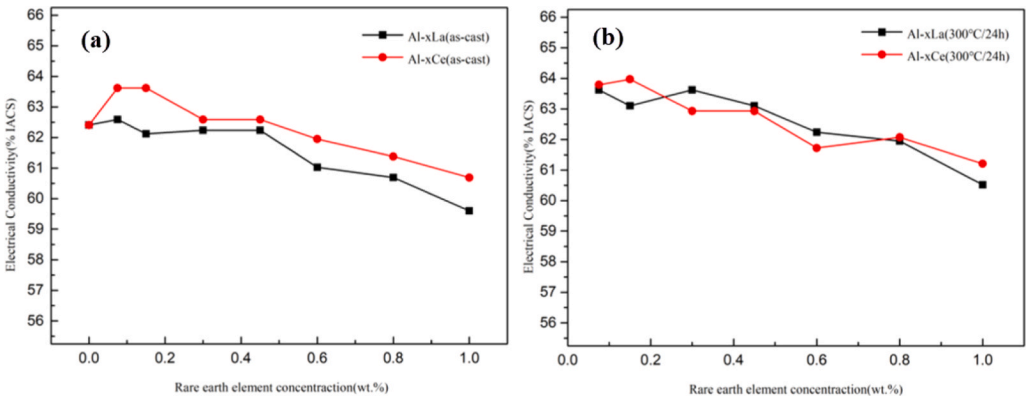

Fig. 5. a) EC of the samples and b) EC after HT of 300 °C for a period of 24 h [70].

and silicon impurities within the aluminum matrix. Scanning electron microscopy images, presented in Figs. 6 and 7, display the microstructures of alloys with different concentrations of cerium and lanthanum, both before and after HT. Fig. 6a shows that at lower cerium levels, the secondary phases are finely dispersed within the aluminum matrix. In contrast, higher cerium concentrations (Fig. 6c) cause these phases to form primarily at the grain boundaries. When lanthanum is added, its less effective purification compared to cerium results in a greater likelihood of forming solid solution atoms within the aluminum matrix, as seen in Fig. 7a, where secondary phases are distributed along the grain boundaries. Increasing the lanthanum concentration further enhances the amount of precipitate at the grain boundaries (Fig. 7c). The observed improvement in EC with cerium additions, rather than lanthanum, can be attributed mainly to these microstructural differences. Following HT at 300°C for 24 h, most of the solid solution atoms precipitate out of the aluminum matrix, leading to similar morphologies as illustrated in Figs. 6b, 6e, 7b, and 7e. This process explains the similar EC values observed after HT.

The addition of cerium and lanthanum significantly enhanced the TS of the resulting alloy, achieving peaks of approximately 80 MPa and 83 MPa, respectively. However, a slight reduction in TS was noted after the HT process. Zhao et al. [71] investigated the influence of iron, silicon, and homogenization on the electrical conductivity (EC) and mechanical properties of Al-Mg-Si alloys. They found that adding iron (0.2 wt%) to an Al-0.5Mg-0.35Si alloy enhanced EC by forming the α-Al8Fe2Si phase, which reduced solid solution resistivity by binding silicon and limiting Mg2Si precipitation. However, this improvement came at the expense of TS. Further silicon additions partially restored mechanical properties, while homogenization optimized both EC and strength by modifying the α-Al8Fe2Si phase. Their findings are supported by microstructural and property analyses (Figs. 8–10), including:

- Fig. 8: EC and mechanical properties of the studied samples.
- Fig. 9: Scanning electron microscopy image of the Al-0.25Zr alloy microstructure.

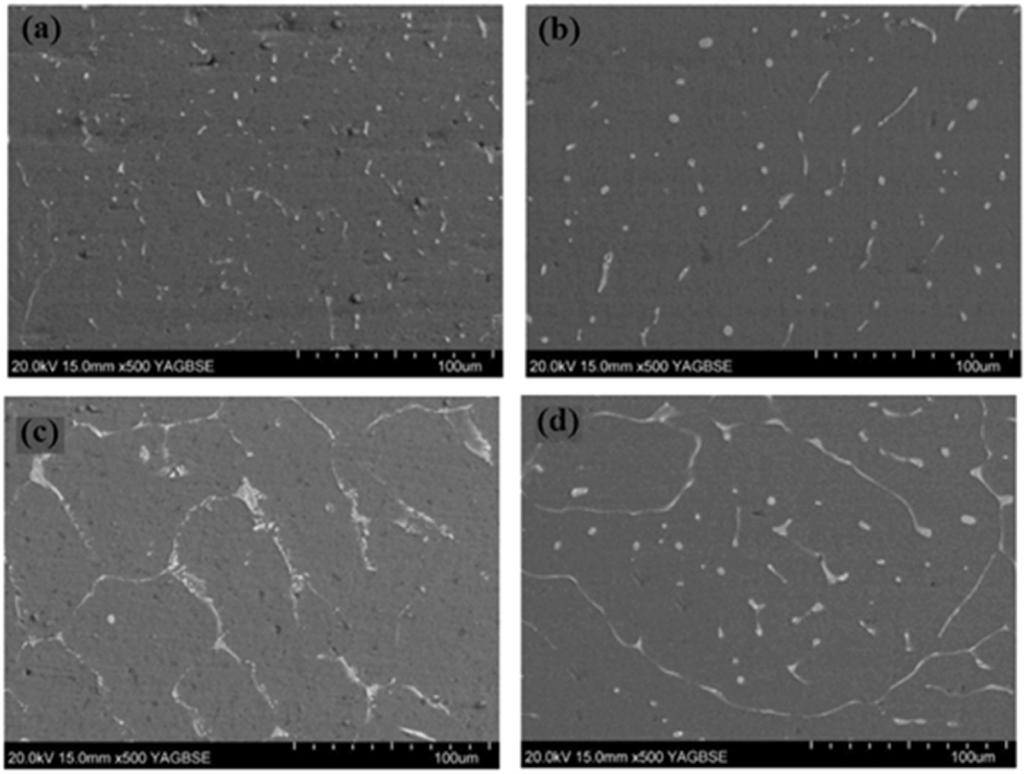

Fig. 6. Scanning electron microscopy images of sample containing cerium element in a) Al-0.3Ce, b) Al-0.3Ce(300°C/24 h), c) Al-0.8Ce and (d) Al-0.8Ce (300°C/24 h) [70].

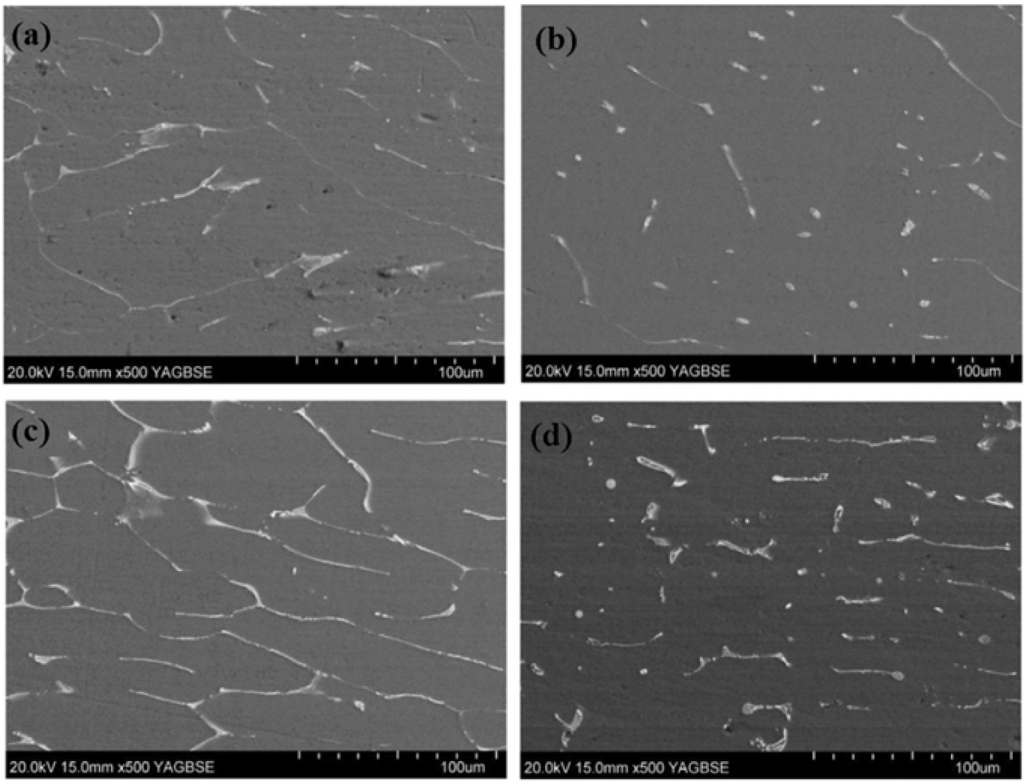

Fig. 7. Scanning electron microscopy images of sample containing lanthanum element in a) Al-0.3La, b) Al-0.3La(300°C/24 h), c) Al-0.8La and d) Al-0.8La (300°C/24 h) [70].

- Fig. 10a: EC of a 9.5 mm wire sample after 100 h, cooled in different environments.
- Fig. 10b: Effect of HT temperature on the EC of the same 9.5 mm wire sample.
- Fig. 10c: Impact of various wire diameters and HT temperatures on the EC of the samples after 75 h.

Majchrowicz et al. [73], demonstrated that hydrostatic extrusion combined with heat HT refines Al-Mg-Si alloys (e.g., AA6201) to ultra-fine grains (300–400 nm), achieving exceptional tensile strength (TS > 330 MPa) and EC up to 58 % IACS. The optimal process—three extrusion passes followed by aging at 180°C for 7 h—yielded 332 MPa TS and 58.4 % IACS EC (see Fig. 11). Microstructural analysis revealed aligned GP zones, β''/β' precipitates, and grain-boundary β particles, which critically influenced properties. Further enhancements were achieved via GR and boron doping, balancing mechanical robustness and EC for overhead conductor application. The study lacks an assessment of the economic viability and industrial scalability of the proposed thermo-mechanical processing, which may hinder practical adoption.

A study by Cui et al. [74], examined the impact of GR and boron addition on the mechanical and electrical properties of 1070 aluminum alloy. Six different compounds were used for GR, with the outcomes presented in Figs. 12a and 12b. The compound Al-5Ti-0.8B-0.2 C was identified as providing the optimal balance of fine grain size and high EC. The formation of TiC and TiB_2 particles from compounds such as Al-Ti-C, Al-Ti-B, and Al-Ti-BC increases the nucleation potential of aluminum and promotes GR during solidification due to their high melting points and low solubility in α-Al. Adding boron is crucial for enhancing the alloy's EC. Boron interacts with transition metals in the alloy, leading to the formation and precipitation of boride particles. According to the principles governing electrical resistance, reducing impurities within the alloy lowers the obstacles to electron flow, thereby improving conductivity. Various aluminum-boron compounds were tested for their effectiveness. The results shown in Fig. 12c indicate that 1 wt% of Al-6B was the most effective in enhancing EC.

In their study, the researchers determined that Al-5Ti-0.8B-0.2 C is the optimal compound for refining the grain structure of 1070 aluminum alloy, while Al-6B is best suited for its purification and enhancement of EC. Figs. 13a and 13b illustrate that the most favorable properties are attained by initially adding 0.2 % Al-6B, followed by 0.5 % Al-5Ti-0.8B-0.2 C. This sequential addition results in superior outcomes. Figs. 13c through 13e illustrate the final microstructure of the 1070 aluminum alloy both before and after the addition of the various grain-refining compounds, along with the relevant stress-strain diagrams.

Xu et al. [67] studied the effects of trace elements on aluminum conductors, with compositions detailed in Table 2. Their findings revealed that high iron/silicon content and Fe/Si ratio improved hardness and mechanical properties through α(Al12Fe3Si2) and β(Al9Fe2Si2) phase formation, albeit at the cost of reduced EC (Fig. 15, Table 3). Boron addition, in the presence of Ti/V, led to (Ti,V)B2 particle formation, which increased nucleation sites but did not consistently refine grain size (Fig. 14), likely due to TiB_2/VB_2 agglomeration during melt storage. Notably, larger grains correlated with lower hardness but higher EC. Also, this study examined specific Fe/Si ratios and boron interactions with Ti/V but did not explore other potential synergistic or antagonistic effects of additional trace elements. Also, while grain size effects were noted, the study did not systematically control solidification conditions, leaving uncertainty about the exact influence of cooling rates on microstructure and properties Fig. 15.

Cui et al. [75] investigated the impact of increasing boron concentration on the EC in the presence of trace amounts of titanium. It was found that titanium in the solid solution adversely affects EC, and minimizing its concentration within the solution enhances conductivity. However, during the process of adding boron alongside titanium, titanium facilitates the precipitation of transition elements in the form of borides, which subsequently enhances the EC of the alloy (refer to Fig. 16a). Typically, the efficiency of boron addition operations is approximately 77.7 %. In the instance of the 1070 aluminum alloy investigated in this study, the EC improved to 64.6 %IACS. Nevertheless,

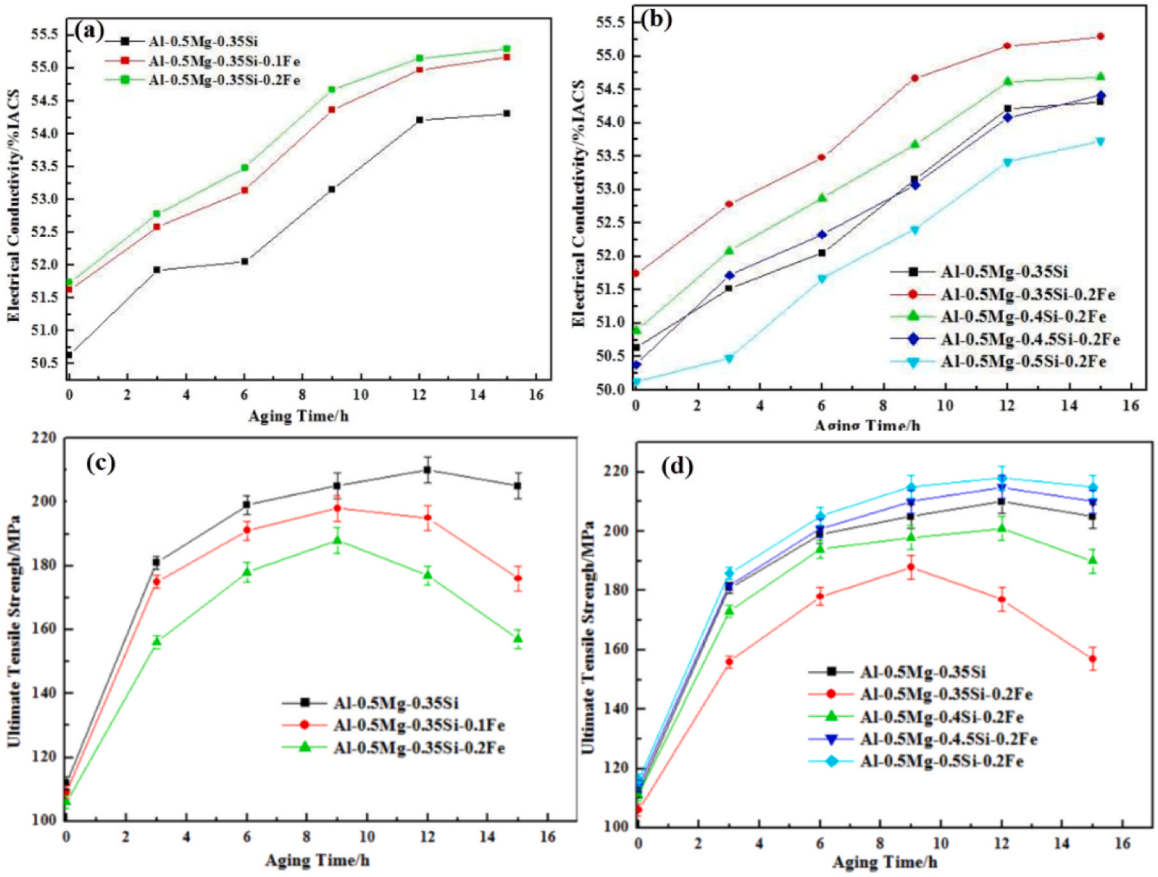

Fig. 8. EC of alloys a) (Al-0.5Mg-0.35Si-xFe) and b) (Al-0.5Mg-xSi-0.2Fe), and final TS of alloys c) (Al-0.5Mg-0.35Si-xFe) and d) (Al-0.5Mg-xSi-0.2Fe) at different HT times [71].

the use of titanium can elevate the process efficiency to 93.3 % and the EC to 65.3 %IACS. The findings demonstrated that most transition elements react and precipitate with the addition of titanium. Consequently, by further reducing the concentration of transition elements in the 1070 aluminum alloy, the distortion of the alloy's crystal lattice is diminished. The reduction in lattice distortion diminishes electron scattering within the crystal structure, thereby enhancing the EC of the alloy. This relationship is visually demonstrated in Figs. 16b and 16c.

In another study by Cui et al. [76] the enhancement of the electrical and mechanical properties of dilute aluminum alloy conductors was investigated. The study specifically analyzed the alloys Al-0.5Mg-0.35Si and Al-0.8Fe-0.2Cu, aiming to balance boron addition with GR to improve the stated properties. The EC of the samples, correlated with varying boron content, is detailed in Table 4. The observed improvements in EC were primarily due to the reaction between boron and the transition elements within the alloy, resulting in the formation and precipitation of borides. One significant concern regarding aluminum alloys is the potential adverse interaction between boron and alloying elements. Fortunately, the study revealed that boron does not react with elements such as iron, magnesium, silicon, and copper. Consequently, the addition of boron has a minimal impact on the distribution of these alloying elements. For instance, Figs. 17a-17c illustrate the microstructure of various regions in the Al-0.5Fe-0.2Si alloy with an addition of 0.12 % boron. These images show white areas corresponding to the AlSiFe phase along the grain boundaries, devoid of any white particles or impurities. This indicates that with a sufficient holding period, numerous transition elements precipitate as borides. Further analyses confirmed the presence of (V,Ti,Al)B_2 particles resulting from boron addition. Overall, the study demonstrated that boron effectively enhances the EC of aluminum alloys without negatively affecting the distribution of key alloying elements, thus achieving a refined grain structure and improved mechanical properties. However, the beneficial effects of boron were observed after sufficient holding time, but the study did not systematically optimize or vary this parameter, potentially overlooking time-dependent precipitation dynamics. Also, while boron improved EC and grain refinement, the long-term thermal and electrical stability of the boride-containing alloys under operational conditions (e.g., elevated temperatures) was not assessed.

Different α-Al grain sizes significantly impact the EC of aluminum, making the relationship between these two parameters both important and vital (Figs. 18 and 19).

In research conducted by Koprowski et al. [77], examined the impact of incorporating trace amounts of magnesium, cobalt, and cerium, as well as the effects of the drawing process, on the mechanical and electrical properties of 1xxx series aluminum alloys. Post-drawing, 99.9 % pure aluminum exhibited a TS of 200 MPa and EC of 61.1 %. The addition of 0.2 % by weight of magnesium, cobalt, and cerium yielded tensile strengths and conductivities of 225 MPa/59.1 %, 203 MPa/60.5 %, and 184 MPa/60.9 %, respectively. The findings indicate that the addition of small amounts of cobalt and cerium had minimal effect on the strengthening of drawn wire compared to 99.9 % aluminum. Conversely, the addition of magnesium had a notable impact, as 0.2 % magnesium remained in solid solution, enhancing the alloy's TS. In a study, Khangholi et al. [78] examined how different levels of silicon affected the hardness and EC of 6xxx series aluminum alloys during HT at 180 °C. The three samples studied in this study included Si4, Si6 and Si9, which represent 0.4 %, 0.66 % and 0.89 % by weight of silicon, respectively, and a constant amount of 0.65 % by weight of magnesium. Figs. 19a and 19b show the micro-hardness and EC of the test specimens with respect to time. As it turns out, the higher

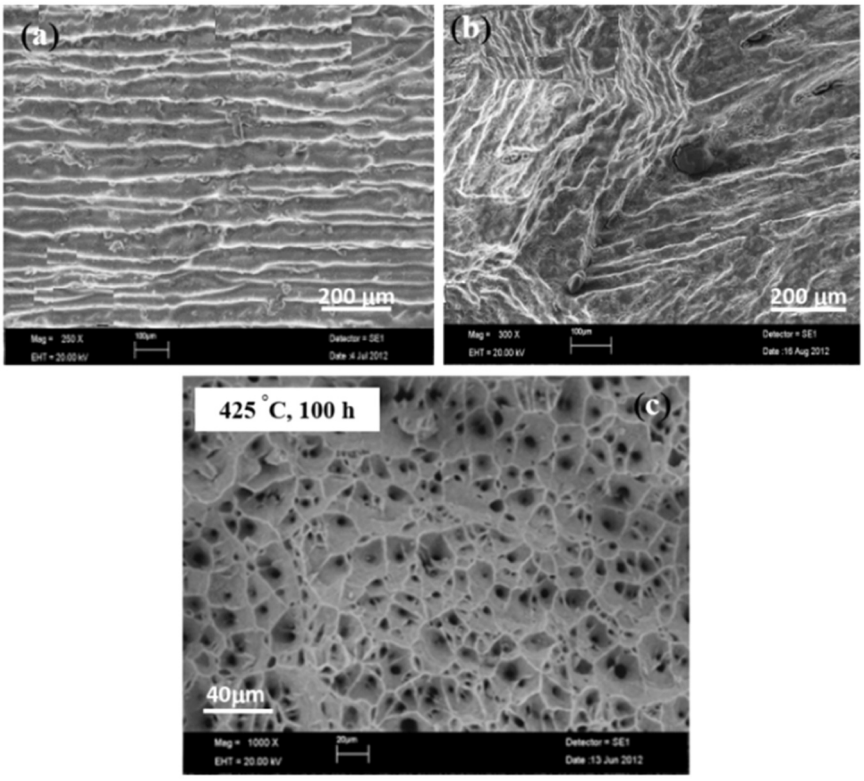

Fig. 9. Scanning electron microscopy image of Al-0.25Zr alloy microstructure a) in the shape of a wire with a final diameter of 9.5 mm, b) continuous casting and drawing of T-bar ingot, and c) 9.5 mm wire microstructure at temperature 425 °C and time 100 h [72].

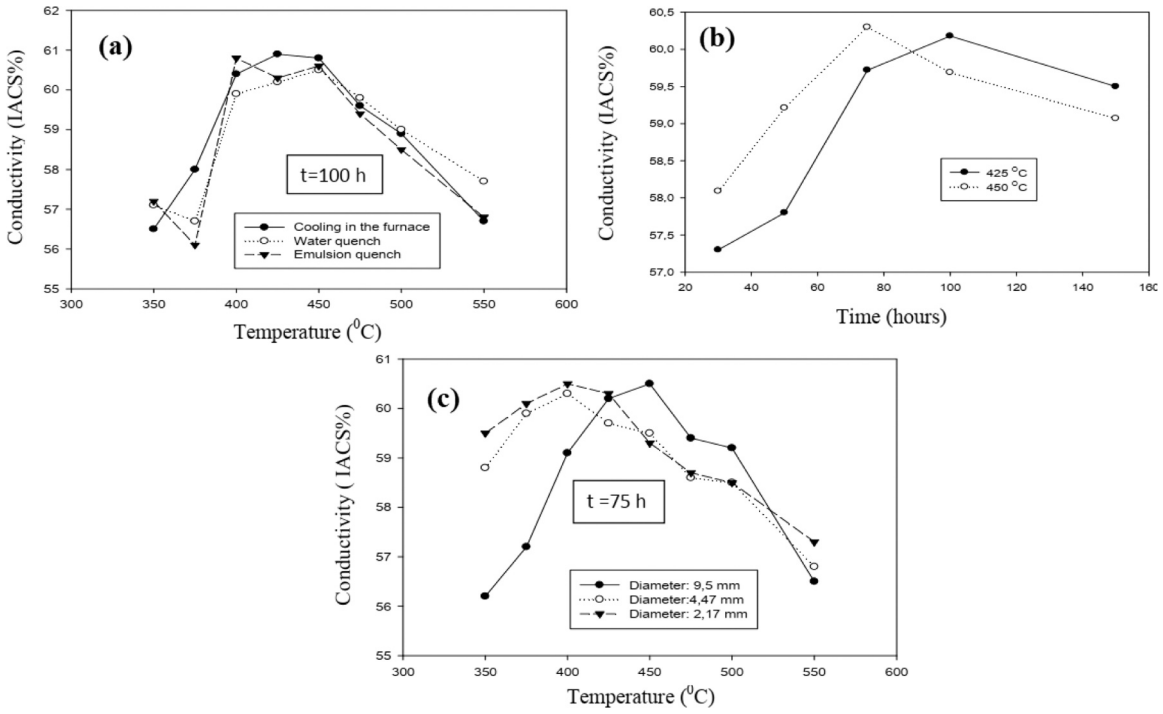

Fig. 10. EC values of a) 9.5 mm wire sample at 100 h and cooling in different environments, b) effect of HT temperature on the EC of the same sample, and c) effect of different wire diameters and different HT temperatures at 75 h on the EC of the samples [72].

the amount of silicon, the harder it is. When the samples reached their maximum hardness, their EC had fallen below the minimum required value (52.5 %IACS). Therefore, there was a need for times during which the EC also improves. According to Fig. 19c, in areas where the EC is less than the target value (51–44 %IACS), the alloy with the highest amount of silicon (Si9) has the highest hardness. However, with increasing EC, the hardness of the Si6 sample was reported to be higher than that of the Si9 sample, and according to Fig. 19d in areas with high EC, the Si6

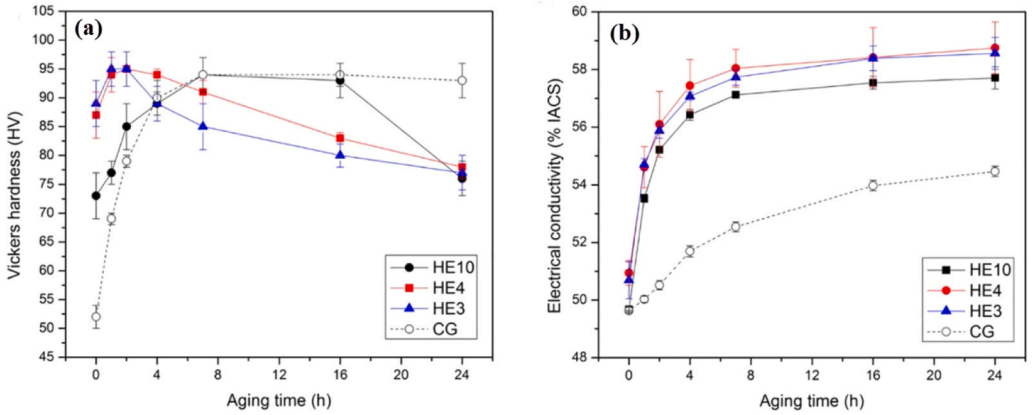

Fig. 11. a) Hardness, and b) EC of 6201 aluminum alloy under different conditions of hydrostatic extrusion and HT at 180 °C and different times [73].

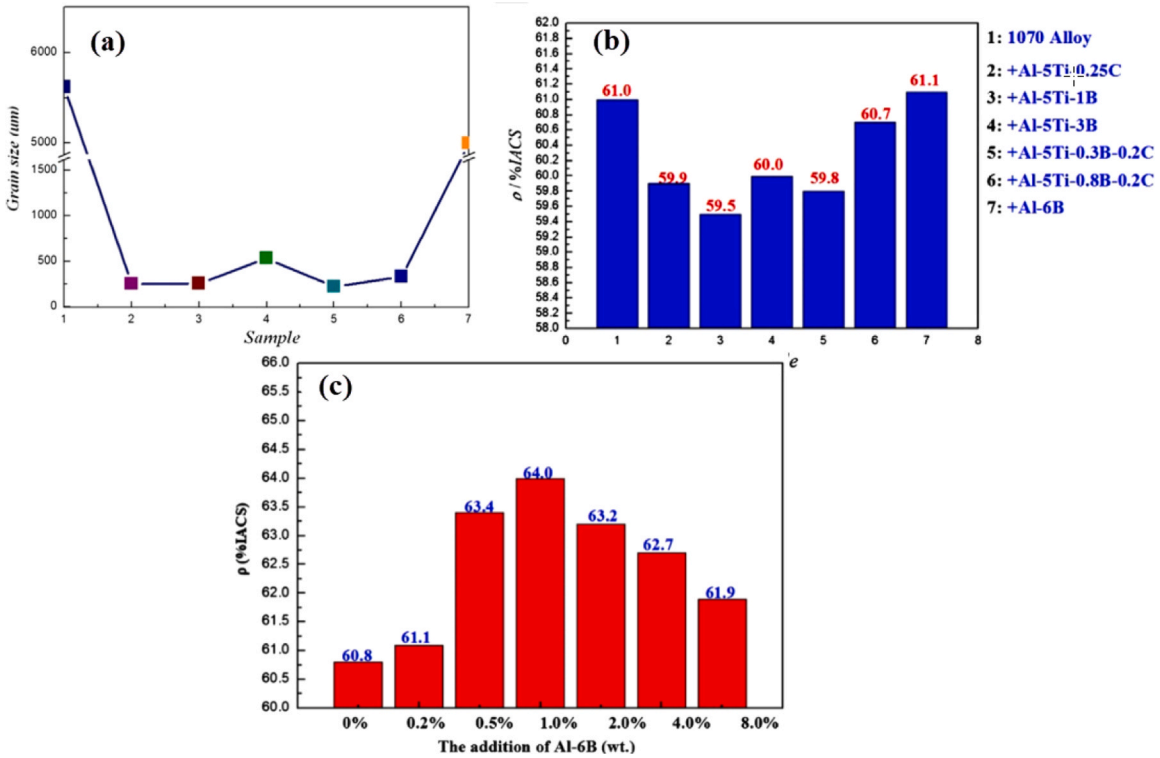

Fig. 12. a) Grain size, b) EC of 1070 aluminum alloy with various additives, and c) EC of 1070 aluminum alloy with different amounts of boron added [74].

sample has the highest hardness among all three samples. In general, the distribution of iron-rich intermetallic particles and the type of these particles after the homogenization operation depend on the Fe/Si ratio (Fig. 20). While mechanical and electrical properties were reported, detailed microstructural evolution (precipitate distribution, dislocation density) was not thoroughly characterized to fully explain the observed property trends.

In the investigation conducted by Langelandsvik et al. [79] investigated the effects of iron precipitate and a novel torsional extrusion method on the electrical and mechanical properties of 1370 aluminum alloy. Initially, 3 mm diameter drawn wires were subjected to solid solution HT at 640 °C for one hour. According to the TTTD in Fig. 21a, maximum iron precipitation occurred at 450 °C. Subsequently, the 1370 alloy underwent a new torsional extrusion process, as schematically shown in Fig. 21b. The association between EC and the duration of solid solution HT across a spectrum of temperatures is depicted in Fig. 21c. The results indicate a slight enhancement in EC resultant from the HT in comparison to the wire-drawing process. Specifically, during HT within the temperature range of 300 °C to 560 °C, the peak EC achieved was 64.5 %IACS at 400 °C after a duration of 96 h. This improvement in conductivity at varying thermal conditions can be fundamentally attributed to the precipitation of supersaturated iron within the solid solution onto intermetallic compounds such as AlFe and AlFeSi, featuring notable phases including $Al_{13}Fe_4$, Al_5Fe, Al_9Fe_2, $Al_{15}Fe_6Si_5$, and $Al_9Fe_2Si_2$. Fig. 22a and b illustrate the increase in iron-rich particles before and after HT. Transmission electron microscopy results of the regions along the extrusion direction are presented in Fig. 22c and d. Analysis of the microstructural images reveals that grain boundaries, highlighted by red arrows, are obstructed by iron precipitates. This obstruction effectively curtails grain boundary migration, recrystallization, and grain growth at elevated temperatures. Moreover, the resultant formation of a $< 001 >$ texture orientation has been linked to an enhancement of the alloy's electrical properties. Furthermore, wires subjected to this torsional extrusion method and subsequently heat

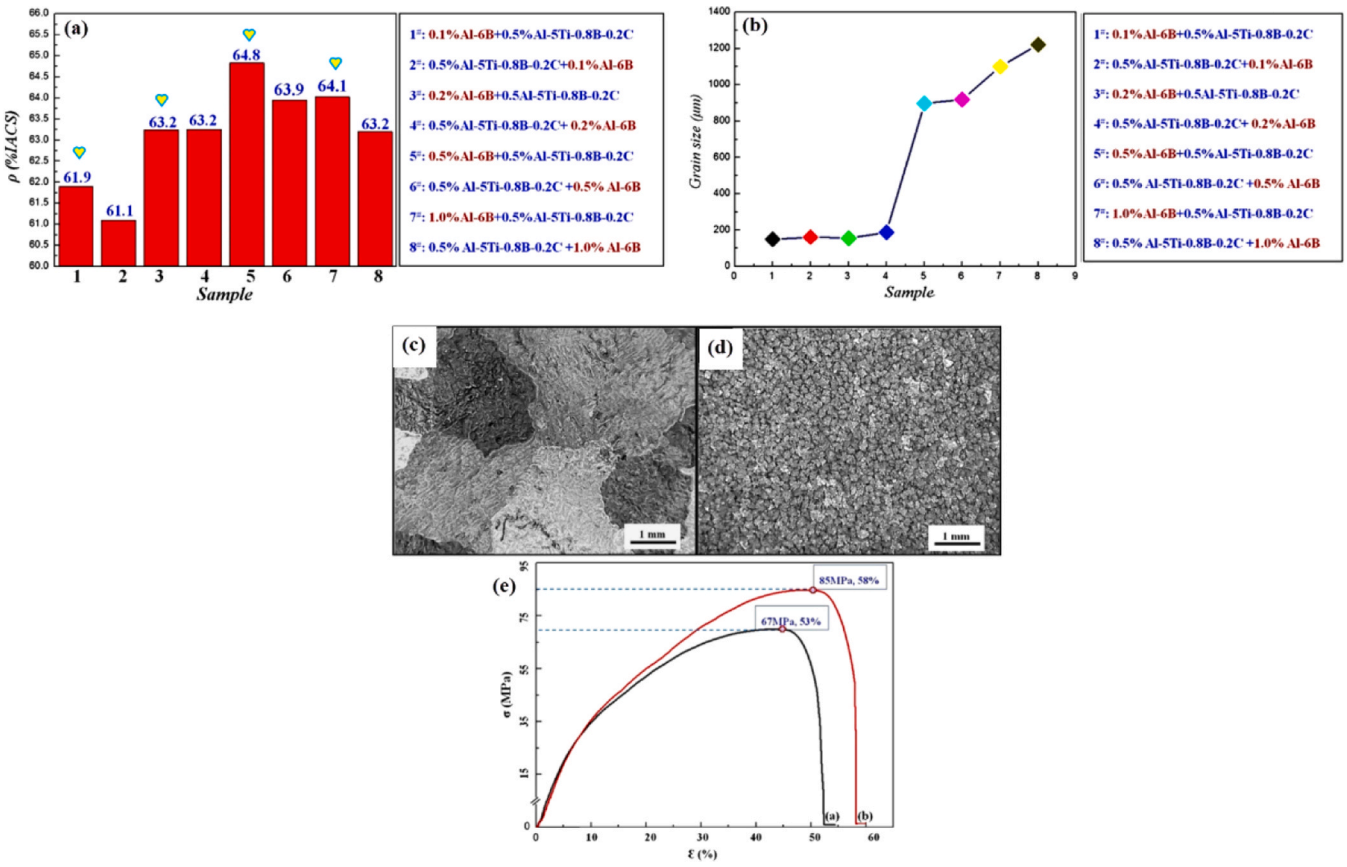

Fig. 13. a) EC of different samples of 1070 aluminum alloy, b) grain size of different samples of 1070 aluminum alloy with 0.5 % additives Al-5TI-0.8B-0.2 C and Al-6B, c) microstructure of 1070 aluminum alloy, d) microstructure of 1070 aluminum alloy with 0.5 % additive Al-5TI-0.8B-0.2 C, and e) their strain-stress diagrams [74].

Table 2
Chemical composition of different aluminum conductors (w%) [67].

Sample	Fe	Si	Ti	V	B	Re	Na	Mg
A−1	0.0641	0.0191	0.0011	0.0003	0.0028	0.0047	0.0054	0.0049
A−2	0.0439	0.0182	0.0011	0.0006	0.0018	0.0046	0.0050	0.0045
A−3	0.0381	0.0149	0.0082	0.0003	0.0057	0.0043	0.0062	0.0057
A−4	0.0244	0.0129	0.0032	0.0179	0.0002	0.0033	0.0070	0.0057

Table 3
Electrical properties of various aluminum conductors [67].

Sample	Temperature (°C)	Electrical resistivity (n.Ω.m)	(EC) (%IACS)
A−1	23.8	28.178	61.19
A−2	23.8	28.145	61.26
A−3	24.0	27.724	62.19
A−4	23.9	27.695	62.25

treated at 450 °C exhibited a commendable synergy of MS, recorded at 65 MPa, alongside an EC value reaching 64.2 %IACS. This exceptional combination underscores the potential of integrated processing techniques in optimizing the performance characteristics of aluminum alloys. The novel torsional extrusion method presents challenges in scalability and industrial implementation compared to conventional processing techniques, potentially limiting its practical adoption. Also, while the study identified 400–450°C as optimal for iron precipitation, it did not fully explore the effects of intermediate temperatures or cooling rates on precipitate formation and distribution. The requirement for extended heat treatment durations (up to 96 h) to achieve peak properties may be impractical for commercial production scenarios where shorter processing times are preferred.

In a study by Jiang et al. [80], the authors investigated the interplay between grain size and the Mg/Si ratio, along with how these factors jointly influence the mechanical, microstructural, and electrical properties of aluminum alloys containing magnesium, silicon, and scandium (Al-Mg-Si-Sc).The study included alloy specimens with varying Mg/Si ratios (both above and below 1.73 % by weight) and grain sizes (coarse and fine). The primary objective of the study was to investigate the effects of grain size and the Mg/Si ratio on characteristics such as hardness and EC at an aging temperature of 200 °C. The alloys analyzed in the research were categorized into two distinct groups. The first group underwent a solid solution HT process at 560 °C for a duration of 2 h, followed by an artificial aging treatment at 200 °C, designated as specimens # 1-I and # 2-I. The second group also experienced initial solid solution HT at 560 °C for 2 h, after which they were extruded to a 9.5 mm diameter at 500 °C and then artificially aged at 200 °C (# 1-II and # 2-II). In coarse-grained alloys, the precipitation of β'' phase and hardening were found to be significantly influenced by the Mg/Si ratio, although this ratio had a lesser effect on EC. The results for hardness and EC in fine- and coarse-grained samples are provided in Fig. 23. In ultra-fine grain alloys, EC was more closely related to hardness than to

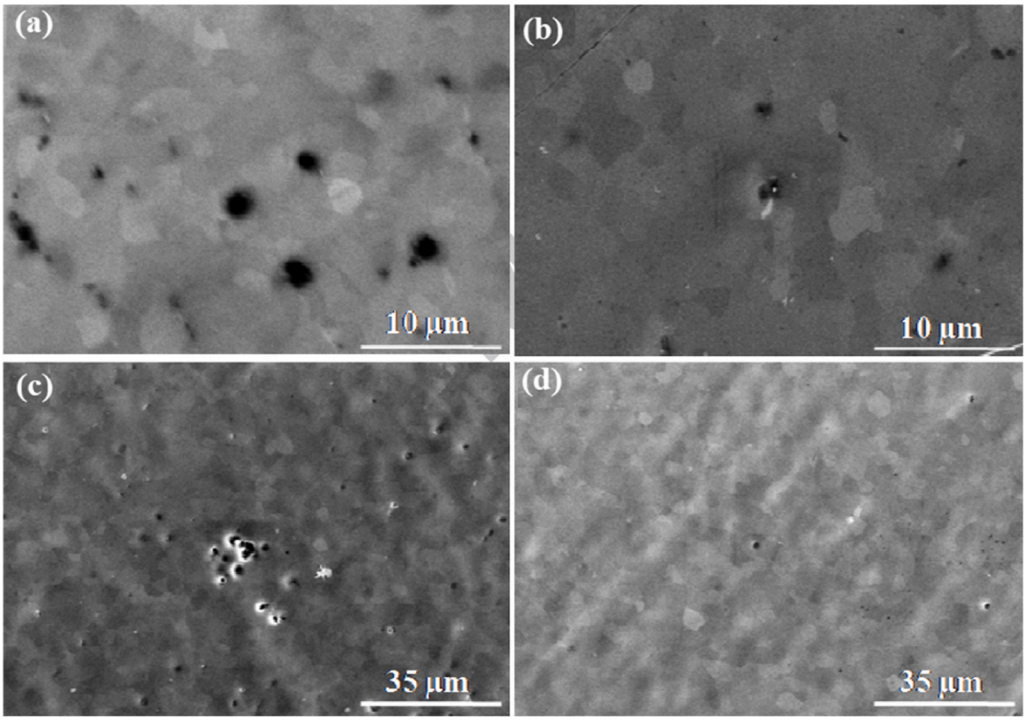

Fig. 14. Microstructure of aluminum conductors: a) A-1, b) A-2, c) A-3, and d) A-4 [67].

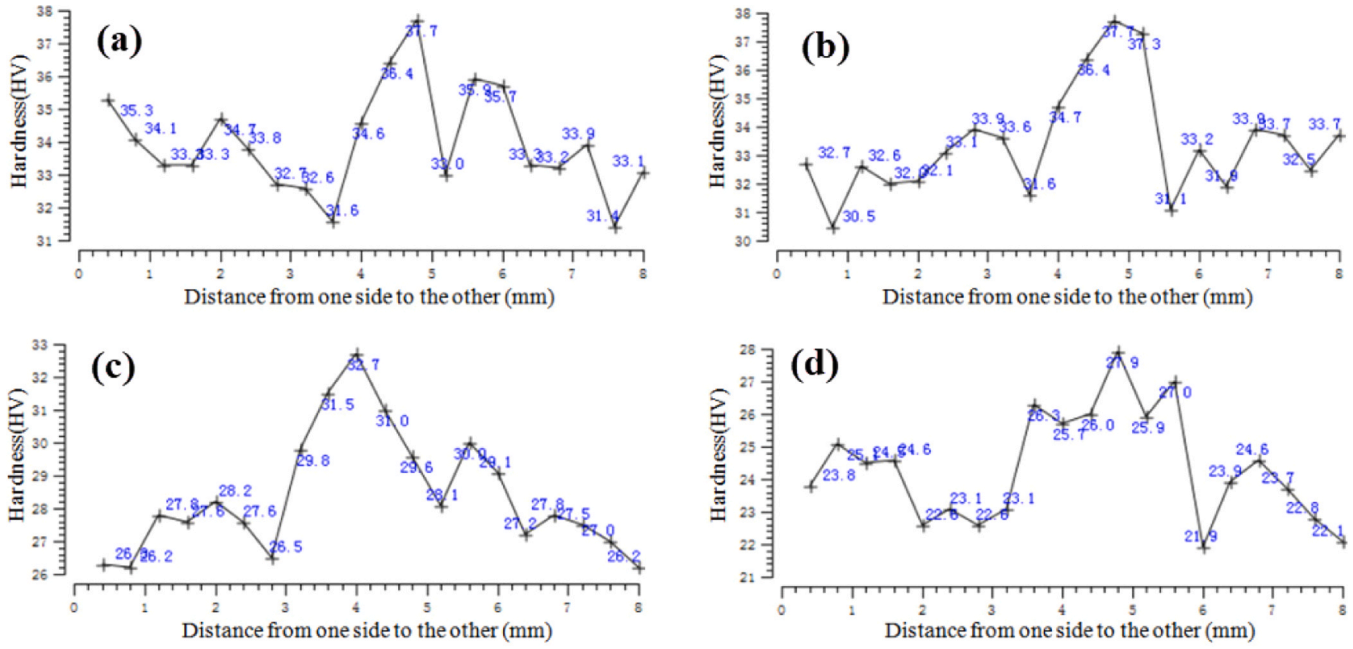

Fig. 15. Hardness of aluminum conductors: a) A-1, b) A-2, c) A-3, and d) A-4 [67].

the Mg/Si ratio. Alloys with higher silicon content exhibited greater EC compared to those with higher magnesium content. This effect is largely due to the influence of silicon on precipitation dynamics at the grain boundaries, which leads to a reduction in the concentration of dissolved atoms and precipitates within the grains themselves. Illustrated in Fig. 24 is the intricate relationship between grain size and the Mg/Si ratio, along with their synergistic effects on both the electrical and mechanical properties of Al-Mg-Si-Sc alloys. The study only examined two specific processing routes (direct aging vs. extrusion + aging), without exploring other thermo-mechanical treatments that could further optimize the property balance. All aging was conducted at 200°C, leaving uncertainty about how different aging temperatures might affect the Mg/Si ratio's influence on precipitation behavior and final properties. Also, the binary classification into "coarse" and "fine" grains oversimplifies the continuous nature of grain size effects, missing potential intermediate optimal grain sizes.

The Al-Si hypoeutectic alloy is commonly used in conductor manufacturing due to its advantageous properties. However, simultaneously enhancing both its EC and mechanical properties is challenging, limiting its wider industrial use. In a study by Cui et al. [81] approaches

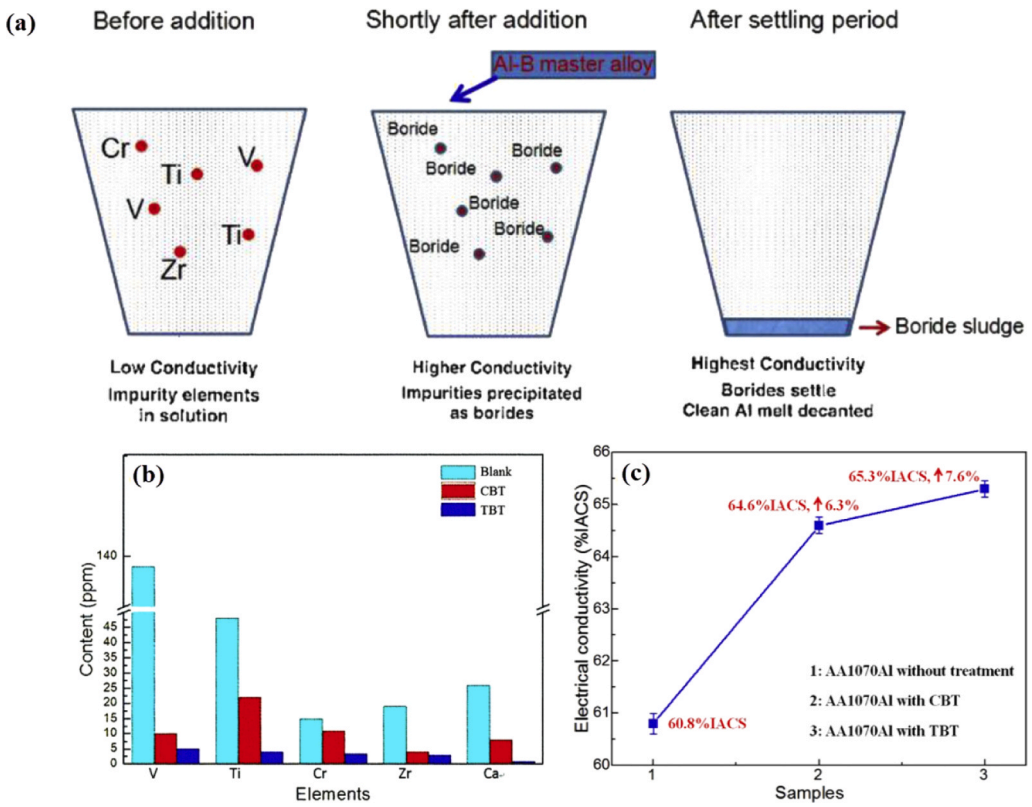

Fig. 16. a) Process of adding boron and precipitation of transition element, b) the amount of impurities in 1070 aluminum alloy in different processes of adding boron, and c) changes in the EC of 1070 aluminum alloy in boron addition processes [75].

Table 4
EC of alloys with the addition of boron (%IACS) [76].

B addition (%)						
Sample	**0**	**0.03**	**0.06**	**0.09**	**0.12**	**0.24**
Al−0.5Mg−0.35Si	52.2	57.0	54.3	53.9	55.0	58.7
Al−0.5Fe−0.2Si	53.0	54.1	56.6	56.9	58.3	57.4
Al−0.8Fe−0.2Cu	56.2	57.0	58.0	58.3	59.8	58.7

to improve the EC of the Al-Si hypoeutectic alloy were explored. This limited improvement is attributed to the negative interaction between boron and strontium. The findings demonstrated that the addition of boron, coupled with the use of titanium, or modification with strontium, effectively enhances EC. Nonetheless, these two methods exhibit differing degrees of effectiveness. Specifically, the EC of Al-7Si was improved to 45.2 %IACS via the TBT process and to 41.6 %IACS through strontium modification. Conversely, the simultaneous application of both TBT and strontium modification resulted in a reduced conductivity of 42.1 %IACS. This diminished improvement is attributed to the negative interaction between boron and strontium. To address this, researchers utilized Al-3B-5Sr, which effectively optimized the microstructure, EC, and mechanical properties all at once. In another study by Murashkin et al. [82],improvements in the mechanical and electrical properties of 6101 aluminum alloys were achieved using the ECAP-C process. This process involved six cycles of ECAP-C at 130 °C on 6101 aluminum alloy, producing an ultra-fine and uniform grain structure with grain sizes between 400 and 600 nm. Figs. 25a and 25b show the microstructure of the 6201-alloy after ECAP-C plastic deformation. The resulting alloy had a TS of 308 MPa and an EC of 53.1 %IACS. HT at 170 °C further boosted EC without sacrificing MS, while treatment at 190 °C reduced TS (Fig. 25c). Additional enhancements were realized by decomposing the solid solution with β' cylindrical precipitates and minimizing the number of alloying elements in the aluminum matrix. The optimal balance of properties, including an ultimate TS of 304 MPa and an EC of 57.1 %IACS, was achieved after six passes followed by 12 h of HT at 170 °C. The ECAP-C process, while effective, is complex and may face challenges in large-scale industrial implementation compared to conventional extrusion or rolling methods. Also, despite improvements, the study did not explore whether higher pass numbers (>6) or alternative post-ECAP treatments could further enhance the strength–conductivity balance.

In their investigation, Pan et al. [83], explored the influence of varying iron content, specifically between 0.3 % and 0.7 % by weight, on the microstructural, electrical, and mechanical characteristics of 8xxx series conductive aluminum alloys. The study comprised three distinct sample groups: Al_3 (0.3Fe), Al_5 (0.5Fe), and Al_7 (0.7Fe). Figs. 26a and 26b depict how the iron content affects UTS, YS, elongation, and EC. Results from this study revealed a consistent increase in both UTS and YS with higher iron concentrations, while elongation values remained relatively stable. This strengthening effect can be traced back to the increased formation of iron-rich intermetallic particles, which impede dislocation motion and grain boundary migration, thereby enhancing the tensile and yield properties. However, the introduction of these intermetallic particles also led to a rise in atomic defects within the aluminum matrix, which hindered the mobility of electrons and subsequently reduced the EC of the alloys. Further assessment was conducted, as shown in Figs. 26c and 26d, to measure the effects of an annealing treatment at 360 °C for 4 h on the samples' mechanical and electrical attributes. Following the annealing process, each of the three alloy samples experienced a 1 % increase in EC. Considering specific application requirements, the Al5 and Al7 samples may be particularly beneficial due to their favorable combination of enhanced MS and satisfactory EC.

Yuan et al. [84], investigated the effects of zirconium incorporation on the properties and thermal stability of Al-Mg-Si aluminum alloy. The study revealed that adding zirconium leads to improved GR and

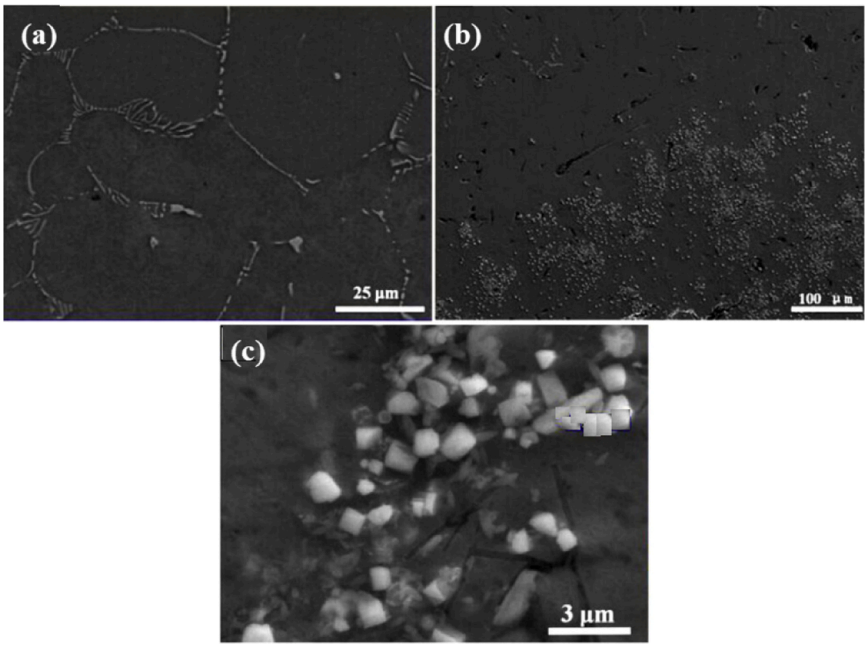

Fig. 17. Microstructure of Al-0.5Fe-0.2Si alloy with the addition of 0.12 % boron; a)upper parts, b) lower parts, and c) morphology of white precipitates [76].

enhanced microstructural stability, attributed to the uniform distribution of Al33Zr particles which act as nucleation sites, as illustrated in Figs. 27b and 27c. Mechanical properties and EC were evaluated following a HT at 190 °C for 3 h, comparing samples with and without zirconium, with results summarized in Table 5. The study concluded that microstructural transformations during HT and deformation significantly influence the mechanical properties of the alloys. Specifically, recrystallization, which typically degrades mechanical properties, is markedly inhibited by the addition of zirconium. This inhibition is attributed to the Zener pinning effect, where dispersed zirconium particles obstruct grain boundary movement, thereby enhancing the alloy's stiffness and TS. In contrast, the incorporation of zirconium results in a decline in EC. This reduction can be primarily attributed to enhanced electron scattering, which occurs as a consequence of the introduction of additional grain boundaries and atomic defects created by the presence of zirconium.

The studies evaluating the thermal stability of the samples included hardness tests under two different HT conditions: 230 °C for 3 h and 180 °C for 400 h. The study only examined a single zirconium addition level (0.145 % Zr), leaving the effects of higher or lower Zr concentrations on property optimization unexplored. Also, while thermal stability was assessed, the longest aging duration was 400 h at 180°C, which may not fully represent long-term performance in real-world applications requiring extended service life.

In their study, Zhao et al. [85] examined the effects of incrementally adding 1 %, 2 %, 3 %, and 4 % by weight of Al-8B-2C on the mechanical and electrical properties of 1070 aluminum (99.7 % purity). The researchers identified an optimal composition through this investigation. As illustrated in Fig. 28a and b, the UTS and elongation percentage were significantly influenced by the proportion of Al-8B-2C added. Specifically, introducing 1–4 % by weight of Al-8B-2C increased the UTS of the 1070 alloy from 66 MPa to 79, 85, 95, and 101 MPa, respectively. Additionally, these additions resulted in more than a 55 % increase in elongation. A primary factor contributing to this improvement is the alteration in grain size of the 1070 aluminum alloy, which varies with different percentages of Al-8B-2C (Fig. 28c). Additionally, the EC of the 1070 alloy was examined in relation to varying amounts of the Al-8B-2C additive, as shown in Fig. 25d. The results indicated an increase in EC from 61.23 %IACS to 61.51 %IACS and 61.87 %IACS with the addition of 1 % and 2 %, respectively. Further addition of 3 % resulted in an EC of 62.06 %IACS, while a 4 % addition led to a slight decrease to 61.83 % IACS. This improvement is likely due to the interaction between AlB2 particles and impurities such as Ti, Cr, and V in the aluminum, which affects electron transfer to primary impurities like Fe and Si.

In a detailed study by Hassanabadi et al. [86], the effects of various grain refiners on the properties of 1370 aluminum alloy were extensively investigated. Different refiners with distinct chemical compositions, as specified in Table 6, were used at a concentration of one percent by weight. The results showed that adding Al-5Ti-1B, Al-3Ti-1B, OPTIFINE, and TIBloy at this level did not notably affect the grain refining of the 1370 aluminum alloy. In contrast, incorporating Al-3Ti-0.15 C was significantly more effective in refining the primary alloy's grain structure. By comparing the lattice parameters of the TiC and TiB_2 particles with those of αAl, it was concluded that TiC particles have a superior ability to create nucleation sites for αAl, thereby achieving greater GR in aluminum alloys. Further investigation into the effects of these additives on the EC of the 1370 aluminum alloy is illustrated in Fig. 29. Initially, the EC for all samples exhibited a slight reduction (indicated by time zero in the diagrams corresponding to the reference sample's conductivity). This decrease was observed to stabilize over time and, in some instances, even reversed. The initial decline in EC is likely due to the accumulation of undissolved titanium particles within the melt post-refinement. The subsequent increase is attributed to variations in the precipitation behavior of particles such as TiB2, TiC, $TiAl_3$, and AlB_2. This behavior is influenced by variations in particle size distribution. This study only examined a single concentration level (1 wt%) for all grain refiners, potentially missing optimal dosage effects that could vary for different refiner types. Also, the EC measurements lacked detailed temporal resolution during the initial stabilization period, obscuring the exact kinetics of conductivity recovery and while different refiners were compared, the study didn't provide quantitative analysis of particle size distributions or interfacial characteristics between nucleating particles and α-Al matrix. Also, all experiments were conducted under identical melting/casting conditions, leaving uncertainty about how varying processing parameters (e.g., cooling rates) might interact with refiner effectiveness.

In a study by Knych et al. [87], the effects of zirconium additions, ranging from 0.05 % to 0.32 % by weight, on aluminum alloys used for overhead conductors were investigated. The samples were subjected to a thermal treatment protocol, wherein they were maintained at

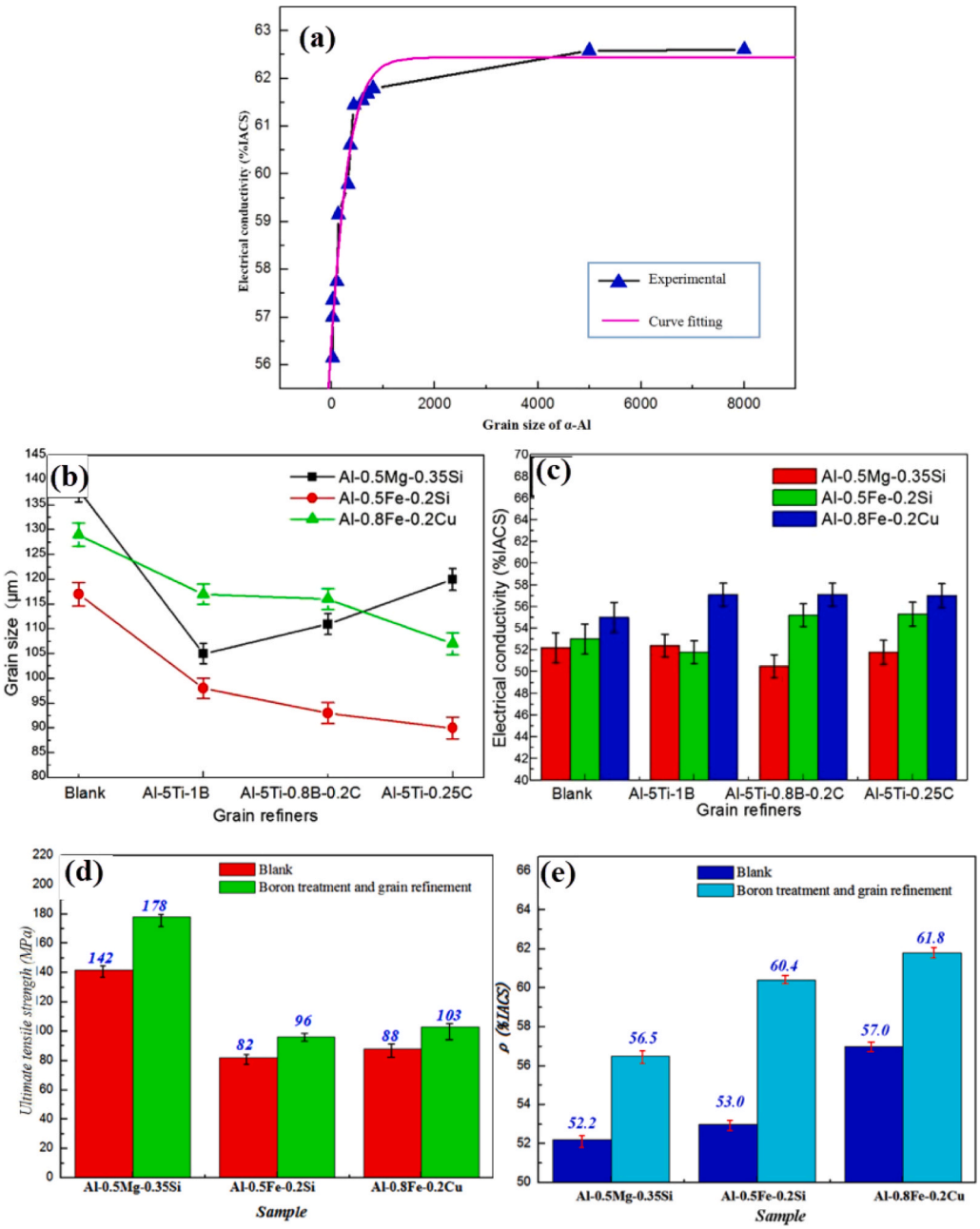

Fig. 18. a) Relationship between αAl grain size and EC, b) effect of addition of grain refiners on grain size, c) EC of aluminum alloys with addition of grain refiners, d) simultaneous effect of boron and grain refiners on mechanical properties, and, e) electrical properties of aluminum alloys [76].

temperatures spanning from 20 °C to 620 °C, with exposure durations set at 24, 120, and 192 h respectively. It was observed that in the AlZr0.05 sample, minor changes occurred in electrical properties, with electrical resistance decreasing from 29 nΩm at 20 °C to 28.4 nΩm at temperatures up to 500 °C. The optimal conditions for this alloy were determined to be 350 °C for 192 h. As the zirconium content increased to 0.09 % by weight, the changes in electrical properties were more pronounced due to the presence of insoluble zirconium in the aluminum solid solution, with optimal conditions being 350 °C for 192 h. For the sample with 0.15 % zirconium, the EC data displayed a U-shaped pattern, with optimal conditions located at the bottom of the U-shape. In alloys containing 0.22 % zirconium, a decrease in electrical resistance occurred between 20 °C and 450 °C due to thermal diffusion activation. However, when the temperature rose to the range of 450 °C to 620 °C, conditions resembled equilibrium due to zirconium's limited solubility and reduced precipitation. The best treatment conditions for these samples were 450 °C for 192 h.

In another study, Pan et al. [88] conducted a meticulous investigation into the influence of partial additions of copper and magnesium on the microstructural characteristics and properties of 8xxx series conductive aluminum alloys. The primary alloys incorporated iron concentrations of 0.3 %, 0.5 %, and 0.7 % (denoted as Al-0.3Fe, Al-0.5Fe, and Al-0.7Fe respectively). The experiment involved the incremental addition of 0.18 % and 0.29 % copper to these baseline alloys, alongside the introduction of 0.025 %, 0.05 %, and 0.1 % magnesium to the Al-0.3Fe-0.18Cu, Al-0.5Fe-0.18Cu, and Al-0.7Fe-0.18Cu compositions. Given iron's notably low solubility in aluminum, iron predominantly precipitated as intermetallic phases within the alloy's microstructure. Post-extrusion processing resulted in these iron-rich intermetallic particles being fragmented into exceedingly fine particles, which were subsequently aligned along the extrusion direction within the aluminum matrix. The inclusion of magnesium and copper

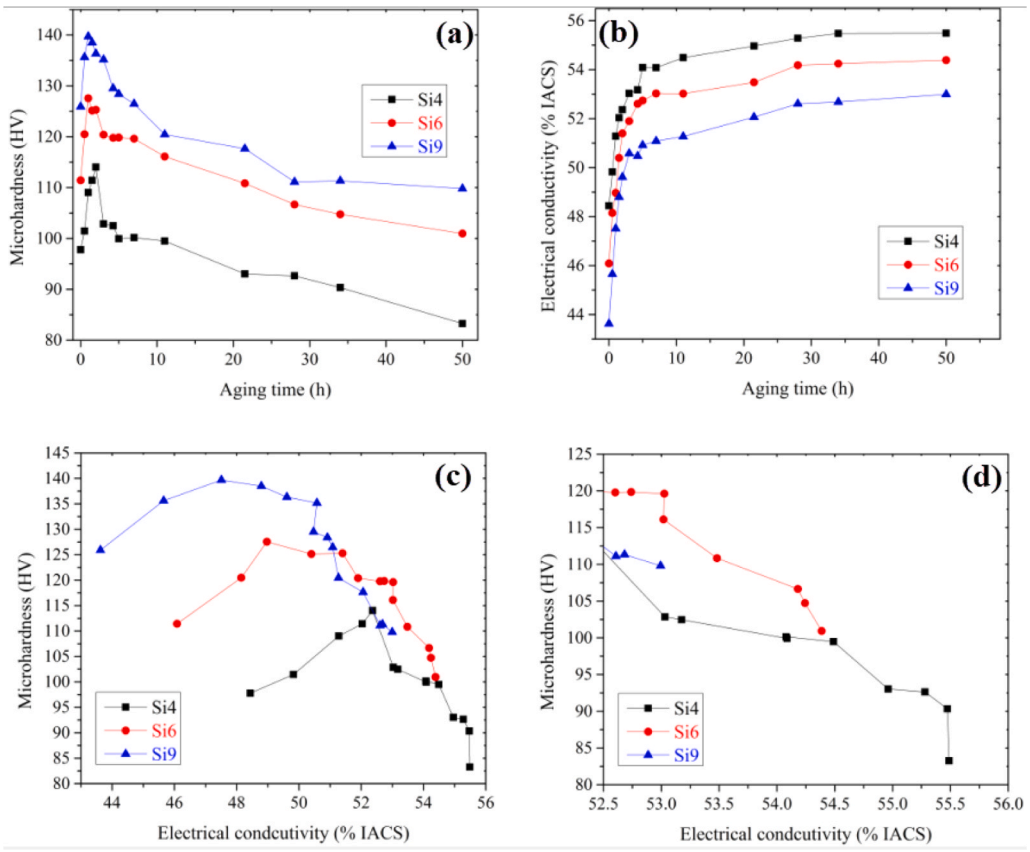

Fig. 19. a) Hardness, and b) EC as a function of time at 180 ° C. c) Hardness versus EC, and d) hardness versus EC in values above 52.5 %IACS [78].

facilitated the process of microstructural recovery post-extrusion, leading to notable alterations in grain size within the alloy matrix. Figs. 30a and 30b delineate the correlation between grain size and the addition of copper and magnesium, exhibiting a marked reduction in grain size with the addition of copper and marginal changes with the inclusion of magnesium. This difference is attributed to the distinct diffusion behaviors of copper and magnesium. Figs. 30c and 30d illustrate the impact of varying amounts of magnesium and copper on EC. It is discernible from these figures that the introduction of magnesium and copper culminates in a diminished EC of the alloy. This diminution in conductivity is predominantly ascribed to the augmented scattering of free electrons, induced by the presence of these solute atoms within the aluminum lattice. Figs. 31a through 31c present the outcomes of UTS evaluations. The data indicates that the incorporation of magnesium and copper substantially bolsters the UTS of the alloys. The enhancement in TS can be primarily attributed to a confluence of mechanisms: solid solution strengthening, microstructural refinement, and the interactions between solute atoms and the aluminum matrix. This research didn't assess long-term thermal stability or aging effects on the developed microstructures and properties.

Chen et al. [89] embarked on a comprehensive study aimed at developing aluminum alloys, specifically of the Al-Fe-(Cu) system, tailored for use in aluminum wires, with a particular focus on their annealing behavior and its consequent effects on mechanical and electrical properties. The study scrutinized two distinct alloy compositions: Al-0.8Fe-0.3Cu (designated as Alloy #1) and Al-0.8Fe-0.1Zr (designated as Alloy #2). These alloys were subjected to a series of annealing experiments at incrementally varied temperatures of 275°C, 300°C, 325°C, 350°C, and 375°C, across different durations extending up to a maximum of 8 h. Microstructural analysis of the extruded alloys #1 and #2 revealed that the morphology of precipitates varied with the number of alloying elements, and that secondary phase distributions were aligned along the extrusion direction. Notably, alloy #1 exhibited a higher prevalence of coarse secondary phase particles compared to alloy #2. The impact of the annealing process on the EC and hardness of Alloy #1 and Alloy #2 is depicted in Figs. 32c and 32d. The findings indicate that EC improves with increasing annealing temperature, reaching its peak at six hours before subsequently declining. The study demonstrated that the addition of 0.1Zr had a more detrimental impact on EC than 0.3Cu. As illustrated in Figs. 32c and 32d, prolonged annealing leads to a decrease in hardness, which eventually stabilizes. The rate of hardness reduction varied across different annealing temperatures. Throughout the annealing process, sample #1 consistently exhibited higher hardness than sample #2, attributable to the greater strengthening effect of 0.3Cu compared to 0.1Zr.

Hou et al. [35], explored the interplay between MS and the anomalous behavior of EC in an Al-1.13 %wt Fe alloy, following eight passes through a drawing process that produced a final diameter of 3.15 mm. The relationship between strength and EC as a function of cross-sectional area is depicted in Fig. 33. The study revealed that as the cross-sectional area diminished, the UTS rose, while EC declined. Notably, upon exceeding a 61.9 % area reduction, both EC and MS experienced concurrent enhancement. For the Al-Fe alloy, the highest levels of electrical strength and conductivity were attained with an area reduction surpassing 86.3 %. The comprehensive results, which include UTS, YS, elongation percentage, and EC at varying degrees of area reduction, are summarized in Table 7. The data indicate that both strength and EC are heavily influenced by microstructural changes that occur during area reduction. These changes contribute to the strengthening mechanisms and impact EC. The primary cause for the observed variations in EC is linked to modifications in the morphology and dimensions of the grains within the alloy matrix. Notably, when the cross-sectional area is reduced by over 61.9 %, there is a pronounced elongation of the grains, which correlates with an enhancement in EC

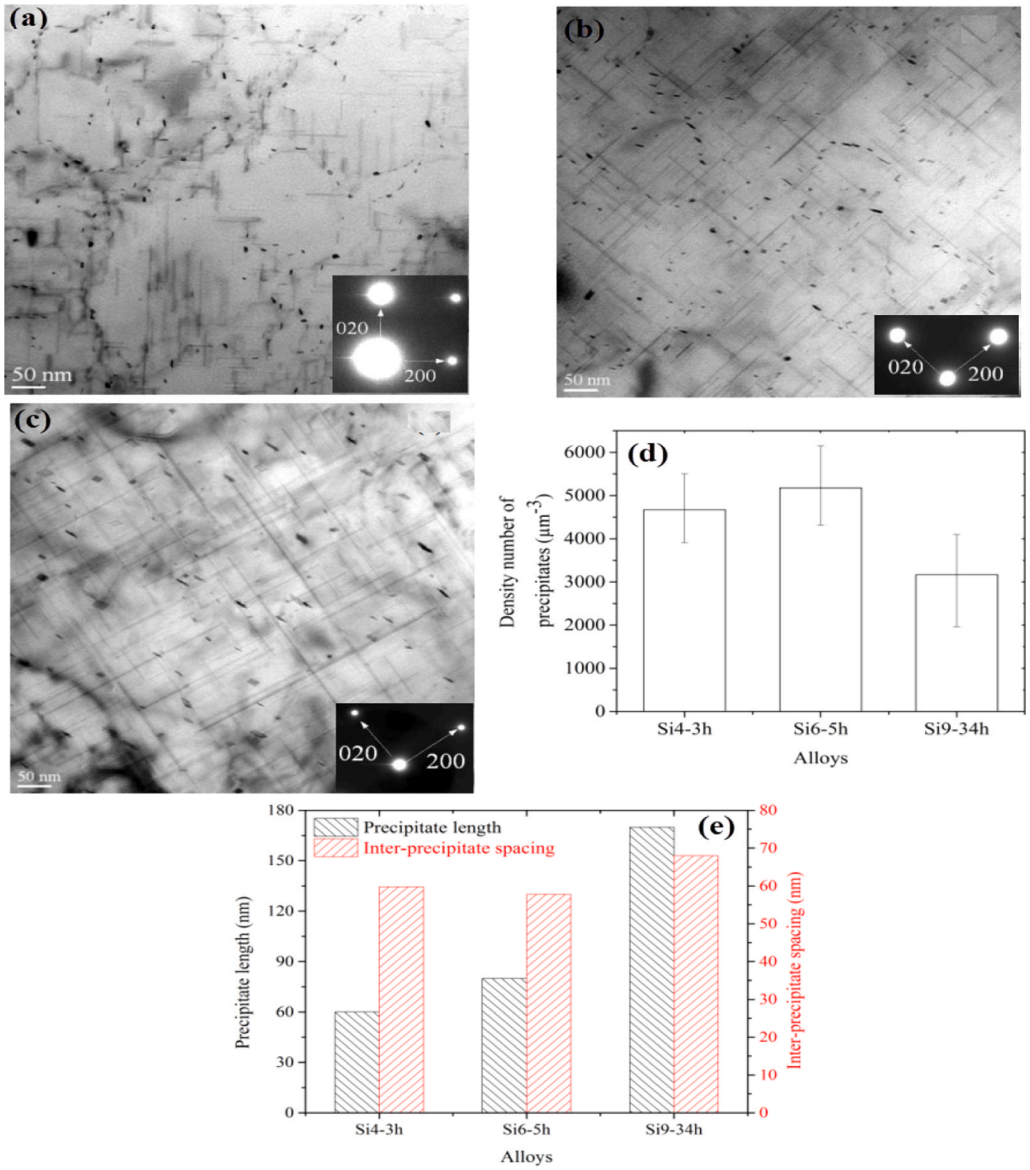

Fig. 20. a) Transmission electron microscopy images of precipitate distribution for Si4 sample after 3 h, b) Si6 sample after 5 h, c) Si9 sample after 34 h at 180 ° C, d) density number of precipitates in all three samples, and e) precipitate lengths and intra-precipitate spacing for all three samples [78].

within this specific range. On the other hand, for area reductions below 61.9 %, the elongation of the grains occurs at a more gradual pace, while there is a concurrent reduction in grain width. This leads to a decline in EC. In this work focused primarily on tensile strength and conductivity, omitting other important properties like fatigue resistance or thermal stability that are critical for practical applications. Also, all processing was conducted at RT, leaving unknown how elevated temperature deformation might affect the observed phenomena.

Zhao et al. [90] systematically investigated the effects of ECAP under different thermal conditions on the MS and EC of an Al-Mg-Si alloy. The study compared three processing routes: RT, elevated temperature (200°C), and a TST involving one initial pass at 200°C followed by seven passes at RT. Samples processed entirely at 200°C exhibited larger grain sizes due to dynamic recovery and excessive decomposition of the solid solution, which reduced solute pinning at grain boundaries and allowed grain coarsening. This led to decreased strength compared to RT-processed samples, where strain hardening dominated. However, the TST approach achieved the highest MS, as the combination of high-temperature initiation and subsequent RT deformation promoted nano-precipitation that effectively locked dislocations, surpassing the strengthening effects of solid solution alone. Additionally, EC improvements were linked to the reduction of solute atoms in the matrix due to precipitate formation, which minimized electron scattering. The study demonstrated that TST optimizes both strength and conductivity by balancing grain refinement, precipitation, and solute distribution, making it a superior processing strategy for this alloy system.

In an independent study, Han et al. [76] explored how varying the Mg/Si ratio impacts the microstructure and the interrelation between hardness and EC in Al-Mg-Si ultra-fine grain alloys. The research focused on four samples with distinct Mg/Si ratios: Sample #1 (Mg/Si = 0.75), Sample #2 (Mg/Si = 1.10), Sample #3 (Mg/Si = 1.48), and Sample #4 (Mg/Si = 1.94). Grain Size Consistency: The grain size in the alloys remained unaffected by changes in the Mg/Si ratio and thermal treatments. Dislocation Density Dependency: Dislocation density did not vary with changes in the Mg/Si ratio. However, it showed significant sensitivity to HT, with a 40 % reduction observed when treated at 170 °C for 4 h. Precipitate Dynamics: The size of precipitates formed was constant regardless of the Mg/Si ratio, but their density was dependent on the ratio. The highest density of β″ precipitates was noted at an Mg/Si ratio of 1.48. Mechanical and Electrical Properties: Increased levels of

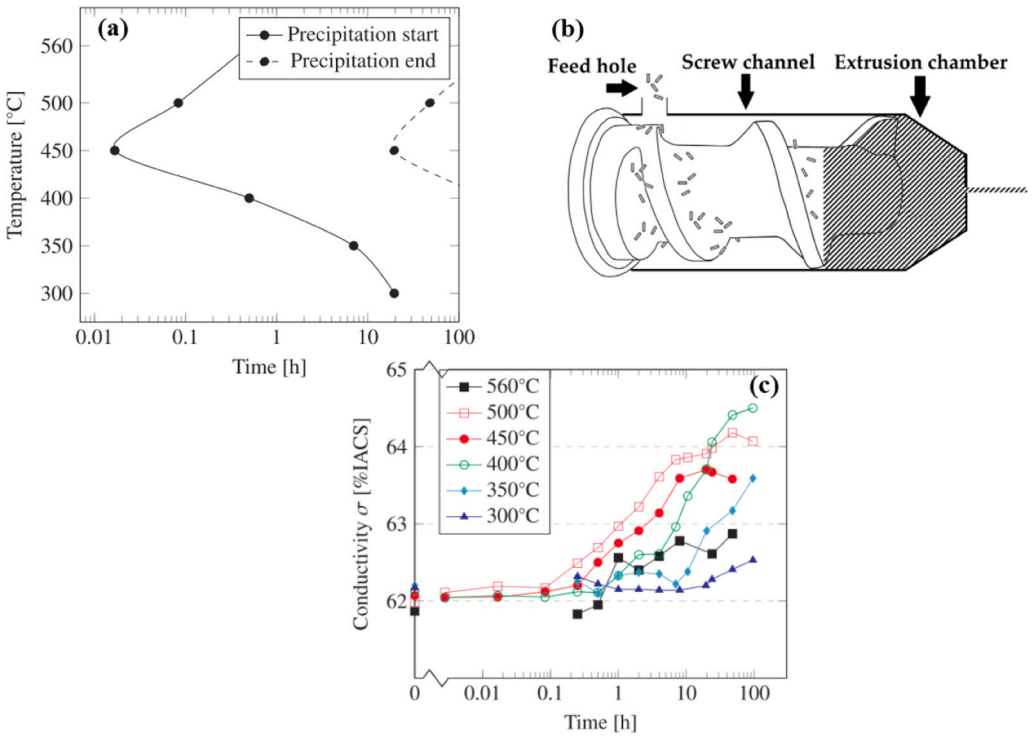

Fig. 21. a) TTT diagram for iron-rich particles of 1370 alloy after solid solution HT and aging, b) schematic of torsional extrusion method, and c) changes in EC versus time at different aging temperatures [79].

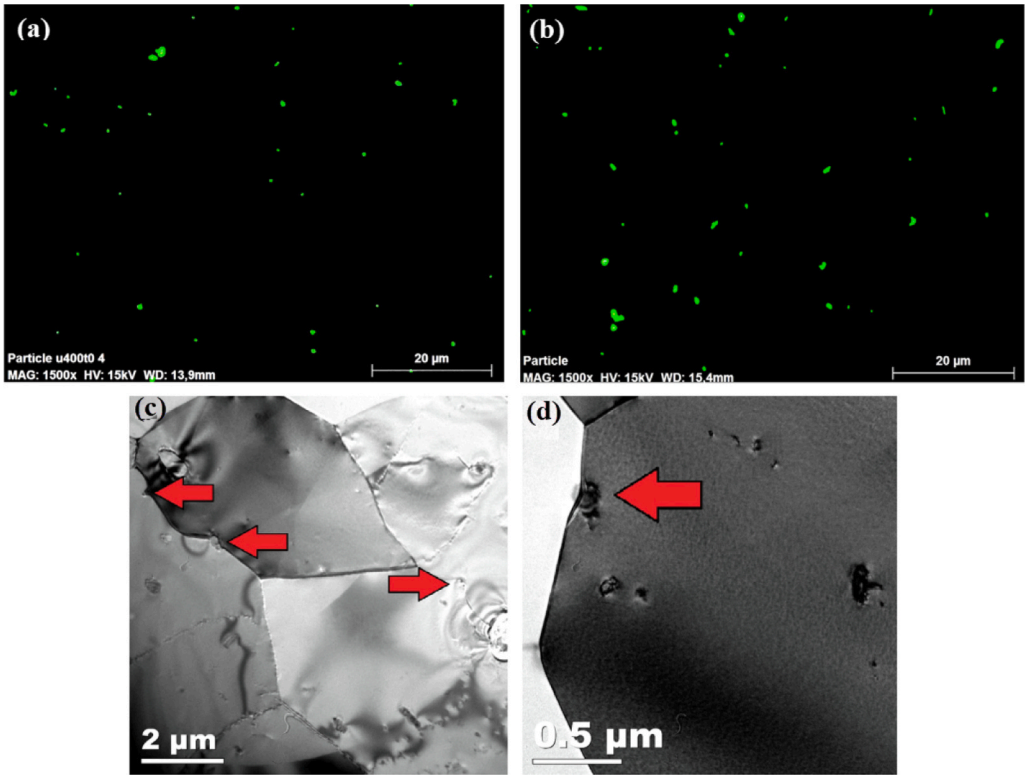

Fig. 22. Scanning electron microscopy images of iron-rich particles: a) before aging and b) after aging. Transmission electron microscopy images of microstructure after torsional extrusion process (c and d). The red arrows indicate that the grain boundaries are locked by iron-rich particles [79].

magnesium and silicon were associated with greater hardness during the CD process, while EC tended to decrease. Post heat-treatment, a noticeable decrease in hardness was observed due to a reduction in dislocation density and their eventual elimination. Strength-Conductivity Correlation: The collective analysis of the strength and conductivity changes across all four alloy samples

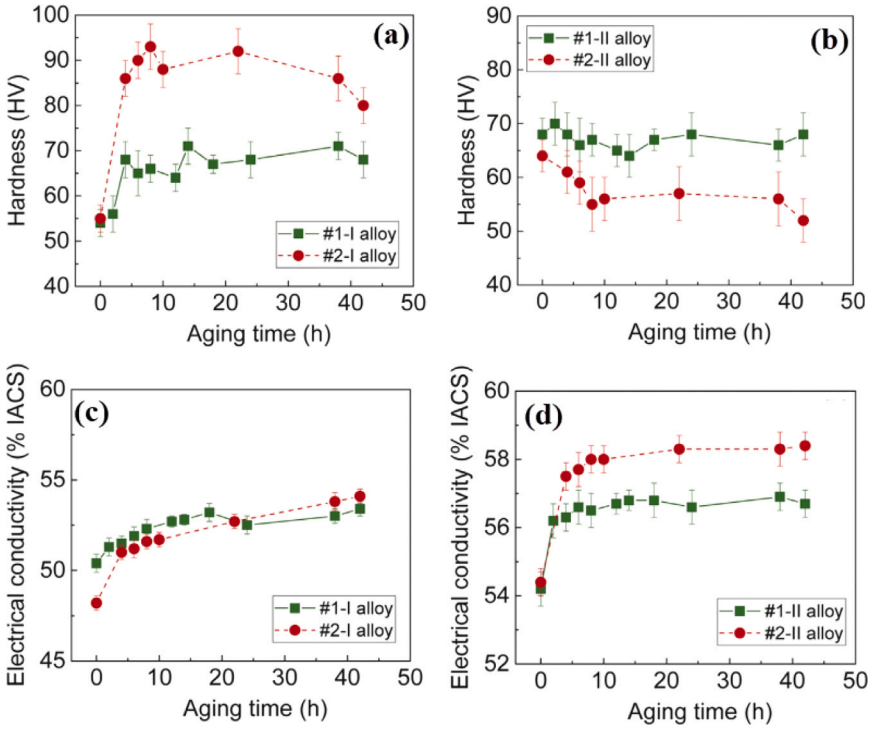

Fig. 23. Hardness changes in a) coarse grain, and b) ultra-fine grain alloys; EC changes in c) coarse grain, and d) ultra-fine grain alloys [80].

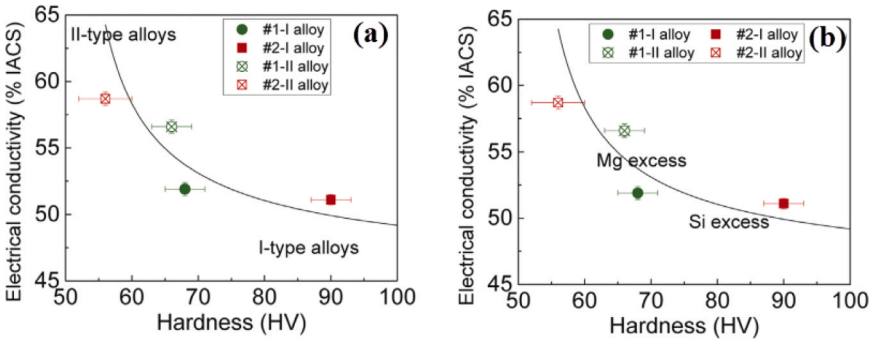

Fig. 24. Correlation between EC and hardness of Al-Mg-Si-Sc alloy relative to a) grain size, and b) Mg/Si ratio [80].

underscored the impact of hardening precipitates. Particularly, the Al-Mg-Si alloy with an Mg/Si ratio of 1.48 exhibited superior hardness along with enhanced conductivity. This study underscores the significant role of the Mg/Si ratio and HT in influencing the mechanical and electrical properties of Al-Mg-Si ultra-fine grain alloys. By optimizing these parameters, it is possible to tailor the alloy's performance for specific applications where a balance between MS and EC is crucial.

In a comprehensive investigation by Feng et al. [91], the effects of lanthanum and titanium incorporation, as well as the role of homogenization, on the electrical properties of pure aluminum were systematically analyzed. This study scrutinized these characteristics both prior to and following homogenization at 500 °C for an extended duration of 8 h. The results, highlighted in Table 8, reveal a notable inverse relationship between the strength and EC of the aluminum matrix as the concentration of the alloying elements escalates.

Specifically, within Al-La samples, variations in EC were observed to occur slowly when the lanthanum content remained under 0.3 % by weight, indicating a threshold effect related to the lanthanum concentration. However, at higher concentrations, these changes accelerated due to the precipitation of silicon, lanthanum, and iron-based compounds, as well as increased lanthanum solubility in the aluminum matrix. In Al-Ti alloys, the introduction of titanium enhanced strength at the cost of EC, likely due to titanium's effect on the solid solution. Lanthanum addition allowed for the precipitation of impurities from the α-Al solution, thereby improving EC, a capability that titanium did not demonstrate. The study also investigated Al-0.3La-xTi alloys (x = 0.1, 0.2, 0.3, 0.4). Results indicated that adding titanium to these alloys resulted in higher EC compared to Al-Ti alloys but lower than Al-La alloys, attributed to the solid solution, titanium precipitates, and increased TS. When both elements were added simultaneously, new Ti2Al20La precipitates formed, which consumed titanium from the aluminum matrix, thereby reducing its concentration and enhancing EC. The results before and after the homogenization process, presented in Table 9, showed that EC improved post-homogenization, due to an increased precipitation of atoms from the solid solution, which significantly affected EC more than precipitates. Moreover, homogenization had its greatest impact on improving EC and the least impact on microstructural changes, mainly through the reduction of casting defects such as the elimination of small and large cavities and microstructural shrinkage.

In a study conducted by Zhao [92], the optimization of Al-Fe-Si alloy compositions aimed to enhance EC and TS. The study focused on

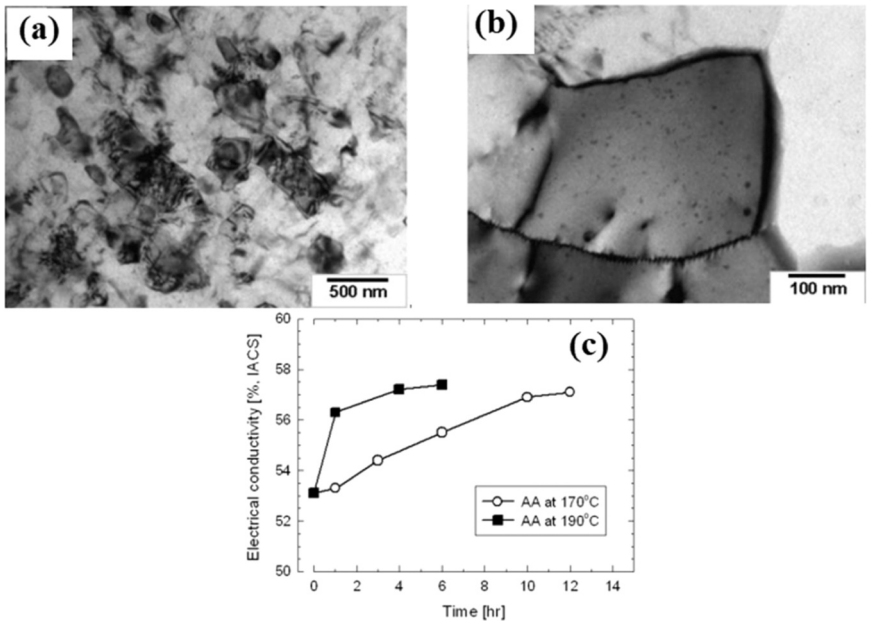

Fig. 25. a) Microstructure, and b) transmission electron microscopy image of secondary phase strengthening precipitates in 6101 alloy after ECAP-C process; c) changes in EC of 6101 alloy after ECAP-C process and HT [82].

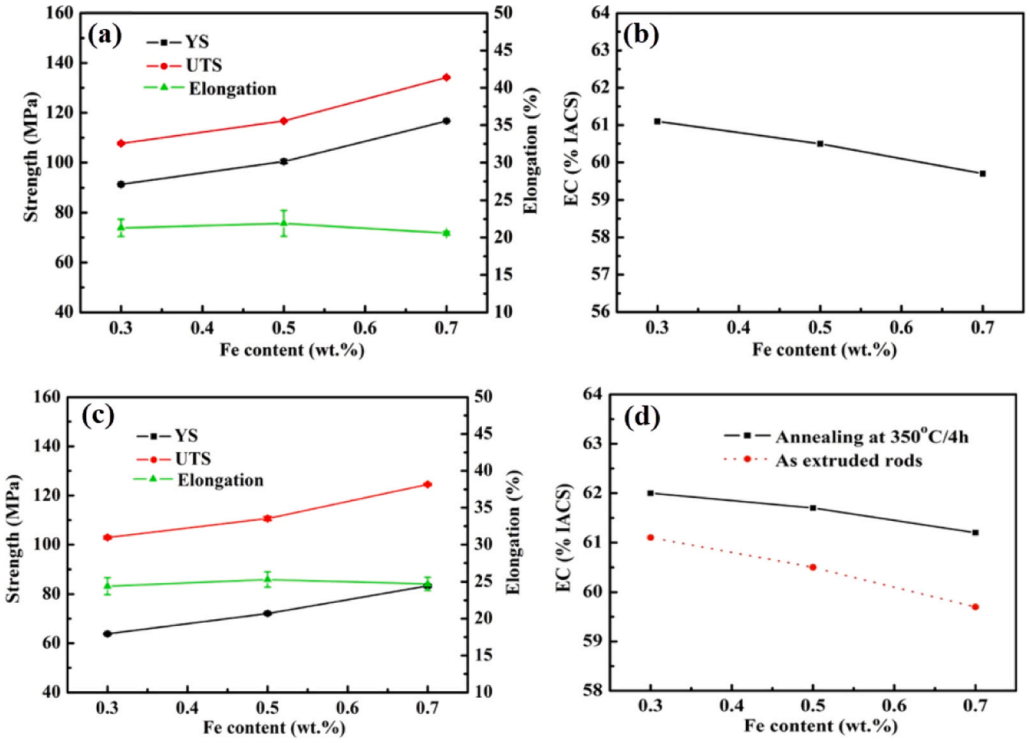

Fig. 26. Changes in a) mechanical properties, and b) EC of samples with different amounts of iron. Changes in c) mechanical, and d) electrical properties of the same samples after HT at a temperature of 360 °C and a time of 4 h [83].

Al-xFe-0.1Si and Al-xFe-0.2Si alloys, where x ranged from 0.1 to 0.5. To assess the effects of homogenization, the Al-0.5Fe-0.2Si alloy was subjected to HT at 570°C, 600°C, and 630°C for varying durations, from 1 to 96 h. The EC outcomes are shown in Fig. 34a. The data indicates that the addition of iron to both alloy samples exhibited a similar trend in EC. Specifically, adding iron up to 0.3 % by weight led to a maximum EC of 62.06 % IACS for the Al-xFe-0.1Si sample and 60.57 % IACS for the Al-xFe-0.2Si sample. Beyond these optimal concentrations, EC began to decline. Microstructural analysis revealed that with increasing iron content, secondary α-Al_8Fe_2Si phases formed at grain boundaries and in dendritic regions. When iron content exceeded 0.4 % by weight, double phases (Al_xFe) appeared, and these precipitates thickened. Adding silicon to pure aluminum led to the formation of insoluble silicon within the aluminum matrix, increasing electron scattering and thus reducing EC. However, iron addition helped purify the matrix from impurities, consequently enhancing EC. Figs. 34b and 34c depict the effects of the homogenization process on the UTS and EC of the Al-0.5Fe-0.2Si alloy. The results indicated an increase in the relative concentrations of iron

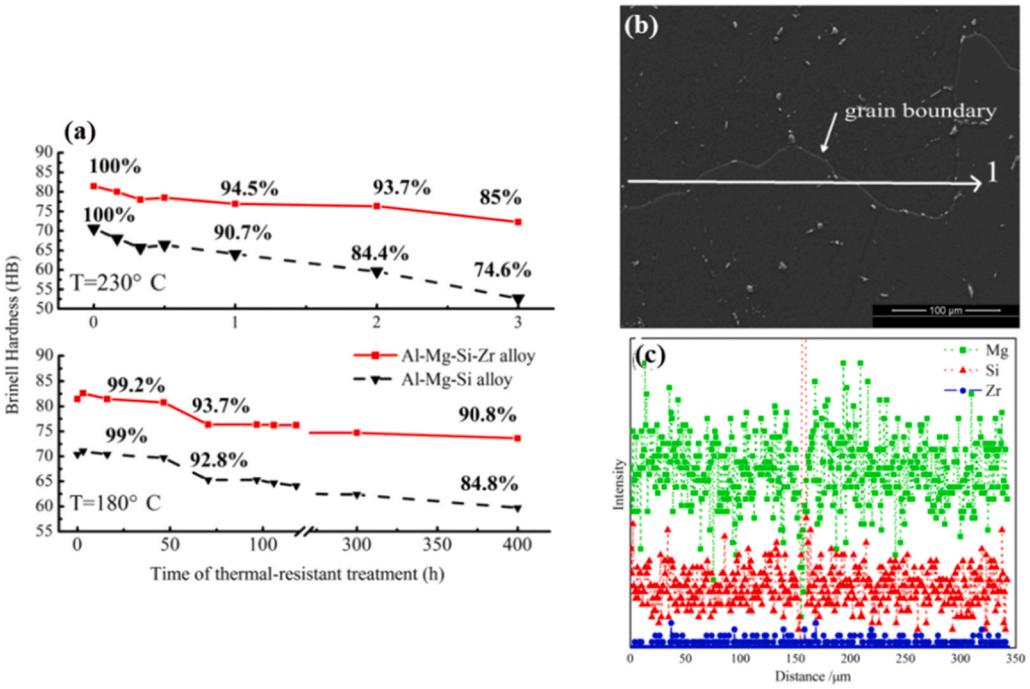

Fig. 27. a) Softening process of Al-Mg-Si and Al-Mg-Si-Zn alloys under different thermal stability operations, b) Al-Mg-Si-Zn alloy microstructure after homogenization HT, and b) and c) distribution of alloying elements in the direction of the arrow [84].

Table 5
Effect of zirconium addition on mechanical and electrical properties of Al-Mg-Si alloy [84].

Alloy	Hardness (HB)	TS (MPa)	Elongation (%)	Conductivity (% IACS)
1# (0 %Zr)	72	220	14.7	55.5
2# (0.145 % Zr)	83	265	20	54

and silicon with extended homogenization time. Additionally, Figs. 34d and 34e show that higher homogenization temperatures improved EC rapidly, although the maximum conductivity remained within a specific range. The UTS were relatively consistent across different homogenization conditions, and intermetallic particles became discontinuous. In this study While UTS was reported, other critical mechanical properties (e.g., fatigue strength, fracture toughness) weren't evaluated despite their importance for conductor applications. Also, all samples underwent conventional casting and homogenization without exploring alternative processing routes like rapid solidification or severe plastic deformation.

Wang et al. [93], investigated the impact of the CD process on the characteristics of Al-Y ultra-fine grain alloy. Their findings showed that the Al-Y cast alloy is composed of α-Al dendrites, accompanied by a eutectic interdendritic structure. The α-Al grains, which are randomly distributed and range in size from 200 to 500 μm, are notably smaller than those of pure aluminum, highlighting the refining influence of yttrium on the microstructure. Microstructural analyses identified both α-Al and β-Al_3Y phases within the Al-Y alloy. Notably, after multiple CD passes, the α-Al filaments aligned with the β-Al_3Y fine particles were observed in the drawing direction. The enhancement of MS is predominantly achieved through advanced SPD techniques, such as HPT, ECAP, CD, and ARB. However, these methods frequently lead to a deterioration in EC. In a striking departure from this conventional understanding, the findings of the current study reveal an unprecedented simultaneous improvement in both mechanical and electrical properties. Specifically, the UTS exhibited a considerable increase from 126 MPa to 232 MPa. This remarkable correlation challenges existing paradigms and invites further exploration into the underlying mechanisms at play. According to Matthiessen's relation, an increase in crystal defects, such as dislocations and voids, leads to higher electrical resistance in alloys. The study indicated that the dislocation density increased electrical resistance by approximately 2.7×10^{-11} Ωm,2.7×10^{-11} Ωm, a negligible amount that suggests dislocations play a minor role in resistance changes. Similarly, the influence of vacancies on electrical resistance was also minimal, with an increase of 2.6×10^{-11}Ωm, 2.6×10^{-11}Ωm. Furthermore, the solubility of yttrium in aluminum is about 0.16 % by weight, contributing approximately= 0.02688×10^{-8}Ωm, 0.02688×10^{-8}Ωm, to the electrical resistance. Even when considering potentially insufficient yttrium dissolution in the matrix, the resistance increase remains significantly lower than that attributed to deformation effects. Consequently, it seems that the observed strength reduction may predominantly arise from the presence of Al3Y intermetallic particles, which possess an electrical resistance of 2.155×10^{-7} Ωm, 2.155×10^{-7} Ωm. The increase in EC of the Al-Y alloy is mainly linked to the orientation of Al_3Y particles along the drawing direction. Furthermore, stacking faults also play a significant role in enhancing both the conductivity and strength of the material. Fu et al. [94] explored how adding zirconium influences the precipitation behavior and properties of Al-Mg-Si conductor alloys. The study analyzed four distinct samples: Alloy1 (0.13 % wt Zr), Alloy2 (0.18 % wt Zr), Alloy3 (0.23 % wt Zr), and a control sample without zirconium. These alloys were subjected to various HTs at 200°C for different durations—2, 4, 6, 12, 24, 36, 48, 72, and 96 h—to evaluate their mechanical and electrical characteristics. The findings indicated an increase in TS with zirconium addition, although the relationship was non-linear. It is suggested that zirconium promotes the diffusion of magnesium and silicon into the aluminum matrix, thereby modifying the precipitation behavior of Mg/Si particles. Microstructural examinations showed a reduction in grain size with higher zirconium content. Additionally, aluminum showed a propensity for dynamic recovery during the hot extrusion process. Consequently, it can be inferred that even a modest zirconium addition significantly inhibits grain boundary migration and suppresses dynamic recovery. Furthermore, both EC and MS are influenced by the

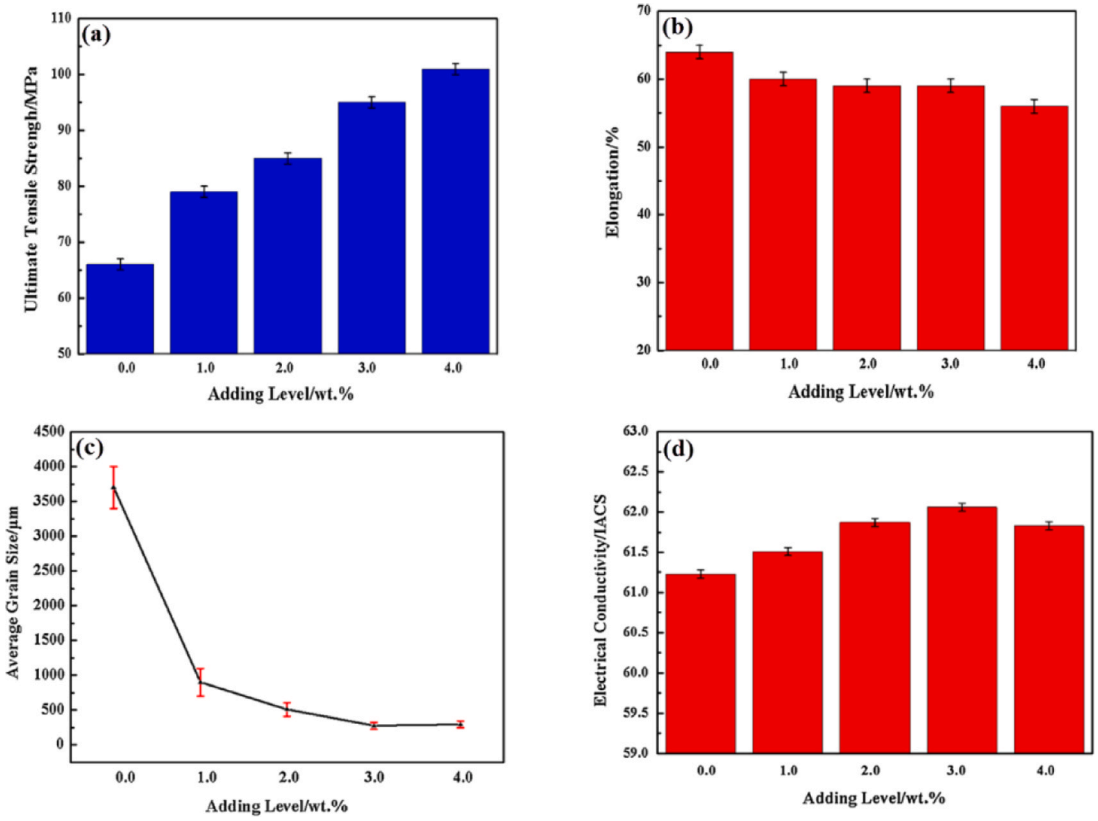

Fig. 28. a) UTS, and b) elongation percentage of 1070 alloy by adding different amounts of Al-8B-2C. Effect of Al-8B-2C addition on c) grain size and d) EC of 1070 alloy [85].

Table 6
Chemical composition of 1370 alloy and various grain refiners [86].

Material	Composition (wt%)									
	Ti	B	C	Fe	Si	V	Cu	Mg	Zn	Al
Commercial pure Al	0.003	0.008	-	0.15	0.007	0.003	0.01	0.01	0.02	99.7
Al−5Ti−1B	5.0	1.0	-	-	-	-	-	-	-	-
Al−3Ti−1B	3.0	1.0	-	-	-	-	-	-	-	-
OPTIFINE	3.0	1.0	-	-	-	-	-	-	-	-
TiBloy	1.6	1.4	-	-	-	-	-	-	-	-
Al−3Ti−0.15 C	3.0	-	0.15	-	-	-	-	-	-	-

precipitation of magnesium/silicon particles, with zirconium playing a pivotal role in this process. As zirconium content increases, the particle size of the magnesium/silicon precipitates diminishes, and zirconium either promotes or inhibits their growth. In zirconium-containing samples, the density of magnesium/silicon particles remained substantially higher than in the samples lacking zirconium. In the absence of zirconium, particle density swiftly decreased with prolonged HT, nearly vanishing after 48 h, as the β′ needle phase transformed into larger β′ and β phases. In contrast, the samples containing zirconium retained a high concentration of magnesium and silicon precipitates even after 96 h. This suggests that zirconium effectively slows the diffusion of these elements Fig. 35.

Hou et al. [95] studied the impact of annealing on the microstructural evolution and the associated decrease in strength of pure aluminum conductors. The cold-drawn specimens underwent annealing at temperatures of 90, 150, 200, 250, and 300 °C. Figs. 36a and 36b depict the correlation between UTS and YS in relation to annealing duration at various temperatures. The results demonstrated a general trend of diminishing mechanical properties as the annealing temperature increased. This decline in mechanical performance is undeniably linked to the microstructural alterations and the strengthening mechanisms that transpire during the annealing process. Texture analysis revealed that the samples exhibited a combination of $< 001 >$ and $< 111 >$ orientations following the CD process. Hence, the strength properties of the samples are intimately linked to the volume fraction of these textures and the directional strength. The calculated mechanical properties related to the sub grains and textures are presented in Fig. 36c, indicating that the reduction in strength with increasing temperature is attributable to a decrease in the sub grain strengthening parameters. In essence, for the sub grains produced during CD, boundaries aligned with the tensile axis play a critical role in enhancing strength. Consequently, an increase in the sub grain width (as shown in Fig. 37b) due to CD and subsequent annealing contributes to a reduction in the sub grain strengthening parameter. Furthermore, texture analysis showed a reduced $< 111 >$ volume fraction in the annealed specimens compared to the unannealed ones (Fig. 37a). This suggests a shift in texture from $< 111 >$ to $< 001 >$. In this study the maximum annealing duration wasn't specified, potentially overlooking long-term stability effects that are crucial for practical applications. Also, the research focused primarily on mechanical properties without correlating

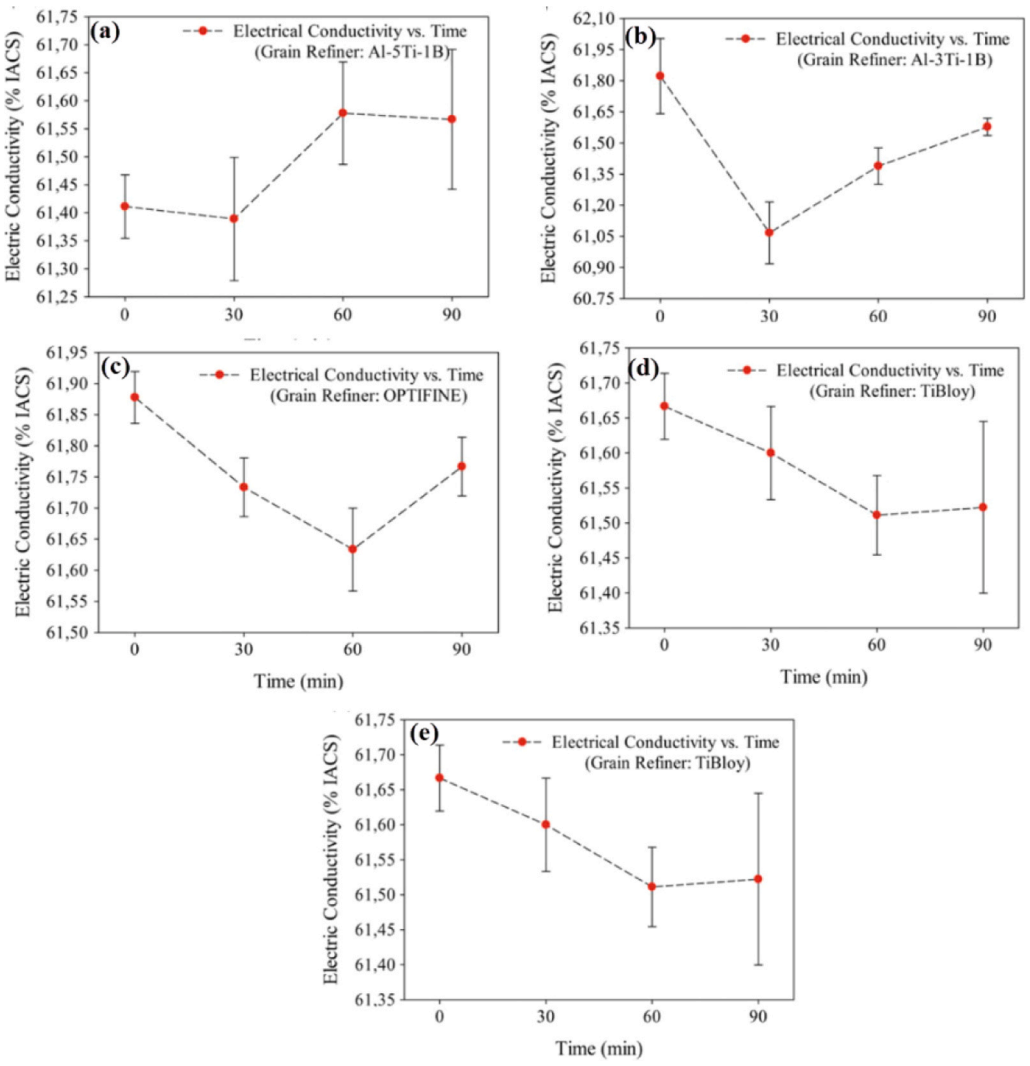

Fig. 29. Effect of different additives on the EC of the 1370 alloy at different times after the addition of a) Al-5Ti-1B, b) Al-3Ti-1B, c) OPTIFINE, d) TIBloy, and (e)Al −3Ti-0.15 C [86].

microstructural changes with electrical conductivity variations, which is critical for conductor applications.

In a study by Wang et al. [96], the microstructural changes and texture of a 1070 cold-rolled aluminum alloy subjected to various annealing processes were examined. The 1070 aluminum underwent a cold rolling process following homogenization at 500 °C for one hour, achieving an 85 % reduction after 12 passes. The samples were then annealed at 200 °C for differing durations of 30, 60, 120, and 240 min, designated as AT30, AT60, AT120, and AT240, respectively. The results demonstrated that after homogenization, the rolling characteristics were preserved, maintaining an initial grain size of around 66 μm. Annealing led to the elongation of grains along the rolling direction, as well as observable recovery and recrystallization processes. During the first 30–60 min, the cold-rolled samples softened primarily through recovery mechanisms, while recrystallization was the dominant softening process at extended durations. Additionally, grain growth was observed at annealing times exceeding 240 min. Remarkably, with extended annealing time, the grain size grew from 10.01 μm to 13.95 μm, then slightly reduced to 12.89 μm. Fig. 38 depict to the changes in EC and hardness of the specimens subjected to different annealing conditions. From this figure, it is evident that the highest EC was observed post-homogenization (61.4 % IACS), while conductivity dropped below this level during the cold rolling process. The measured hardness exhibited a significant increase following the cold rolling due to work hardening effects but decreased with prolonged annealing time.

Li et al. [97], examined the improvement in strength and EC of an Al-0.3Ce alloy by co-adding Ti (C, N) nanoparticles. These nanoparticles, characterized by an approximate grain size of 50 nm, were incorporated into the Al-0.3Ce alloy via an ultrasonic method at a temperature of 720 °C for 15 min. Microstructural analyses revealed that as the volume fraction of nanoparticles increased from 0.5 % to 2 %, the size of the nanoparticles diminished significantly; specifically, at a 1.5 % volume fraction of Ti (C, N) nanoparticles, the particle size reduced from 960 μm to 132 μm. Following the ultrasonic addition of these nanoparticles, the aluminum microstructure transitioned from coarse columnar grains to coaxial grains. The cavitation effect during ultrasonic processing helped reduce the aluminum grain size in the melt. Notably, the introduction of Ti (C, N) nanoparticles improved the MS but led to a decrease in EC, likely due to the GR induced by the nanoparticles. Table 10 provides a summary of the Al-0.3Ce alloy properties after nanoparticle addition. As observed, there was a concomitant reduction in grain size and EC alongside improvements in MS and elongation percentage following nanoparticle incorporation. Moreover, HT at 570 °C for 4 h increased the EC from 62.2 % IACS to 64.0 % IACS. This improvement is attributed to the precipitation of cerium with iron and silicon, which facilitates the removal of cerium from the aluminum matrix.

In their study, Liao et al. [98] examined the impact of cerium

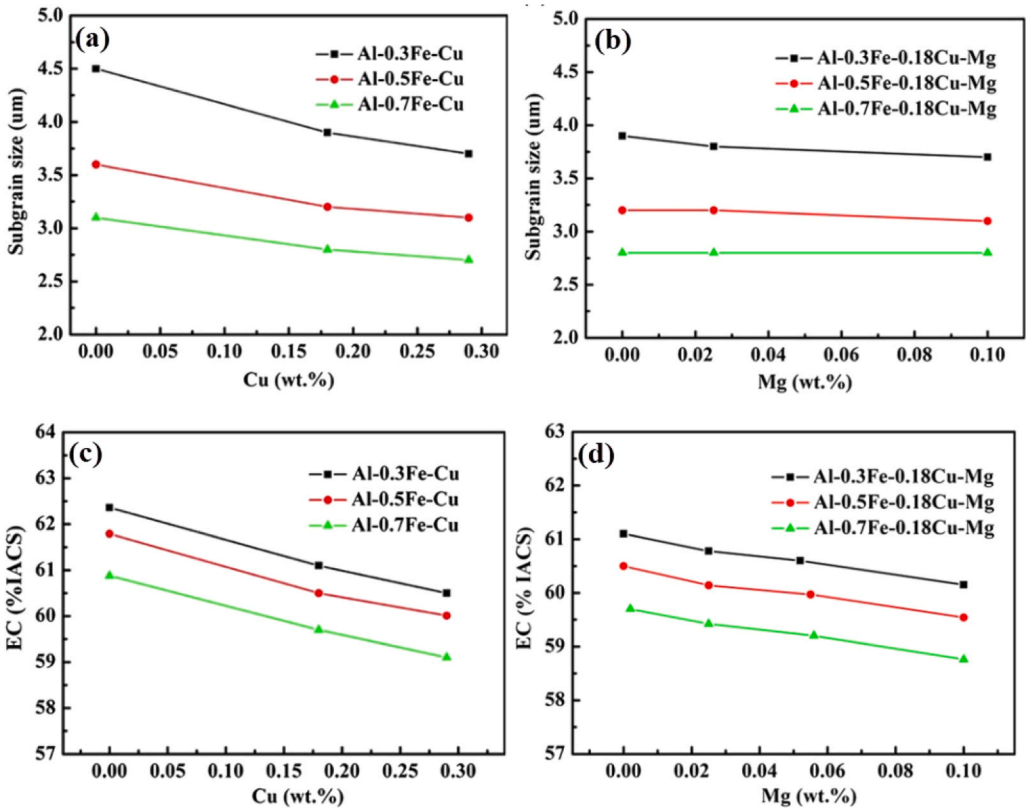

Fig. 30. Grain size changes and EC of different samples by (a and c) adding copper element and (b and d) adding magnesium element [88].

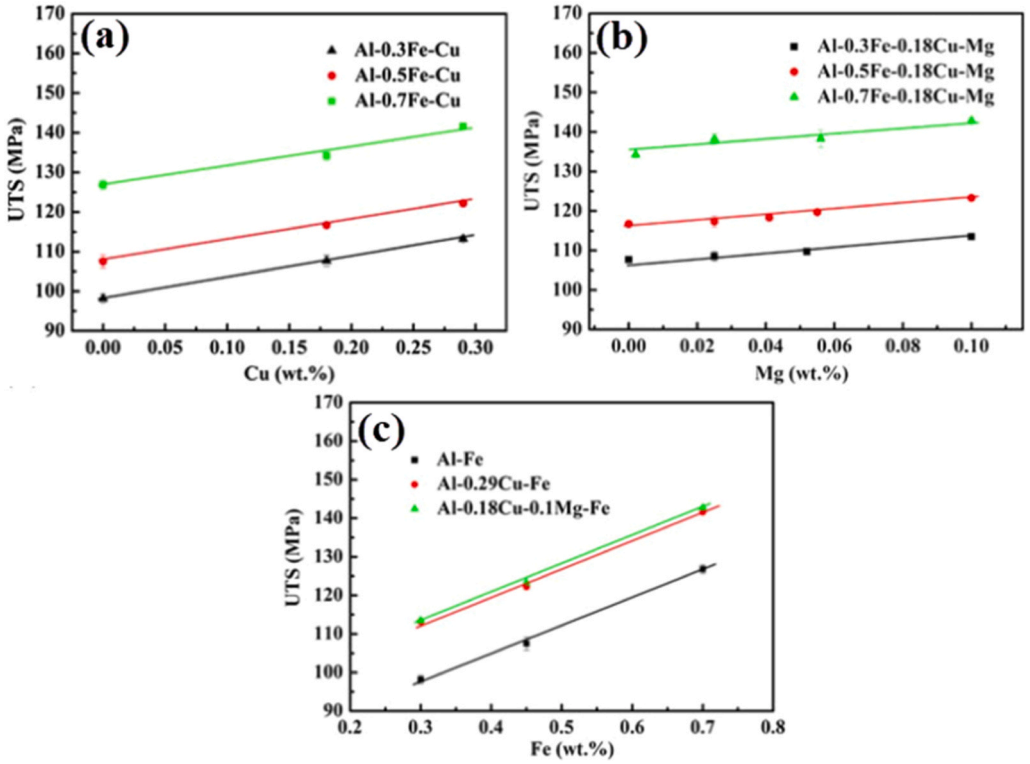

Fig. 31. Effect of adding copper, magnesium and iron elements on the UTS of samples (a, b and c) [88].

addition on the properties of Al-0.3Si-0.2Mg alloy. Four distinct alloy samples were prepared: Alloy 1 (without cerium), Alloy 2 (0.1 % by weight of cerium), Alloy 3 (0.2 % by weight of cerium), and Alloy 4 (0.3 % by weight of cerium). As depicted in Fig. 39, which illustrates the microstructure of the different alloys, the quantity of secondary phase particles-specifically those rich in iron and silicon-increased with the

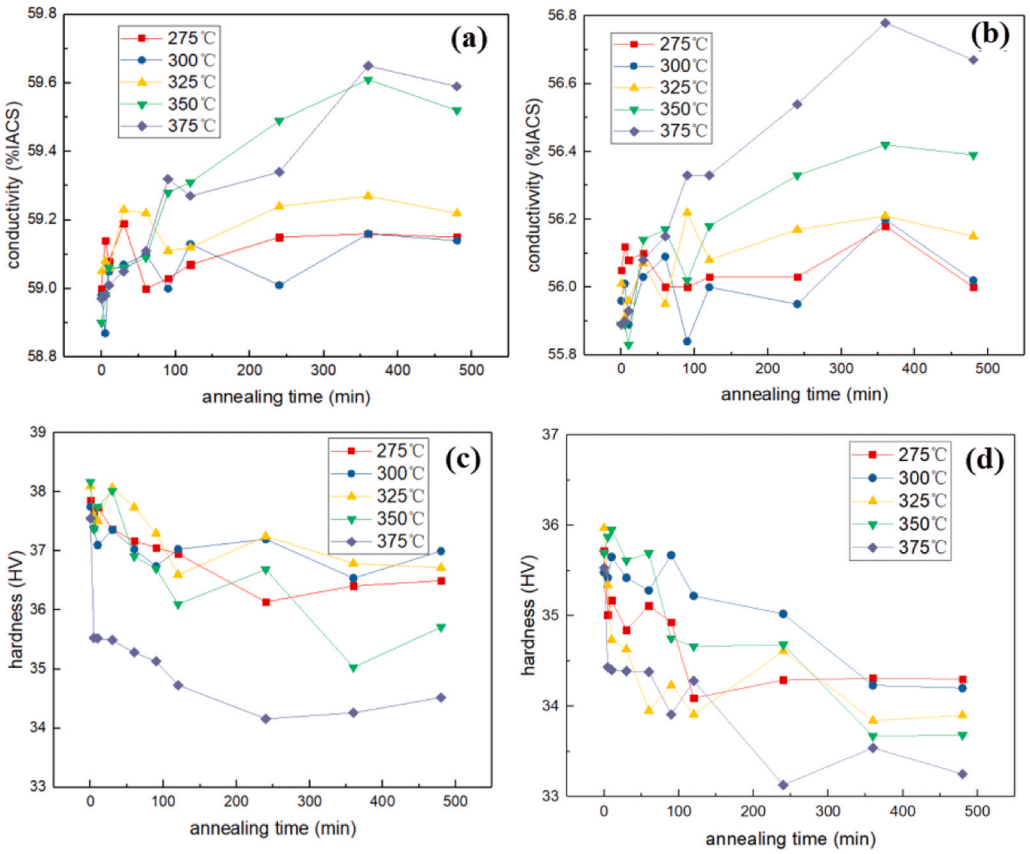

Fig. 32. Changes in EC with annealing time for samples a) 1# and b) 2#; hardness changes with annealing time of samples c) 1# and (d) 2# [89].

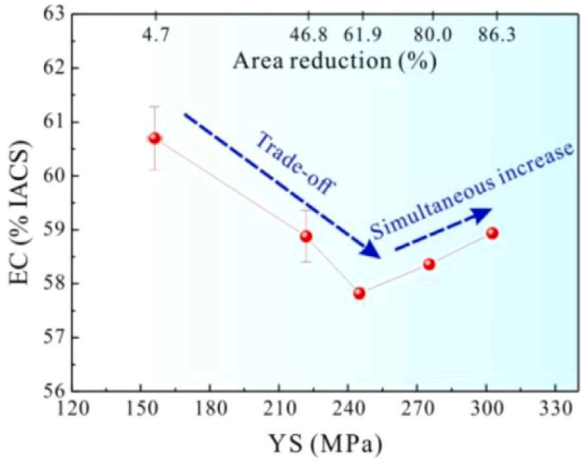

Fig. 33. Relationship between strength - EC of Al-Fe alloy at different area reduction percentage [35].

addition of cerium. Since soluble iron and silicon particles in the aluminum matrix negatively impact the EC of the alloys, the inclusion of cerium was found to reduce the presence of these elements, thereby enhancing conductivity. The effects of cerium addition on hardness, YS, TS, and elongation of the investigated samples are displayed in Figs. 40a-40c. The findings reveal that the inclusion of cerium significantly increased the hardness in both the cast specimens and those treated under T7 heat conditions. The observed reduction in grain size attributed to cerium addition was identified as a contributing factor to the improvement in mechanical properties. Furthermore, Fig. 40d highlights the findings concerning the EC of the samples under varying

Table 7
YS, UTS, elongation percentage and EC of Al-Fe wires at different area reduction percentages [35].

Area reduction (%)	YS (MPa)	UTS (MPa)	Elongation (%)	EC (%IACS)
4.7	156.1 ± 3.4	161.7 ± 0.9	9.1 ± 1.0	60.70 ± 0.58
46.8	221.8 ± 0.4	228.3 ± 0.7	5.3 ± 0.3	58.88 ± 0.48
61.9	245.1 ± 0.5	249.5 ± 0.5	5.1 ± 0.1	57.82 ± 0.10
80.0	275.3 ± 0.8	278.0 ± 0.4	3.6 ± 0.1	58.36 ± 0.08
86.3	302.7 ± 0.6	306.8 ± 0.7	3.1 ± 0.2	58.94 ± 0.07

Table 8
The EC and mechanical properties of Al-La, Al-Ti, and Al-La-Ti samples with varying percentages of lanthanum and titanium [91].

Material		TS/MPa	YS/MPa	Elongation/%	IACS/%
Al-La	Al−0.075La	63	61	30.44	60.35
	Al−0.15La	64.5	57	34.83	60.69
	Al−0.30La	66	61.3	24.33	60.35
	Al−0.45La	73.3	67	35.11	57.24
Al-Ti	Al−0.06Ti	23	9	45.33	55.17
	Al−0.1Ti	76	40	51.00	53.8
	Al−0.2Ti	77.7	67.3	38.33	51.21
	Al−0.4Ti	79	79	41.67	50.17
Al-La-Ti	Al−0.3La−0.1Ti	74.7	38	34.3	56.72
	Al−0.3La−0.2Ti	76	32	31.43	56.03
	Al−0.3La−0.3Ti	78	38	31.43	54.83
	Al−0.3La−0.4Ti	80	39	35.85	52.76

Table 9
EC of samples before and after homogenization operation at 500 °C for 8 h [91].

Sample	IACS%	
	As-cast	Homogenized
Al−0.3La	60.35	63.28
Al−0.2Ti	51.21	55.29
Al−0.3La−0.1Ti	56.72	58.28
Al−0.3La−0.2Ti	56.03	57.29
Al−0.3La−0.3Ti	54.83	54.53
Al−0.3La−0.4Ti	52.76	53.45

conditions. The data indicate that the inclusion of cerium led to improved EC. The presence of solute elements in solid solution generates strain within the crystal lattice, negatively affecting EC; consequently, the removal of these impurities—including the deleterious effects of iron and silicon-facilitates a rise in conductivity. Additionally, the T7 condition facilitates the precipitation of Mg2Si, which additionally enhances the EC. The research exclusively used T7 heat treatment conditions, leaving unexplored how alternative aging treatments (e.g., T6 or natural aging) might affect the cerium-modified alloys. Also, didn't assess long-term thermal stability of the cerium-modified microstructures or potential aging effects on properties.

In their research, Yuna and colleagues[99] delved into the influence of homogenization temperature on the microstructure and EC of an Al-Mg-Si-Ce alloy. The alloy synthesis involved a precise amalgamation of pure aluminum ingot, Al-Si, Al-Ce, Al-B master alloys, and pure magnesium ingot. The homogenization treatments were conducted at 535°C, 560°C, and 580°C for a consistent duration of 6 h.

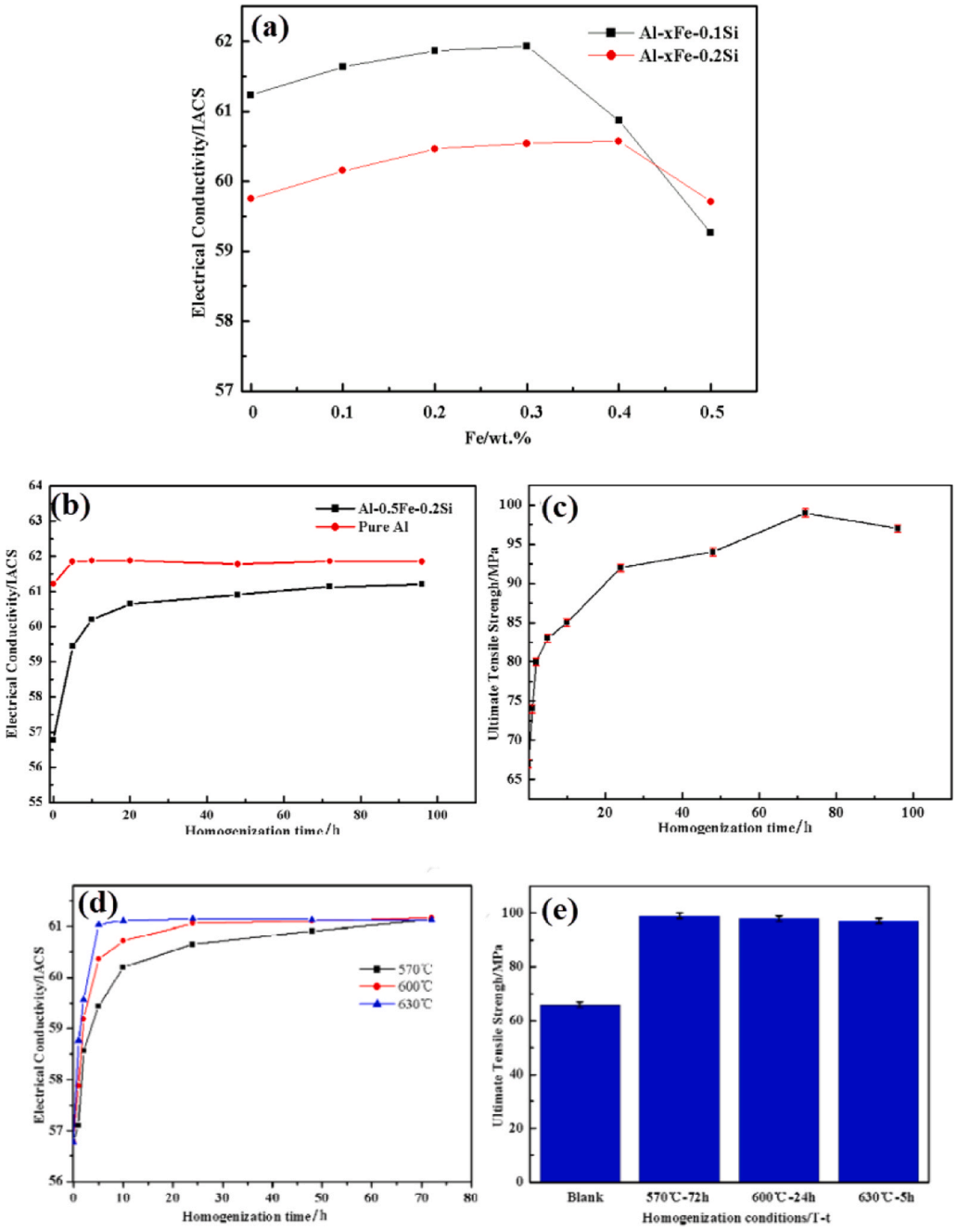

Fig. 34. a) EC of Al-Si alloy with different percentages of iron; UTS and EC of Al-0.5Fe-0.2Si alloy at different times (b and c) and different homogenization temperatures (d and e) [92].

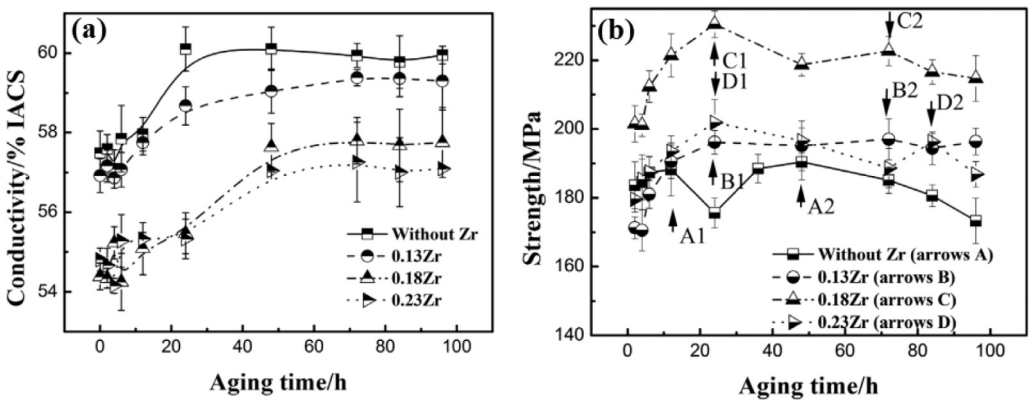

Fig. 35. Changes in the properties of Al-Mg-Si alloy with zirconium content: (a) EC, and (b) MS [94].

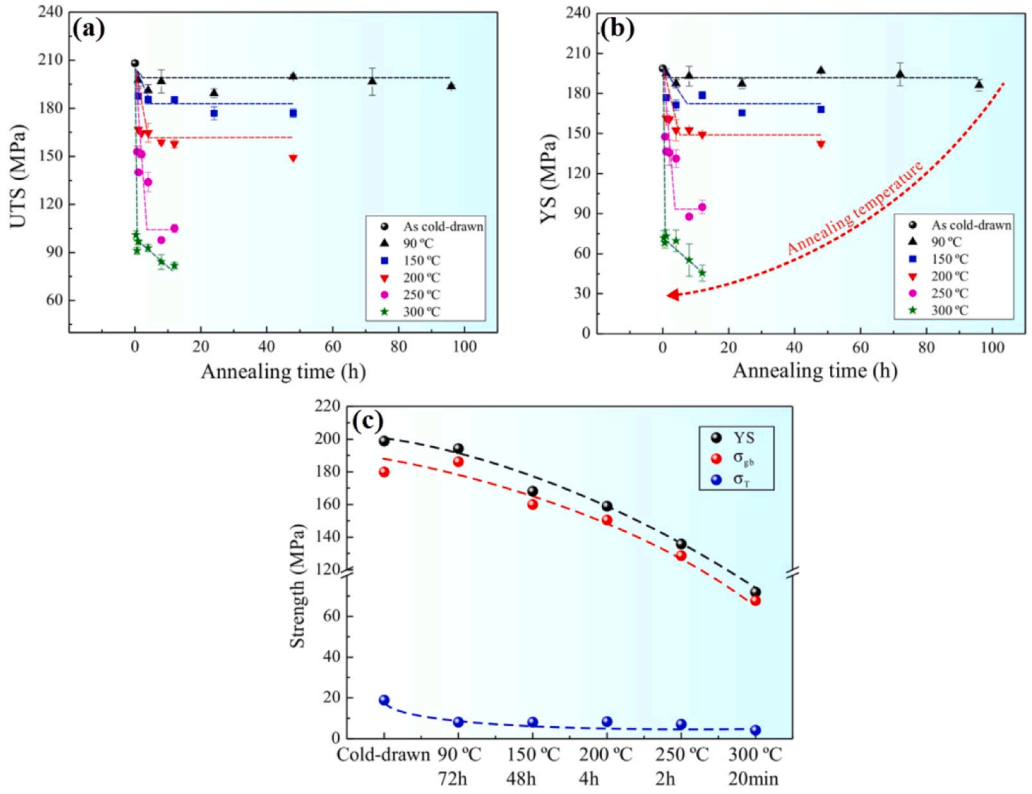

Fig. 36. Relationship between a) UTS and b) YS of different specimens with respect to different time and temperatures; c) YS and strength of subgrains and texture of cold drawn specimens before and after annealing process [95].

Microstructural: Analysis Prior to homogenization, the secondary phases in the Al-Mg-Si-Ce alloy were noted to be distributed along the grain boundaries as well as in discrete forms within the grains. The homogenization process at temperatures up to 560 °C exhibited no significant alteration to these secondary phases. Nevertheless, upon elevating the temperature to 580°C, a significant morphological transformation was observed, with specific lattice phases disintegrating into rod-like or dot-like particles. Notably, no new phases emerged during the homogenization processes, and the existing phases remained intact, indicating their substantial stability, as supported by X-ray diffraction analysis depicted in Fig. 41a. **EC:** Fig. 41b illustrates the findings related to EC. It is evident that conductivity increased with rising homogenization temperature, reaching a peak before subsequently declining at higher temperatures. As homogenization temperature escalated, there was an increase in vacancy concentration coupled with a decrease in lattice parameters. This pattern persisted until lattice strain was re-established, leading to the observed decrease in conductivity. Mechanical properties: The analyzed results are depicted in Fig. 41c. The YS and UTS showed a decreasing trend following the different homogenization treatments. This decline was attributed to the unchanged grain size and morphology of the cerium phases, which was further connected to the reduction in the lattice parameter.

In their research, Murashkin et al. [100] investigated the characteristics of an Al-Mg-Zr alloy subjected to the ECAP-Conform process followed by CD. To encourage the formation of Al_3Zr precipitates and maintain an ultra-fine grain structure at higher temperatures, an initial HT at 385°C was crucial. Analysis of the wire's microstructure after a 120-hour HT at this temperature revealed the formation of Al_3Zr particles alongside a semi-stable microstructure. After six passes through the ECAP-Conform process at RT, the researchers attained an ultra-fine grain microstructure with grain sizes between 600 and 800 nm. Notably, this intense plastic deformation process did not alter the

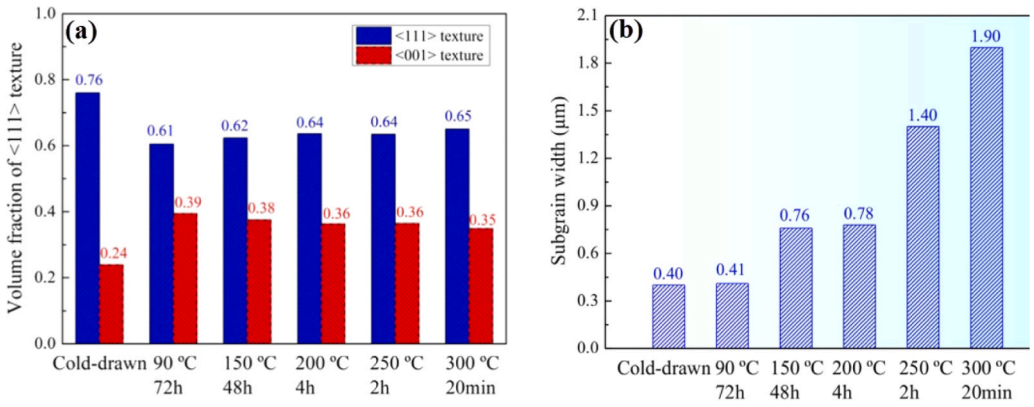

Fig. 37. a) Statistical results of volume fraction of different textures before and after annealing operation, and b) width of subgrains of cold drawn samples before and after annealing operation [95].

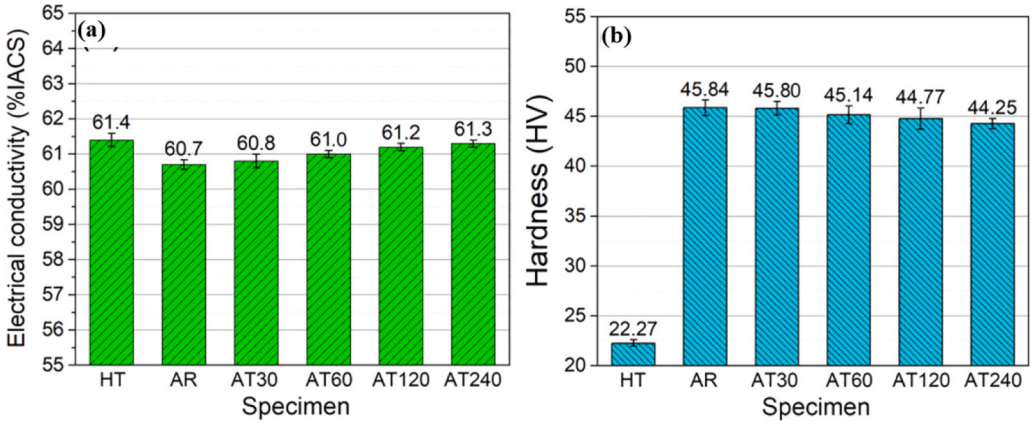

Fig. 38. Changes in a) EC, and b) hardness of samples under different conditions (HT = Homogenized and AR = As-rolled specimens) [96].

Table 10
Effect of addition of Ti (C, N) nanoparticles on grain size, mechanical properties and EC of Al-0.3Ce alloy [97].

Alloys	Grain size (μm)	σ_{UTS} (MPa)	Elongation (%)	(EC) (% IACS)
Casting refining pure Al	959	63	30	63.5
Al−0.3Ce	577	70	34	63.2
Al−0.3Ce+ 1.5 vol% Ti(C,N)	123	84	47	61.2
Al−0.3Ce + 1.5 vol% Ti(C,N) annealed at 570℃ & 4 h	-	79	47	64.0

morphology of the Al_3Zr precipitates. Assessments of strength, ductility, and EC in the samples post-ECAP-Conform and CD indicated that the ultra-fine grain structure contributed to improvements in YS and UTS. The CD phase after ECAP-Conform resulted in increased dislocation density and further GR, ultimately achieving a substantial 30 % increase in the strength of the ultra-fine grain structure. To evaluate the samples' thermal stability, a HT at 230°C for one hour was performed. Notably, the surface morphology of the ultra-fine grain particles remained largely unchanged due to the presence of Al_3Zr nanoparticles. However, this annealing operation led to a reduction in dislocation density, which resulted in an approximate 10 % decrease in UTS. Additionally, no alteration in the alloy's lattice parameter was observed following HT at 385 °C, indicating a stable concentration of magnesium and zirconium within the aluminum solid solution. Consequently, the observed rise in electrical resistance of the samples after the ECAP-C process and CD (from 30.18 nΩm and 29.93 nΩm to 29.42 nΩm) appeared related to variations in grain size. The combined ECAPC and CD process presents significant challenges for industrial scale-up due to its multi-step nature and specialized equipment requirements. Also, focused on a single Al-Mg-Zr composition, leaving unexplored how varying Mg/Zr ratios might affect property optimization. In a study conducted by Morozova et al. [101], the influence of silicon and zirconium on the microstructure and properties of Al-Fe-Si-Zr alloys was thoroughly investigated. The research primarily focused on the resulting microstructural modifications, micro-hardness, and EC attributed to the addition of these elements. Zirconium promotes the formation of Al3Zr particles, making its optimal concentration crucial for enhancing the desired properties. The study revealed that adding more than 0.3 % by weight of zirconium led to the distribution of Al_3Zr particles in dendritic regions, which negatively impacted mechanical properties. Therefore, the zirconium content should remain below this threshold to avoid deteriorating the properties, although minimal additions might not result in significant improvements Silicon, in particular, was noted for its significant effect on enhancing both hardness and EC. Moreover, without silicon, the formation of detrimental needle-shaped Al_3Fe particles after annealing were more likely. HT within the 400–450°C range facilitated the dispersion of Al_3Zr nanoparticles, thereby achieving maximum hardness and strength. A key factor affecting EC is the decomposition of the solid solution, which notably influences the electrical properties examined in this research. Fig. 42 provides an overview of the variations in hardness and EC of Al-1 % Fe-Si-Zr alloys due to the addition of zirconium and silicon. The study underscores the nuanced role of these elements in shaping the microstructural and functional attributes of the alloys. While this study provides valuable insights into the effects of silicon and zirconium, several limitations should be noted. First, the narrow

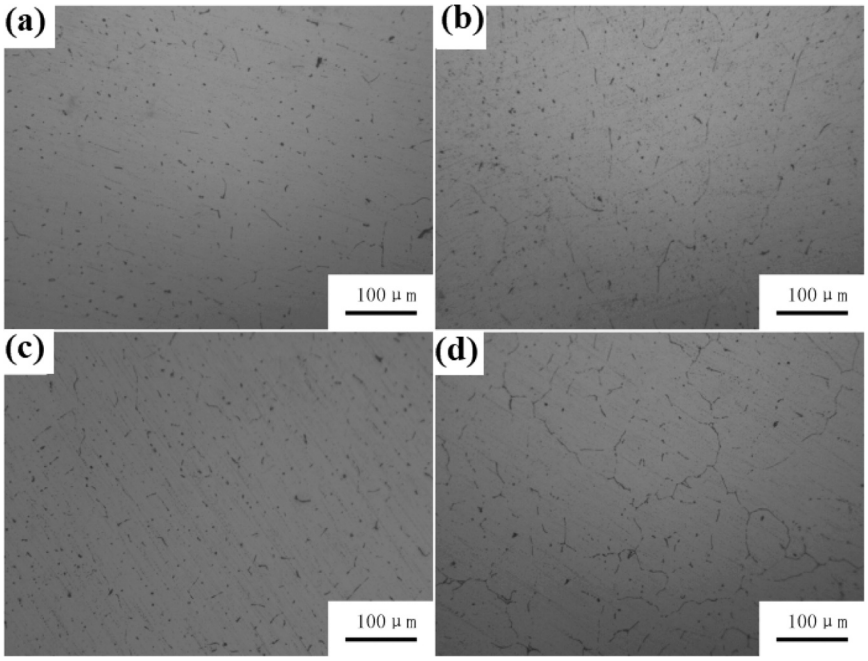

Fig. 39. Optical microscopy images of microstructure of Al-0.3Si-0.2Mg cast alloy in different amounts of the element cerium: a) 0 %, b) 0.1 %, c) 0.2 %, and d) 0.3 % [98].

compositional range investigated (zirconium up to 0.3 %) may restrict the findings to specific conditions and overlook effects at higher concentrations. Second, the research did not address industrial processing conditions such as varying cooling rates or solidification process modifications. Third, although hardness and electrical conductivity were measured, more in-depth microstructural analyses (TEM characterization of Al_3Zr particle distribution) were not performed. Finally, the study did not evaluate long-term effects such as thermal stability under operational conditions.

Kalinenko et al. [102] explored how varying the rolling temperature, along with subsequent annealing, impacts the EC and MS of an aluminum alloy. They specifically used an Al-1 % Fe-0.25 % Si-0.3 % Zr alloy, rolling it at two different temperatures: 300°C and 400°C. Post-rolling, the alloy underwent a HT process at 400°C for a duration of three hours. Transmission electron microscopy (TEM) images, depicted in Figs. 43a and 43b, illustrate the microstructure of the alloy rolled at these temperatures, which shows alignment in the rolling direction. The analysis revealed that as the rolling temperature increased, the transverse distance between subgrains also increased, while the density of dislocations decreased. This suggests that higher rolling temperatures lead to more pronounced microstructural change and dislocation density reduction. The in-depth analysis reveals the pivotal influence of rolling temperature and subsequent annealing on the optimization of both EC and MS in the aluminum alloy.

Fig. 43c displays the results of EC measurements under different conditions. It is evident that rolling at higher temperatures had a negligible effect on EC. In contrast, subsequent HT markedly changed the conductivity due to the decomposition of the solid solution. The fraction of solid solution decomposition was found to be 0.46 after rolling and increased to 0.57 following the HT. Additionally, Fig. 43c includes data on the mechanical properties of the samples. These findings indicate that rolling at different temperatures increased strength but decreased ductility. The dynamic recovery of the microstructure at higher temperatures plausibly accounts for the observed reduction in MS. Conversely, annealing at 300°C led to diminished mechanical properties as a result of decreased dislocation density. Overall, annealing contributed to the breakdown of the solid solution and the distribution of precipitates, which in turn influenced the alloy's electrical and mechanical characteristics. Guo et al. [103], conducted a study to investigate the impact of erbium addition on the microstructure and various properties of an Al-0.4Fe-0.5Si alloy. Their microstructural analysis revealed the formation of several phases including Al_3Er, Al_3Fe, Al_6Fe, ErSi, and $Al_{10}Fe_2Er$ during the alloying process. Notably, the presence of the Al_3Fe phase during solidification, due to the heterogeneous nucleation interface of the liquid phase, led to an increased nucleation rate. This rise in nucleation rate contributed to the refinement of the alloy's microstructure. The findings from this study underscored that the optimal quantity of erbium for microstructural GR is 0.3 % by weight. A critical factor impacting the EC of aluminum alloys is the presence of impurities like iron and silicon in the matrix. According to Matthiessen's law, these impurities adversely affect conductivity. The researchers in this study stated that during the solidification process, erbium plays the role of iron adsorbent in the remaining liquid phase and prevents the accumulation of iron and its conversion into coarse Al_3Fe particles. Conversely, the inclusion of erbium significantly affects silicon as well. The formation of ErSi with silicon reduces the silicon content within the aluminum solid solution. Another very important effect of adding RE elements such as erbium is the removal of impurities such as chromium, titanium and vanadium from the alloy during the melting process. As mentioned, the reactions between iron and silicon with erbium and the removal of impurities have a positive effect on improving the EC of the alloy, as the study showed a one percent increase in EC by adding the RE element erbium. HT at 260 °C for one hour increased the atomic radius of Al_3Fe phase, which resulted in a growth of 22 MPa in the UTS. The optimal balance of mechanical and electrical properties was achieved with 80 % cold deformation followed by HT at 260°C for one hour. Medvedev et al. [104] conducted a study to enhance the mechanical and electrical properties of aluminum alloys incorporating RE elements by optimizing their concentration and employing thermomechanical treatments. Aluminum alloys containing RE elements (Al-RE) are recognized as ideal materials for manufacturing HTLS conductors due to the near-zero solubility of RE elements in the aluminum matrix, which minimally impacts EC. The study examined three alloy samples with varying concentrations of RE elements: 0.9 % lanthanum and 1.6 % cerium ("2.5"), 2.9 % lanthanum and 1.6 % cerium ("4.5"), and 3.1 % lanthanum and 5.4 % cerium ("8.5"). The

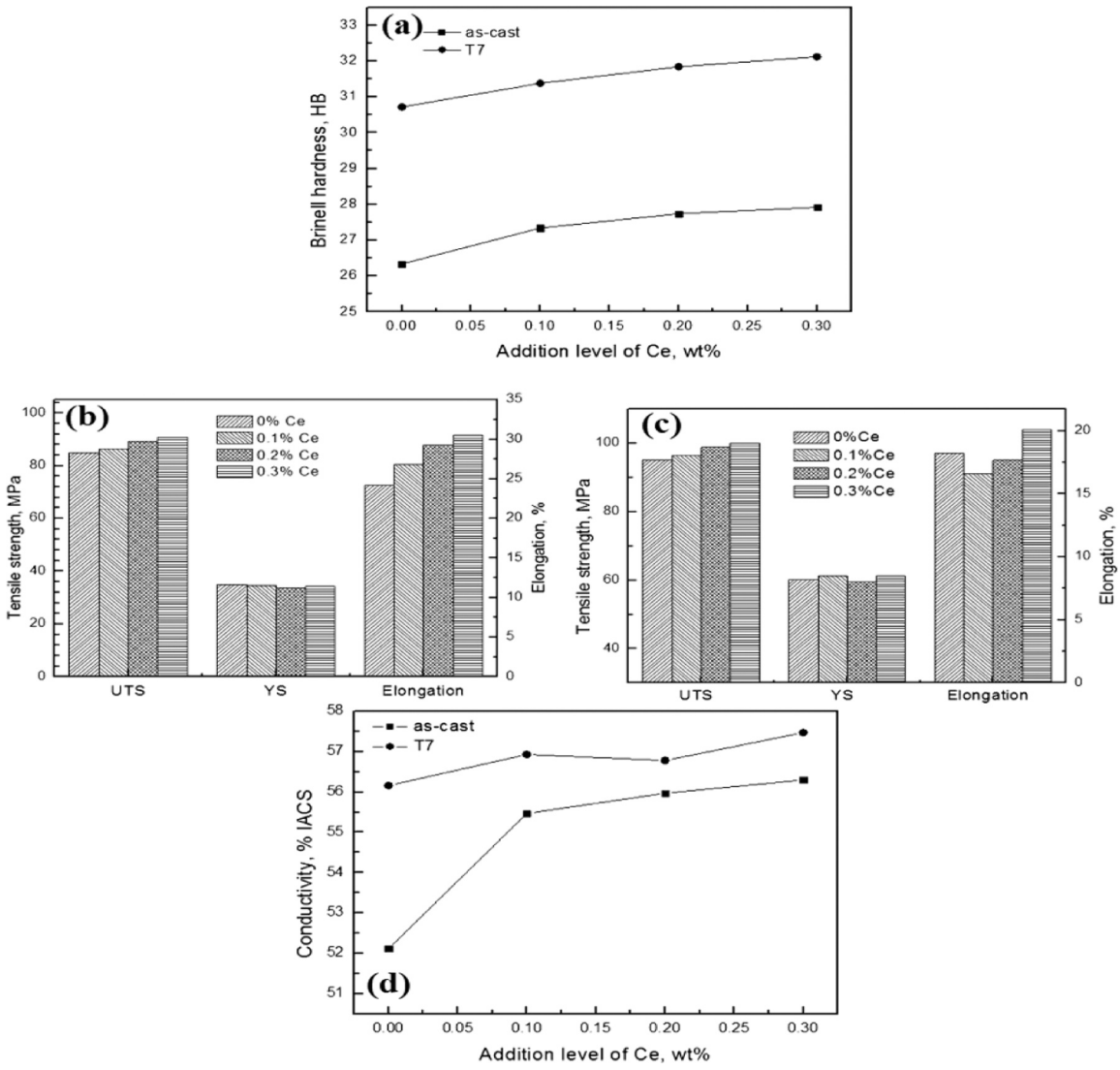

Fig. 40. a) Brinell hardness of Al-0.3Si-0.2Mg alloys with various amounts of cerium, b) tensile properties of Al-0.3Si-0.2Mg alloys with various amounts of cerium as cast, c) tensile properties of Al-0.3 alloys Si-0.2Mg with different amounts of cerium as T7 HT, and d) EC of Al-0.3Si-0.2Mg alloys with different amounts of cerium [98].

samples were treated with HPT at RT, followed by annealing at temperatures of 230°C, 280°C, and 400°C for one hour. The resulting mechanical and electrical properties, after HPT and the annealing process, are detailed in Table 11 and illustrated in Fig. 44. This research demonstrates that by optimizing the concentration of RE elements and employing suitable thermomechanical processing, the properties of aluminum alloys can be significantly enhanced. These improvements make the alloys particularly suitable for advanced applications such as HTLS conductors.

It is well established that SPD profoundly influences the microstructure and properties of an alloy. According to the findings detailed in Table 11, the HPT process at RT results in the formation of an ultra-fine grain microstructure and the precipitation of $Al_{11}(Ce, La)_3$ intermetallic particles. This microstructural evolution leads to increased MS but a reduction in EC. Naturally, adding more RE elements (RE) further enhances mechanical properties while reducing EC, necessitating an optimal composition that balances these attributes. A key finding of this study is that a brief, one-hour annealing at temperatures below 280 °C improves EC without significantly compromising mechanical properties. The researchers identified that the ideal combination of properties was achieved in Al-(3.5–4.5) RE samples subjected to the HPT process at RT and then annealed within the 250–280 °C temperature range.

In a study by Pozdniakov et al. [105], examined the effect of zirconium on the microstructure, recrystallization behavior, mechanical properties, and EC of Al-Er-Y alloys. Microstructural analysis revealed that the primary intermetallic compounds in the Al-Er-Y alloy include Al_3Y, Al_3Er, and $Al_3(Er, Y)$. The introduction of zirconium resulted in the formation of the $Al_3(Er, Y, Zr)$ phase. When the Al-Er-Y sample was annealed at 300°C, its hardness increased, which was attributed to the formation of eight-nanometer dispersed $Al_3(Er, Y)$ particles. The addition of zirconium led to a more pronounced improvement in hardness, likely due to the formation of five-nanometer $Al_3(Er, Y, Zr)$ particles. Specialized mechanical analysis determined that the recrystallization temperature of the Al-Er-Y alloy was about 365°C. With zirconium addition, this temperature increased to over 400°C. The study found that the inclusion of zirconium boosted UTS and YS by approximately 30 MPa after annealing. However, despite these enhancements in mechanical properties and the higher recrystallization temperature, the alloy's EC decreased by around 6 % IACS. This decrease in conductivity is mainly due to the higher density and smaller size of the $Al_3(Er, Y, Zr)$ particles In another study by Barkov et al. [106], the effects of thermomechanical operations on Al-Er-Yb-Sc alloys were examined. The number and density of precipitates were found to depend on the specific thermomechanical treatments and chemical compositions, directly

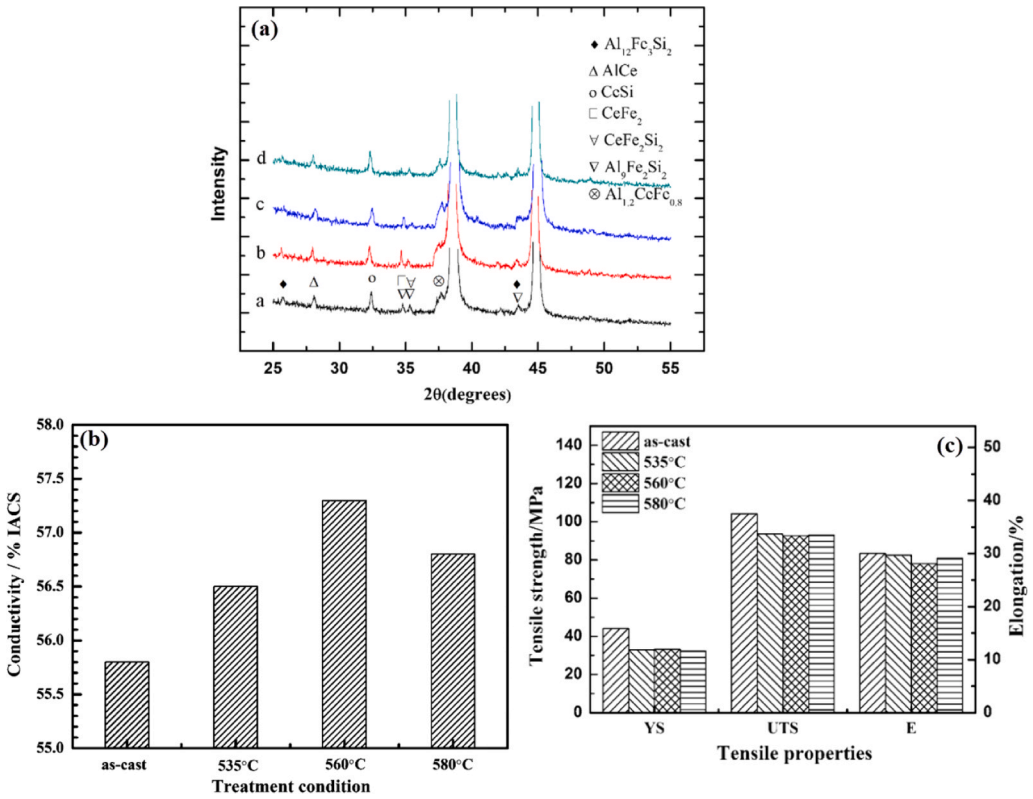

Fig. 41. a) X-ray diffraction pattern of Al-Mg-Si-Ce alloy (casting sample), b) EC of Al-alloy Mg-Si-Ce before and after homogenization operation, and (c) tensile properties of Al-Mg-Si-Ce before and after 6 h HT [99].

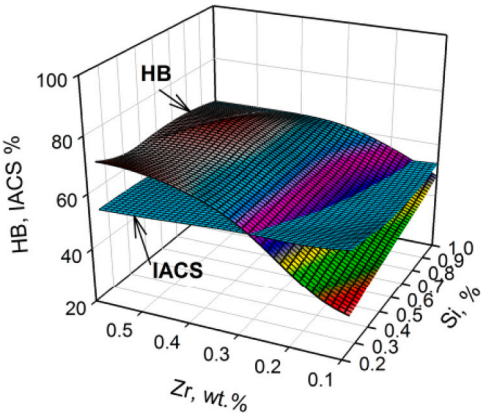

Fig. 42. Effect of adding zirconium and silicon on the EC and hardness of Al-1 % Fe-Si-Zr alloys [101].

impacting various properties. Therefore, optimizing these factors is crucial to achieving a balanced property profile. The study used Al-Er-Yb-Sc alloys with varying scandium content. Microstructural observations showed that the aluminum solid solution is saturated with scandium, erbium, ytterbium, and eutectic Al_3(Er, Yb) particles sized between 50 and 200 nm. Annealing the cast samples at 300 °C resulted in the precipitation of Al_3(Sc, Er, Yb) particles, measuring approximately 4–8 nm, significantly enhancing hardness through precipitation hardening. Overall, Al-Er-Yb-Sc alloys exhibited TSs ranging from 142 to 231 MPa, elongation percentages between 3.6 % and 13.5 %, and electrical conductivities of 54.8–60.9 %IACS. Remarkably, the characteristics like ST and hardness experienced a minor reduction following 100 h of annealing at 300 °C, highlighting the high thermal stability of the alloys. In a study conducted by Mamala et al. [107], aluminum-silver alloys were developed to enhance EC and increase current-carrying capacity. For this purpose, Al-Ag samples containing 0.1 %, 0.25 %, and 0.54 % by weight of silver were tested, alongside pure aluminum as a reference. The impact of silver on EC under various conditions is presented in Fig. 45a. The study found that for each group of specimens, the EC was nearly identical under casting, quenching, and cold deformation conditions. Cold deformation slightly reduced EC, likely due to the formation and accumulation of crystal structure defects. The researchers inferred that in all samples, silver atoms were incorporated into the aluminum solid solution. Fig. 45b shows the EC results for samples with less than 0.1 % by weight of silver. Homogenization and quenching processes had minimal impact on EC. However, in the sample containing 0.1 % by mass of silver, EC decreased by approximately 1 % compared to pure aluminum. Fig. 45c depicts the EC of cold-drawn samples in wire form. Observations indicated that the EC of the drawn samples was less than that of the cast and quenched samples. The results imply that while silver addition affects the EC of aluminum alloys, the impact is relatively slight and differs depending on the processing conditions. The incorporation of silver into the aluminum solid solution and subsequent processing methods play significant roles in determining the final electrical properties of the alloy.

In their study, Ji et al. [108] analyzed the microstructure and properties of Al-Mg-Si alloys applied in aluminum conductors, particularly focusing on the processes of horizontal continuous casting and continuous extrusion. The experimental method is illustrated in Fig. 46a. The alloy composition included 0.58 % Si, 0.65 % Mg, 0.17 % Fe, 0.002 % Cu, 0.03 % B, and the remainder aluminum. The study's findings on alloy hardness at various temperatures, along with its EC during aging at 155 °C, are presented in Figs. 46b and 46c. The hardness testing revealed that while the rate of achieving maximum hardness increases with higher aging temperatures, the hardness value itself decreases. The peak hardness and its most stable state were observed during aging at 155 °C. Additionally, EC measured at 155 °C improved

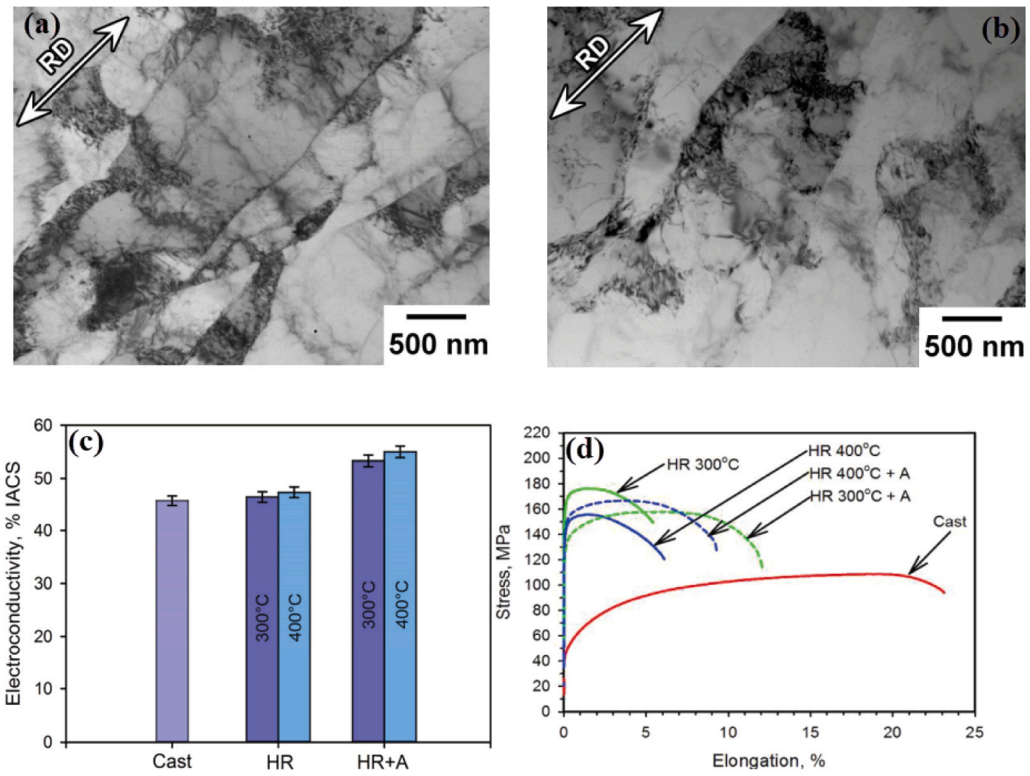

Fig. 43. Transmission electron microscopy images of Al-1 % Fe-0.3 % Zr-0.25Si alloy in rolling after a) 300 °C, b) 400 °C, c) effect of temperature on EC, and d) mechanical properties of Al-1 % Fe-0.3 % Zr-0.25Si alloy (HR = Hot Rolling, HR + A = Hot rolled samples were annealed) [102].

Table 11
Properties of Al-RE alloys after HPT process at RT and followed by annealing for 1 h [104].

Alloy	Annealing temperature (°C)	Mechanical properties			Conductivity	
		σ_y (MPa)	σ_{UTS} (MPa)	ε_t (%)	ω (MS/m)	IACS (%)
Al	-	137 ± 7	195 ± 5	28.3 ± 1.7	35.2 ± 0.2	61.7
Al−2.5RE	-	265 ± 8	297 ± 4	18.5 ± 2.1	32.8 ± 0.6	56.6
	230	195 ± 7	225 ± 2	21.6 ± 2.5	34.9 ± 0.2	60.2
Al−4.5RE	-	489 ± 10	580 ± 9	17.3 ± 2.4	26.4 ± 0.2	45.5
	230	520 ± 12	585 ± 12	12 ± 1.9	29.2 ± 0.3	50.3
	280	455 ± 9	500 ± 15	17 ± 2.1	30.3 ± 0.2	52.2
	400	150 ± 8	192 ± 6	22.6 ± 1.8	33.3 ± 0.1	57.4
Al−8.5RE	-	475 ± 20	637 ± 16	18.2 ± 1.4	23.0 ± 0.2	39.7
	230	506 ± 20	670 ± 15	12.4 ± 2.4	25.0 ± 0.2	43.1
	280	460 ± 20	620 ± 5	13.7 ± 2.1	25.9 ± 0.2	44.7
	400	150 ± 10	240 ± 5	18.7 ± 1.4	30.4 ± 0.2	52.4

over time, attributed to the decomposition of the supersaturated solid solution, reduced precipitation, and the presence of the required thermal energy to recover and reduce dislocations. The optimal properties were achieved by aging for 3 h at 155 °C, resulting in a TS of 334.7 MPa and an EC of around 55.7 % IACS Fig. 47 provides microstructural studies of the diverse processes. This figure demonstrates that the high solidification rate of the continuous casting process results in reduced grain size, while subsequent extrusion breaks down the dendritic microstructure into small, coaxial grains roughly 50 μm in size. Throughout the drawing process, the microstructure is compressed radially while being stretched in the direction of drawing, resulting in a refined grain structure. In this study the economic feasibility of the continuous process versus batch processing wasn't addressed. Also, the study didn't compare the results with conventional casting and extrusion methods to quantify process advantages.

In a study by X Zhang et al. [109], the microstructure and properties of an Al-0.7Fe-0.24Cu conductor alloy were analyzed following the processes of horizontal continuous casting and extrusion. The alloy, comprising 0.70 % Fe, 0.24 % Cu, 0.03 % Mg, 0.07 % Si, 0.009 % B, with the remainder being aluminum, was initially cast into a 12 mm diameter form and subsequently extruded to a 9.5 mm diameter. Results demonstrated that the extrusion process (Conform) reduced particle size and promoted the precipitation of the Al_7Cu_2Fe phase due to deformation. This led to an alloy exhibiting an optimal combination of mechanical properties and EC, primarily attributed to GR and the uniform distribution of stable precipitate phases such as Al_7Cu_2Fe and AlFe. Khanh et al. [110] report that ACSR wires, with a maximum operating temperature of 90°C, do not achieve the necessary EC and TS after repeated exposure to 180°C. This study investigates the production of thermal-resistant Al-Zr-Si-Fe alloy wires. The alloy is created in an electric furnace, cast into a mold, extruded, cold-drawn, and then annealed at 350–450°C for 10 h. The initial high resistivity results from the complete dissolution of zirconium in aluminum. Annealing at 400–450°C significantly enhances TS and reduces resistivity due to the

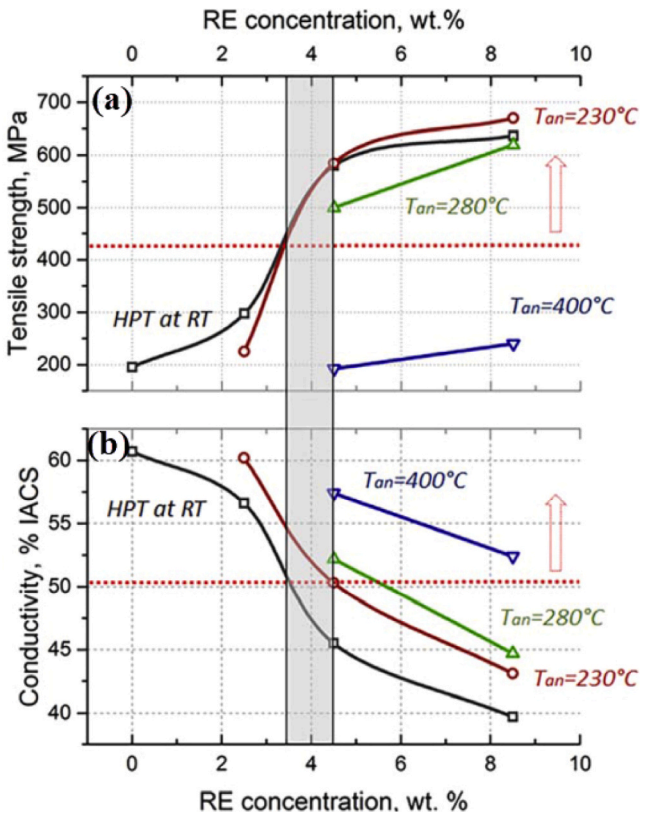

Fig. 44. Characteristics of Al-RE alloys relative to the amount of RE elements for different annealing temperatures: a) TS, and b) EC [104].

precipitation of Al_3Zr (L12) particles. The final product adheres to the IEC 62004 AT1 standard for mechanical, electrical, and thermal properties. Huynh et al. [111] investigated how HT affects the mechanical properties of 6201 aluminum alloy wires. The samples were divided into two groups: A and B. In group A, wires with a diameter of 4.7 mm were annealed at 480°C for 4 h before being drawn to a diameter of 2.7 mm. Some of these 2.7 mm samples were then aged at 170°C for durations of 5, 6, or 7 h, or for 5 days without prior solubilization. Other samples underwent solubilization at 520°C followed by aging at 150, 160, or 170°C for 5, 6, or 7 h. In group B, wires were directly drawn from 4.7 mm to 2.7 mm without annealing. Some of these samples were aged at 170°C for 5, 6, 7, or 8 h, or for 5 days without solubilization, while others were solubilized at 520°C for 1 h and then aged at 150°C for 5, 6, or 7 h. The results showed that optimal aging times and temperatures without solubilization enhance the strength to meet or exceed standards like ASTM B398. For example, a group A sample that was annealed before drawing reached a TS of 340.46 ± 38.97 MPa after artificial aging at 170 °C for 5 h. Conversely, a group B sample, which bypassed initial annealing but was aged at 170 °C for 7 h post-drawing, achieved a TS of 383.9 ± 12.68 MPa. The study further revealed that optimizing solubilization time and temperature can yield enhanced strengths. In group A, samples achieved a strength of 360.55 ± 22.70 MPa after solubilization at 160 °C for 7 h, and 342.35 ± 10.39 MPa after solubilization at 150 °C for 7 h, underscoring the importance of precise HT parameters in achieving superior mechanical properties. In a rigorous investigation conducted by Kang et al. [112], the influence of homogenization on the microstructure, micro-hardness, and EC of Al-Sc-Zr-Er dilute alloys, with varying zirconium concentrations (0.03 % and 0.06 % by weight), was meticulously examined. The microstructural assessment disclosed that both cast alloy samples exhibited an axial columnar microstructure accompanied by relatively coarse grains. In these cast specimens, zirconium atoms were found to be segregated within the dendritic regions, while scandium atoms were predominantly situated in the interdendritic zones. Additionally, the incorporation of erbium contributed to the formation of the Al3Er phase, while the remaining erbium formed discontinuous phases at grain boundaries in conjunction with iron and scandium. During the homogenization treatment, the sample with a higher zirconium content demonstrated the presence of coarse precipitates due to zirconium segregation. The study's results, as illustrated in Fig. 48, indicate that homogenization at 640 °C significantly impacted the EC of both alloy variants. Furthermore, the micro-hardness was evaluated after undergoing homogenization and subsequent age hardening at 400 °C for 24 h. This comprehensive analysis underscores the critical role of homogenization in optimizing the microstructural and functional properties of Al-Sc-Zr-Er alloys with varied zirconium contents.

The duration of homogenization for the investigated samples depends on the degree of zirconium segregation within the dendritic structure. For example, a homogenization at 640 °C for two hours effectively dissolved the Al_3Er phases, along with the iron- and scandium-rich phases. However, extending the homogenization time resulted in the formation of coarse phases in alloys with elevated zirconium content, which negatively impacted the maximum potential for age hardening. Ultimately, the optimal conditions for enhancing hardness and refining homogenization properties were established at a temperature of 640 °C with a duration of 24 h. Liao et al. [113] investigated the enhancement of EC in aluminum alloys through the addition of cerium. The researchers found that incorporating the appropriate amount of cerium significantly improves EC. This improvement can be attributed to the facilitated formation of double, triple, or even quadruple compounds involving iron, silicon, cerium, and aluminum, which ultimately reduces the concentration of dissolved iron and silicon atoms in the aluminum matrix. The impact of cerium content on the EC of two different alloys is illustrated in Fig. 49. The study identifies two primary mechanisms responsible for the observed enhancement in EC with cerium addition. Firstly, the reduction in the number of soluble iron and silicon atoms in the aluminum matrix diminishes lattice strain, thereby facilitating electron movement and enhancing EC. Secondly, the introduction of cerium appears to induce alterations in the electron energy band structure of the aluminum lattice, which may increase the effective number of electrons that contribute to conduction.

Al-0.3 wt% Si-0.2 wt% Mg [113].

In a study conducted by Luo et al. [114], explored how various CD techniques influence the microstructure and mechanical performance of pure aluminum wires subjected to strain. The study included a detailed schematic (refer to Fig. 50a) that depicted the CD methodology utilized. The analysis revealed that the aluminum wires exhibited an inhomogeneous microstructure when exposed to different levels of strain during the CD process. This variation in strain contributed to the observed differences in the microstructural properties of the wires. Specifically, the central regions of the drawn wires predominantly exhibit a $< 111 >$ crystallographic direction, whereas the surface regions display a $< 112 >$ direction The study attributed the inhomogeneity in the microstructure to the shear stress generated during the CD process. It was also observed that the grain size near the surface of the aluminum wires was smaller compared to the grain size in the central regions. Figs. 50b and 50c were used to illustrate the mechanical properties and EC of the samples. These figures demonstrated that the CD process increased the YS significantly while keeping the electrical resistance almost unchanged. The enhancement in MS was primarily due to the increased dislocation density and the formation of high-angle grain boundaries. However, these factors also led to a slight decrease in EC, as the higher dislocation density and high-angle grain boundaries caused electron deflection. Overall, the study underscores the complex interplay between mechanical strengthening and EC, highlighting how the CD process can optimize the performance of pure aluminum wires by altering their microstructure. The $< 111 >$ and $< 112 >$ orientations were identified, but the study didn't provide complete pole figures or orientation distribution functions to fully characterize the texture

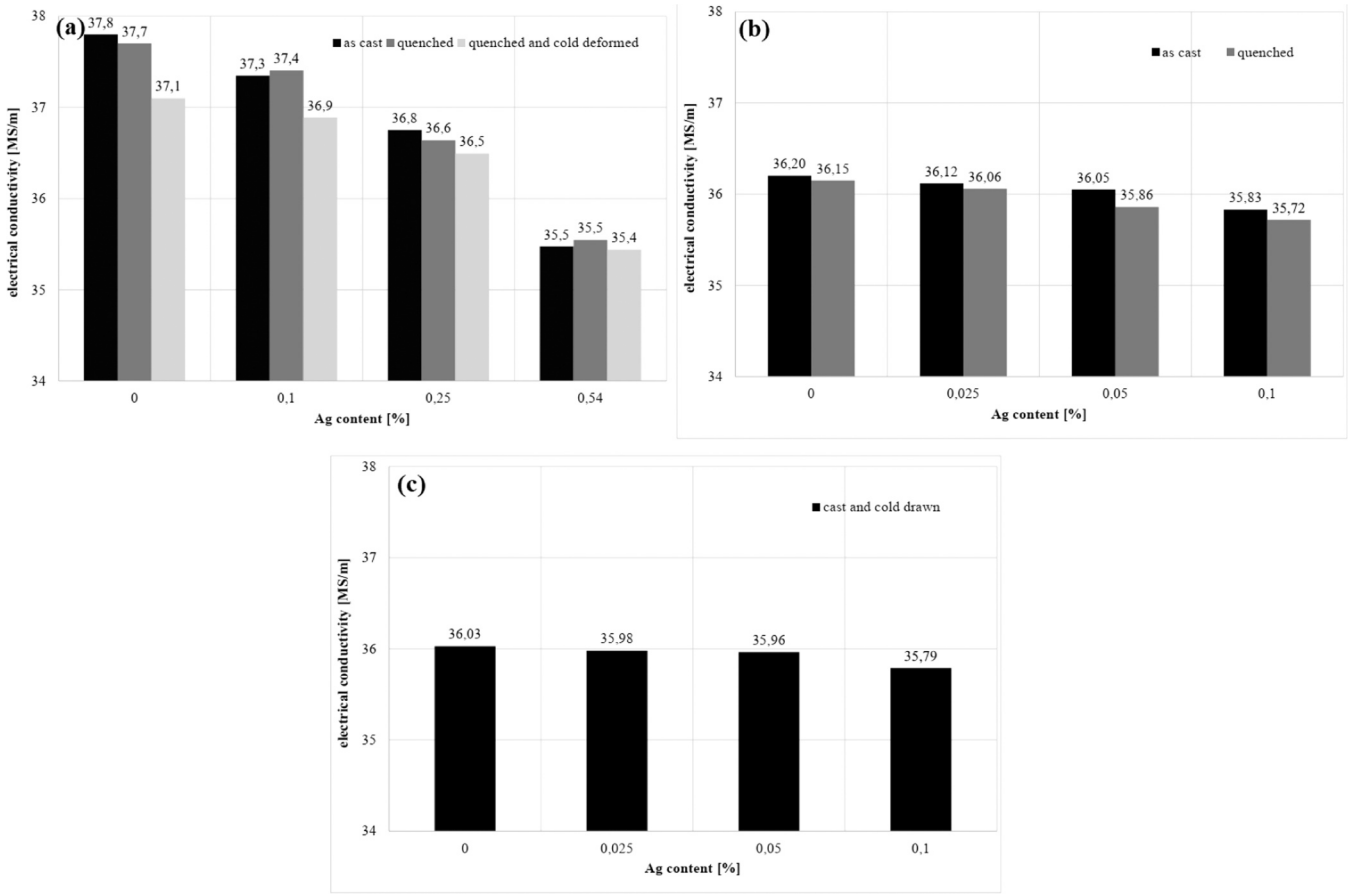

Fig. 45. (a) Effect of silver addition on the EC of the samples at RT, (b) samples with a silver content of less than 0.1 % by weight, and (c) samples drawn to obtain the wire [107].

development. Also, didn't evaluate how the developed microstructures might evolve during subsequent annealing or under long-term service conditions.

In a comprehensive study, Yang et al. [115] explored the impact of deformation via RS on the electrical properties and TS of 1070 aluminum alloy. The alloy was subjected to various strains during the RS deformation process. The findings revealed that the RS process induced significant elongation and a notable reduction in the grain size of the aluminum alloy. This grain elongation substantially increased the sub-grain boundaries and low-angle grain boundaries. The investigation into the micro-hardness and EC, depicted in Fig. 51, demonstrated that micro-hardness increased with higher strain levels due to the RS process, reaching a hardness of approximately 39.5 HV at a strain equivalent to 2.54 %. This improvement in hardness was attributed to the formation of a fine-grained microstructure. Furthermore, the study emphasized that if the microstructure is aligned with the direction of current flow, it facilitates electron transfer. However, the increase in grain boundaries, while beneficial for enhancing MS, results in a reduction in EC. This research focused exclusively on RS deformation without comparing with alternative severe plastic deformation methods (e.g., ECAP, HPT) that might yield different microstructure-property combinations. Also, didn't assess the thermal stability of the refined microstructure or long-term performance under operational conditions.

Chuvil'deev et al. [116] meticulously explored the thermal stability and mechanical attributes of Al-Mg-Zr-Sc (Yb) aluminum alloys used in conductors. The research highlighted that the Al-0.6Mg-Zr-Sc alloy, when annealed at 400 °C for 100 h, exhibited an ultra-fine grain structure with sizes between 2.4 and 2.8 μm. This HT led to a micro-hardness spectrum of 405–440 MPa, an UTS of 160–170 MPa, and elongation percentages falling between 12 % and 12.7 %. It was emphasized that an initial annealing stage at 320 °C for 2 h before the drawing process notably improved the alloy's thermal stability. This preliminary annealing induced the formation of intermetallic $Al_3(Sc_xZr_{1-x})$ nanoparticles and facilitated the precipitation of scandium and zirconium from the aluminum solid solution. In contrast, the magnesium-free variant, Al-Zr-Yb, did not demonstrate significant thermal stability due to the emergence of coarse particles during the primary annealing. For this alloy, annealing at 400 °C for 100 h resulted in increased grain sizes of 4.1–4.8 μm and a micro-hardness range of 305–315 MPa. Cui et al. [117] explored the influence of semi-stable phase precipitation on the electrical characteristics of the Al-0.96Mg2Si alloy. Their findings revealed that during the aging process, the predominant precipitates were β′and β′ phases. The behavior and impact of these precipitates were significantly influenced by both the duration of aging and the temperature. Notably, at an aging temperature of 175 °C, the primary precipitates observed were needle-shaped β′phases. These phases exhibited size growth over time, although this growth was constrained within a particular range. The changes in EC, in contrast to the consistently high hardness, were directly linked to microstructural alterations and the emergence of various phases during the aging process. Aging at 190 °C, unlike at 170 °C which induced only one precipitation phase, resulted in the formation of both β′ and β′ phases. This significantly influenced the alloy's relative electrical resistance (Δρ). As the temperature rose, the ratio of β′ to β′ phases decreased, leading to a rapid reduction in Δρ and a noticeable decline in peak hardness. Zhang et al. [118] conducted a thorough investigation into the effects of deformation and annealing on the mechanical, electrical, and textural properties of Al-Mg-Si alloy, which is commonly utilized in the fabrication of conductive wires. The 6xxx series aluminum alloys are recognized for their balanced medium MS and high EC, making them ideal for such applications. In this study,

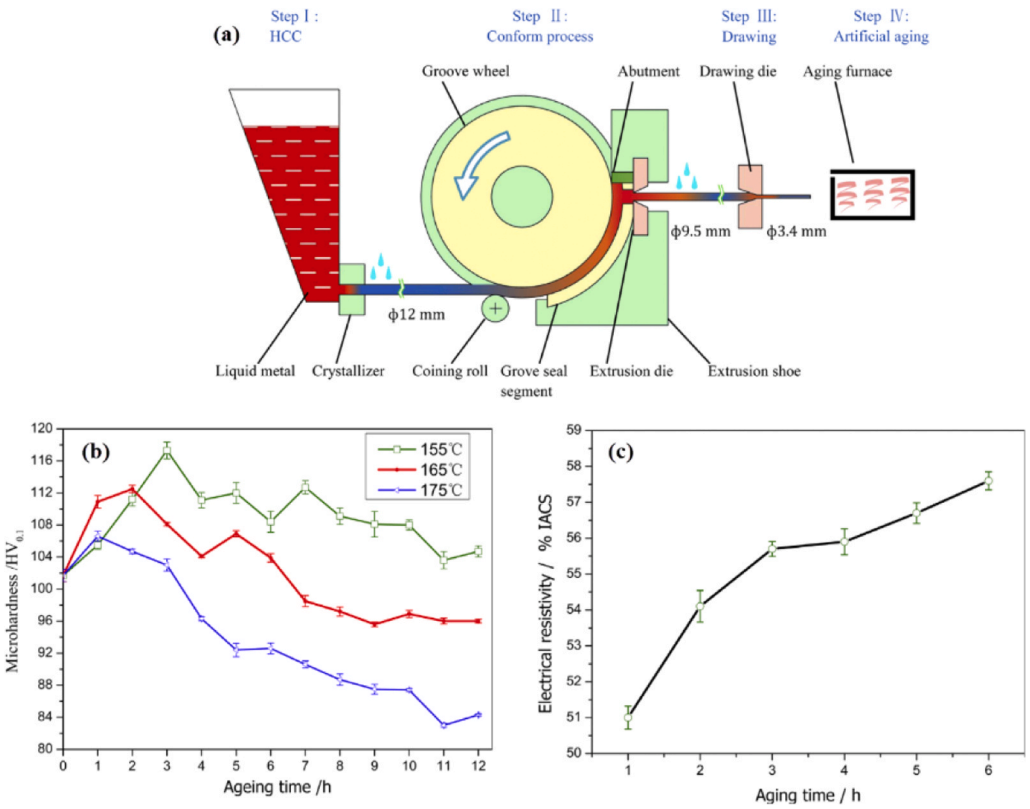

Fig. 46. a) Schematic of horizontal continuous casting, extrusion, drawing and aging operation processes, b) micro-hardness of Al-Mg-Si alloy wire at different temperatures and times of aging, and c) EC measured in aging operation at 155 °C [108].

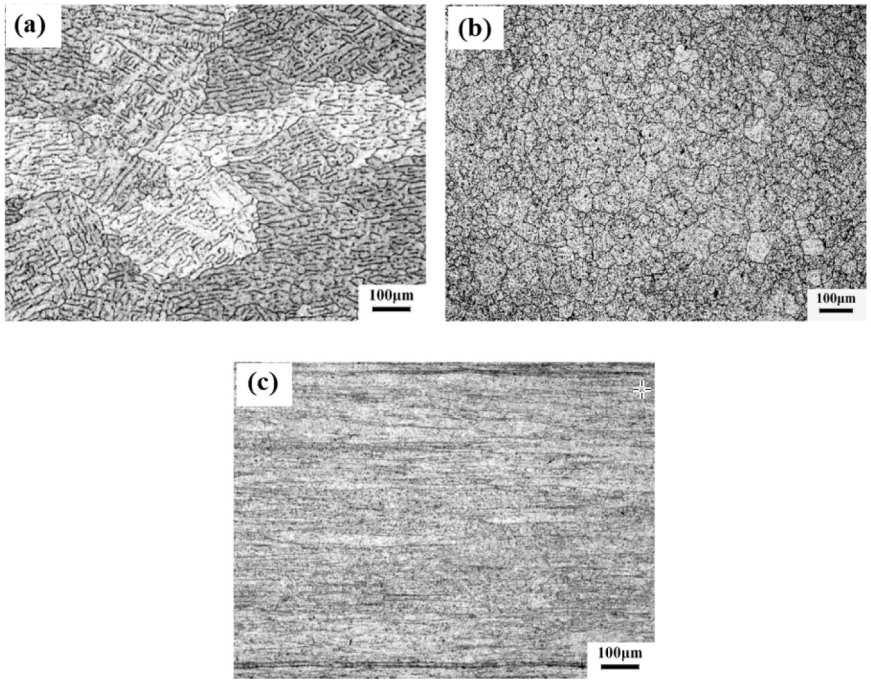

Fig. 47. Optical microscopy images of the microstructure of Al-Mg-Si alloy cast by a) continuous method, b) after extrusion process, and c) after drawing process [108].

the researchers applied a combination of deformations resulting in strains of 0.98 (sample A), 1.73 (sample B), and 2.24 (sample C), followed by annealing operations within the temperature range of 200–500 °C to optimize the alloy's properties. As depicted in Fig. 52, a deformation strain of 2.24 led to a maximum YS of 315 MPa, with an approximate grain size of 34.8 μm and a minimum EC of 43.9 %IACS. Microstructural analysis revealed significant changes post-annealing, transforming the normal state microstructure into a fine-grained,

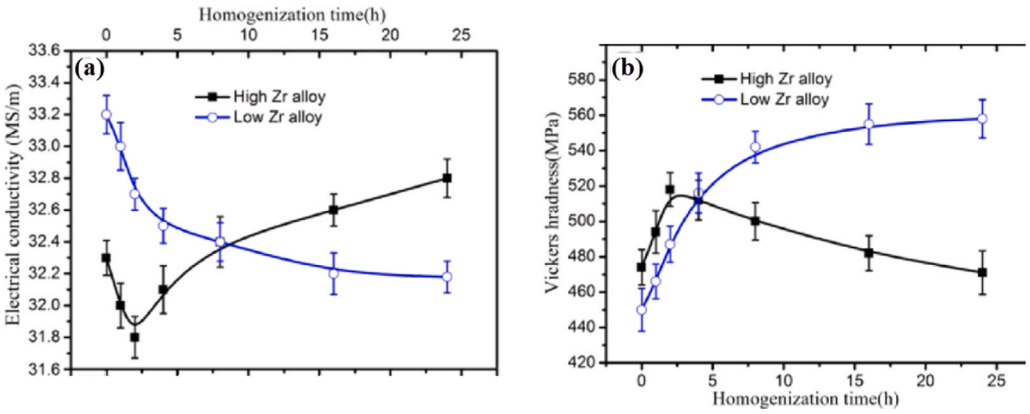

Fig. 48. a) EC changes of Al-Sc-Zr-Er alloys with different amounts of zirconium in homogenization operation at 640 °C, and b) hardness changes after age hardening operation at 400 °C and 24 h time in addition to previous operation [112].

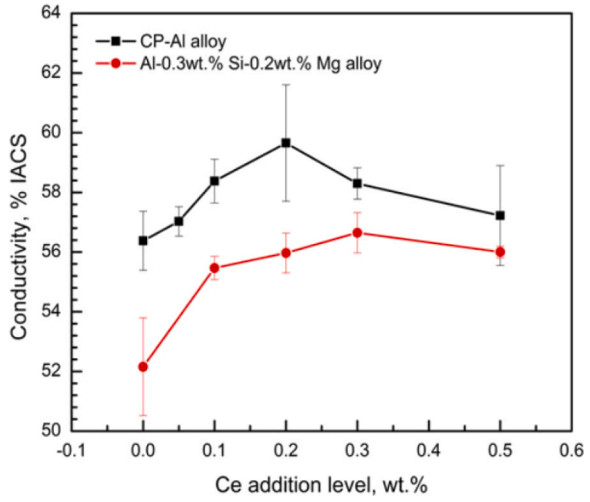

Fig. 49. Effect of cerium addition on EC of commercial pure aluminum and.

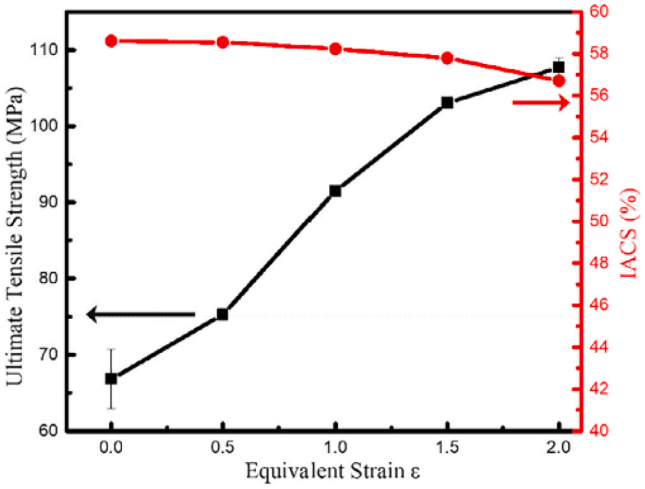

Fig. 51. EC and UTS of 1070 alloy versus applied strain [115].

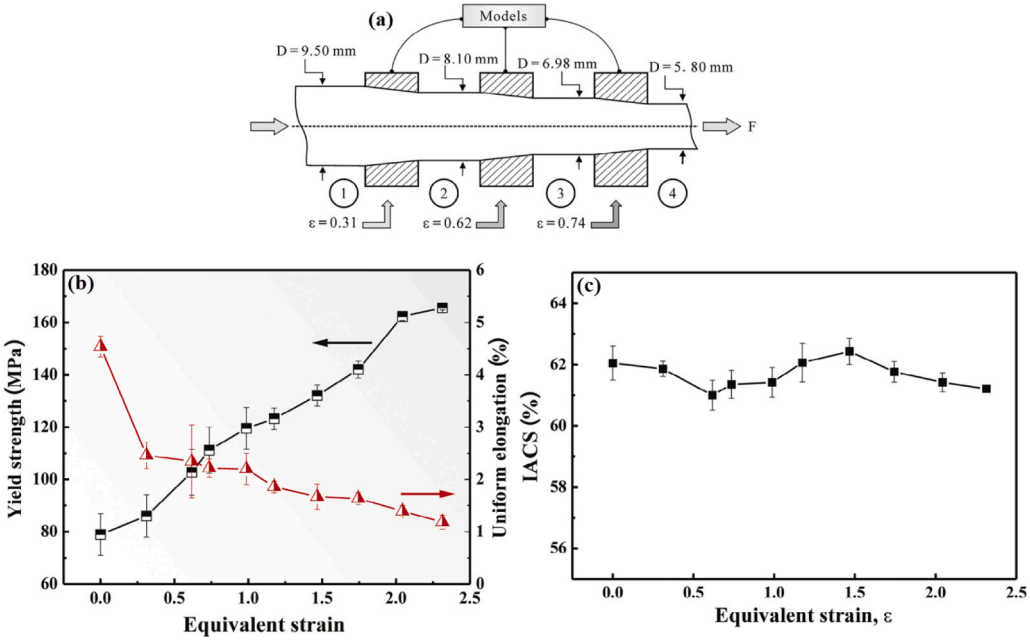

Fig. 50. a) Schematic of the CD process and the amount of strain after each stage of drawing, b) the YS and the percentage of elongation of the sample at different strains applied, and c) the relationship between EC and applied strain during the drawing process [114].

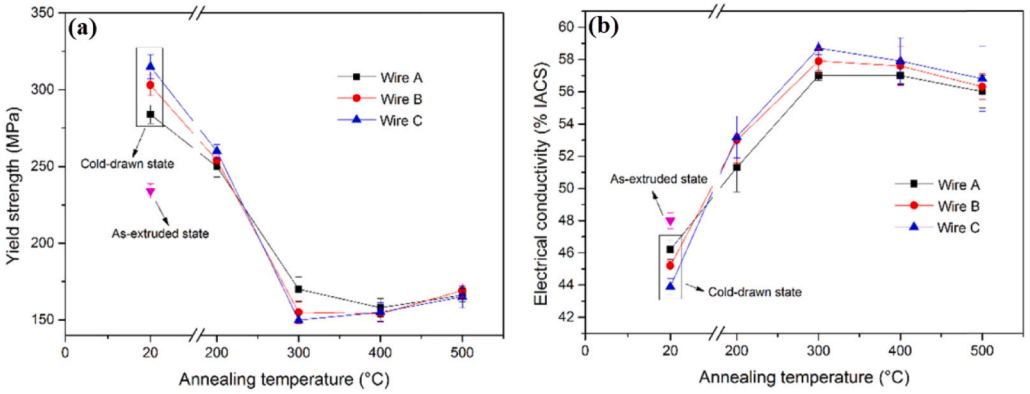

Fig. 52. (a) YS and (b) EC of wires drawn at different temperatures of annealing operation [118].

equiaxed structure. The annealing effect also reduced YS while enhancing EC. For instance, annealing sample A at 300 °C for 3.5 h resulted in a decrease in YS by 165 MPa and a 15 % increase in EC. These improvements were attributed to alterations in grain boundary conditions and dislocation densities. This comprehensive study highlights the critical impact of precise deformation and annealing treatments in enhancing the performance characteristics of Al-Mg-Si alloys, thus optimizing them for use in conductive wire applications.

Recent studies have optimized Al-Mg-Si alloys for power transmission by balancing strength and conductivity. Nikzad [119] demonstrated that an Mg/Si ratio of 1.5 provides the best compromise, achieving IACS> 52.5 % conductivity while maintaining strength through modified thermo-mechanical treatments and Ag/Cu additions. Similarly, Li et al. [120] identified Al-0.7Mg-0.5Si-0.2Fe as the optimal AA6101 composition, reaching 56.3 % IACS conductivity and 91.3 Hv hardness after homogenization. Both studies revealed that lower Mg/Si ratios increase strength but require longer aging, while proper Fe content helps control Si distribution. The research highlights that microstructural optimization through controlled precipitation hardening and careful alloying element selection can overcome the traditional strength-conductivity trade-off in aluminum conductors. These findings provide practical guidelines for developing high-performance transmission line materials with simultaneously enhanced mechanical and electrical properties.

Deokhyun et al. [121] note that, in recent years, overhead copper transmission lines have been replaced by lightweight aluminum lines to reduce costs and prevent sagging associated with heavier copper. High-strength aluminum alloys are used as the core of these lines to address the low strength of the aluminum conductor. Alloying aluminum with copper, however, reduces EC due to the formation of a solid solution. This study examines various Al/Cu ratios (9:1, 7:3, 5:5) to develop a high-strength Al-Cu alloy with minimal conductivity loss using powder metallurgy. Extruding Al/Cu powder at a low temperature of 350ºC minimizes alloying reactions. The resulting microstructure was analyzed, identifying phases such as Cu_9Al_4 and $CuAl_2$. Findings indicate that the TS of the samples improves significantly, while conductivity sees a slight decrease but remains within acceptable operational limits In an innovative study by Hou et al. [122], a novel method was developed to create nano size precipitates aimed at enhancing the mechanical and electrical properties of an aluminum alloy. The chemical composition of the aluminum alloy used in this research was as follows: Si 0.50, Fe 0.20, Mg 0.67, La-Ce (RE) 0.12, B 0.02, Cu < 0.05, Mn < 0.03, Cr < 0.03, Zn < 0.05, and Al bal. The study compared the properties of the alloy in its initial condition, pre-aged state, and pre-soluted condition. The pre-aged state exhibited the optimal combination of mechanical and electrical properties, achieving a UTS of 352.3 MPa and EC of 56.0 %IACS. This was markedly superior to the initial condition (UTS = 342.2 MPa and 49.3 %IACS) and the pre-soluted condition (UTS = 371.0 MPa and 47.8 %IACS). The creation of nano size precipitates effectively mitigated the conventional trade-off between MS and EC, a significant challenge for researchers working with alloys for conductor applications. The researchers noted that the radius of these precipitates substantially influences changes in both strength and conductivity. Mechanically, the improvements were linked to precipitation strengthening mechanisms involving dislocation bypassing and dislocation shearing. Increasing the precipitate radius enhanced EC, thereby achieving a desirable balance between conductivity and MS. This study by Hou et al. provides valuable insights into the manipulation of nano size precipitates, offering a promising avenue for advancing the performance of aluminum alloys in conductive applications.

Li et al. [123] conducted an in-depth investigation into the strengthening mechanisms during the CD process of pure aluminum wire. The study's findings revealed that as the area reduction during wire drawing increases, two critical transformations occur within the aluminum grains and microstructure. Specifically, the axial grains become elongated while the radial grains undergo refinement. Additionally, a notable change in the microstructure orientation is observed, shifting from $< 001 >$ to $< 111 >$. These phenomena were identified as the primary contributors to the increased YS observed in this study. The GR within the microstructure and the formation of specific crystalline orientations significantly enhanced the strength of the aluminum wire. In a comprehensive study by [124], the influence of zirconium addition on the precipitation and dynamic softening behavior of the Al-Fe-Zr alloy was thoroughly examined. The study found that the optimal temperature for the precipitation of Al_3Zr particles is 350 °C. Microstructural analysis of the Al-Fe-Zr alloy revealed that the extruded microstructure comprised butterfly-shaped Al_3Zr particles and rod-shaped Al3Fe particles. The introduction of zirconium into the alloy increased the volume fraction of Al_3Zr particles, whereas the volume fraction of Al3Fe particles remained unchanged. It is essential to highlight that the presence of these particles within the aluminum matrix contributes to the pinning of dislocations. At lower zirconium concentrations (0.1–0.2 % by weight), the pinning force of Al_3Zr is less significant than that of Al_3Fe. However, as the zirconium content increases, this pinning force also increases. During the extrusion process in this study, phenomena such as dynamic recovery and dynamic recrystallization were observed. The study found that a higher pinning force enhances the dynamic recrystallization behavior. Consequently, increasing the zirconium content from 0.1 % to 0.4 % by weight led to a change in the fraction of recrystallized grains from 44.2 % to 86.9 %.

Allamki et al. [125] studied the 6201-T81 alloy, an aluminum-magnesium-silicon alloy used in electrical conductors for overhead and distribution lines. This alloy is valued for its light weight and high mass conductivity but suffers from issues like creep, corrosion, and power loss. To enhance its properties, researchers applied solution HT at 510°C followed by ice-water quenching, then precipitation HT at 150–200°C for 2–24 h. The study found improved strength and hardness at lower temperatures (150°C, 165°C, 175°C) due to fine Mg2Si

precipitates. Higher temperatures (185°C, 200°C) led to decreased properties due to larger precipitates. EC increased with temperature and time, peaking at 60 %IACS. The best combination of properties was achieved with 165°C treatment for 18 h, showing a strength of 313 MPa, elongation of 8 %, hardness of 95 HV, and conductivity of 57.7 %IACS. Micrographs confirmed the correlation between grain size and properties. In their research, Smyrak et al. [126] investigated the impact of chemical composition on the mechanical and electrical properties of Al-Mg-Si wires. As illustrated in Fig. 53, wires with increased concentrations of magnesium and silicon demonstrate enhanced TS while maintaining a relatively constant EC. For instance, at an electrical resistance of 33.5 nΩm, the AlMg0.72Si0.71 alloy achieves the highest TS of 380 MPa, whereas the AlMg0.49Si0.48 sample exhibits a TS of 330 MPa. It is crucial to emphasize the EHC and HSC regions depicted in Fig. 53, which illustrate the developmental trends of Al-Mg-Si alloy wires. Furthermore, the researchers observed that artificial aging performed at temperatures ranging from 100 to 240 °C for durations of 2–24 h failed to yield HSCs and EHCs, thus posing a significant challenge for various studies in this domain.

Recent research has demonstrated several effective approaches for improving aluminum conductor performance. Erturk et al. [127] found that zirconium addition enhances thermal stability through Al3Zr precipitates that inhibit recrystallization by restricting grain boundary movement at elevated temperatures (150–200°C). Jiang et al. [128] developed SiCp/Al 6082 composites via squeeze casting, showing that 2 wt% SiC loading significantly improves mechanical properties (72.7 % increase in YS, 25.2 % in hardness) while reducing porosity. Alshwawreh et al. [129] demonstrated that thermal processing optimizes properties in cold-drawn 6201 AAAC wires, with different diameter wires (1.7 mm and 3.5 mm) showing varied responses to heat treatments (130–250°C). Hou et al. [63] compared electric-heated and A-H treatments on Al-Mg-Si wires, revealing that E-H treatment at moderate temperatures (160–185°C) accelerates precipitate coarsening, increasing conductivity but reducing strength. Orlova et al. [130] achieved optimal properties in Al-0.4Zr alloy (YS=163 MPa, EC=55 % IACS) through combined annealing and HPT processing, attributed to ultra-fine grain microstructure and grain boundary effects. These studies collectively highlight the importance of microstructural control through alloying, composite reinforcement, and thermal processing for enhancing aluminum conductor performance.

Although previous research has examined aging hardening behavior and rolling processes in alloys, the interplay between multi-stage rolling and staged aging in Al-Mg-Si alloys remains poorly understood. Through advanced microstructural characterization techniques, this study by chen et al. [131] reveals that combining two-stage rolling with aging treatment promotes a strong > 111 < crystallographic orientation while

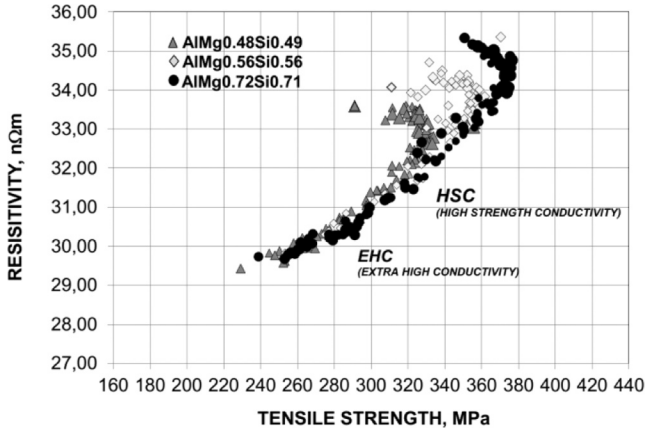

Fig. 53. TS and electrical resistance of Al-Mg-Si wires with different ratios of magnesium and silicon [126].

significantly refining grain structure and β" precipitates. The thermo-mechanical processing also leads to a substantial increase in dislocation density. These microstructural modifications simultaneously enhance mechanical strength and electrical conductivity compared to conventional aging treatments. The improved performance stems from multiple strengthening mechanisms, including grain boundary strengthening, precipitation hardening, and dislocation interactions, alongside reduced electron scattering due to optimized solute distribution. The findings demonstrate that tailored rolling and aging strategies can effectively tailor the microstructure of Al-Mg-Si alloys to achieve superior properties for electrical transmission applications.

Murashkin et al. [132], examined the mechanical and electrical properties of an Al-8.5 wt% RE (where RE consists of 5.4 % Ce and 3.1 % La) alloy with an ultra-fine grain structure, utilizing a high plastic deformation technique. Their findings, summarized in Table 12, reveal that the HPT process facilitated the creation of a homogeneous ultra-fine grain microstructure with an average grain size of 136 nm, incorporating $Al_{11}RE_3$ intermetallic particles. Additionally, the high plastic deformation process led to the incorporation of non-degradable RE atoms into the aluminum matrix, forming a supersaturated solid solution. Remarkably, subsequent annealing at temperatures of 280 °C and 400 °C for one hour did not result in significant grain growth, and the high plastic deformation contributed to enhanced thermal stability of the alloy. Improved mechanical properties after high plastic deformation processes and annealing operations are related to reasons such as GR of microstructure and related strengthening mechanism and formation of RE atomic nanoclusters. (Al-RE) alloys offer significant promise for the production of aluminum conductors because of their superior thermal stability up to 310°C and impressive mechanical characteristics.

Bobruk et al. [133] showed that SPD of Al-Mg-Si alloys produces ultra-fine grain structures with nanoparticle precipitates, simultaneously enhancing mechanical properties via Hall-Petch strengthening and electrical conductivity through matrix purification. Wang et al. [134] optimized Al-0.5Mg-1.0Si alloys with Ce/Cu additions, achieving peak properties (326 MPa UTS, 49.6 % IACS) through 160°C/10 h aging, where precipitate coarsening balanced strength and conductivity. Allamki et al. [21] established that T6 tempering (155°C/30 h) of 6201 alloy yielded an optimal TS/EC balance (326 MPa, 58.6 % IACS), demonstrating the precipitation-hardening trade-off. Pozdniakov et al. [135] developed thermally stable Al-0.2Y-0.2Sc conductors containing nanoscale $Al_3(Sc,Y)$ L_{12} precipitates that maintained 61 % IACS conductivity and 200 MPa UTS up to 300°C by pinning dislocations and grain boundaries, with 400°C annealing providing optimal particle distribution before coarsening occurred at longer durations. These studies collectively highlight three effective approaches for conductor optimization: SPD-induced grain refinement, precipitation engineering through aging treatments, and rare-earth phase stabilization - all while carefully balancing the fundamental strength-conductivity trade-off in aluminum alloys. In a comprehensive study conducted by Jiang et al. [136], researchers thoroughly analyzed how the RE element lanthanum affects the properties and characteristics of the 8167-aluminum alloy (Al-0.5Fe). The researchers found that the incorporation of lanthanum leads to the refinement of αAl grains and an enhancement in the $Al_{13}Fe_4$ intermetallic phases. As shown in Fig. 54, varying the concentrations of lanthanum has a notable impact on both the EC and the mechanical properties of the 8167-aluminum alloy. The findings indicated that adding lanthanum up to 0.08 % by weight markedly enhances both the mechanical and electrical properties. In spite of this, when the lanthanum concentration exceeds 0.1 % by weight, the formation of $Al_{11}La_3$ particles diminishes the elongation percentage. Additionally, the improved $Al_{13}Fe_4$ phases promote effective interaction between silicon and iron elements, which helps remove these elements from the matrix, thereby enhancing the alloy's EC.

The research by Mansurov et al. [137] aims to develop an aluminum-based alloy specifically designed for power line applications.

Table 12
Effect of HPT and annealing process on mechanical properties and EC of Al-8.5RE alloy [132].

Material	Condition	Mechanical properties				EC	
		σ_y (MPa)	σ_{UTS} (MPa)	ε_u (%)	δ (%)	ω (MS/m)	IACS (%)
Al−8.5RE	As-received	73 ± 5	175 ± 4	17.2 ± 1.2	33.0 ± 1.8	28.7 ± 0.1	49.5
	HPT	475 ± 11	537 ± 5	4.9 ± 0.4	18.2 ± 1.5	23.0 ± 0.2	39.7
	HPT+ 280℃	495 ± 10	553 ± 3	1.3 ± 0.2	17.1 ± 2.1	25.9 ± 0.2	44.7
	HPT+ 400℃	255 ± 8	274 ± 4	1.4 ± 0.3	23.4 ± 1.4	30.4 ± 0.2	52.4
CP Al	As-received	46 ± 4	87 ± 4	30.2 ± 1.6	36.3 ± 2.0	35.8 ± 0.1	61.7
	HPT	127 ± 7	195 ± 5	5.6 ± 0.4	28.3 ± 1.8	35.2 ± 0.2	60.7

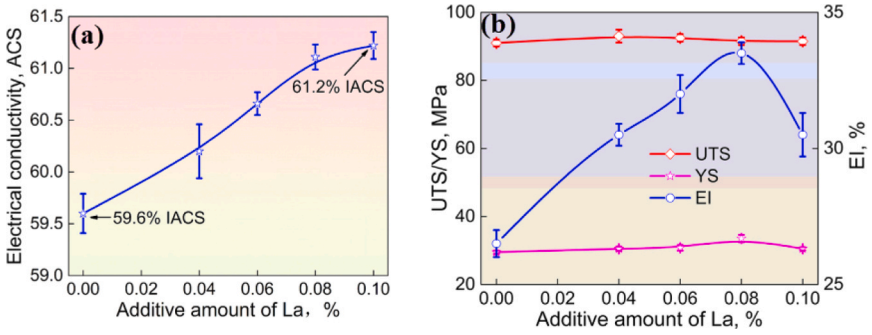

Fig. 54. Changes in a) EC and b) mechanical characteristics of the 8167 alloy as a function of different lanthanum addition levels [136].

It utilizes A7 grade aluminum that meets stringent purity requirements, maintaining impurities below 0.3 wt% to achieve optimal mechanical and electrical features. The alloying procedure incorporates several elements, notably potassium fluorozirconate, which help to enhance the characteristics of the alloy. Production occurred in both laboratory and industrial electric resistance furnaces, with meticulous control over melting and pouring temperatures to ensure consistency. Extensive analytical techniques, including light optical microscopy and scanning electron microscopy, were employed for microstructural analysis, along with measurements of EC that adhered to state standards. The project's objective was to formulate an alloy that offers a favorable combination of high EC and desirable MS, making it well-suited for rigorous power transmission applications. In their research, Sidelnikov and colleagues [4] investigated the impact of chemical composition on the mechanical and electrical properties of Al-Mg-Si wires. The study employed aluminum alloys where zirconium was a primary alloying element, along with varying amounts of iron and magnesium. These alloys were derived from commercial aluminum grades, which were melted in a high-frequency induction melting unit to achieve the desired compositions. The molten aluminum was then cast into ingots using molds, followed by advanced processing techniques such as combined rolling-extrusion and ingotless rolling-extrusion. These techniques were selected for their efficiency in producing elongated semi-finished products that are ideal for wire drawing. Comprehensive metallographic studies and mechanical testing allowed the researchers to examine the microstructure and assess critical mechanical properties such as TS and elongation, as well as the electrical resistivity, to understand how variations in chemical composition influence the overall performance of aluminum alloy wires in electrical applications. The findings regarding the structure and properties of the deformed semi-finished products created using the ingotless rolling-extrusion method are displayed in Fig. 55.

Sharifian et al. [138] developed a novel copper-clad aluminum (Cu/Al) composite wire using extrusion and wire drawing with intermediate annealing at 300°C, achieving a uniform interface without thick intermetallic compounds. The wire exhibited > 66.8 % IACS conductivity and significant strength improvements (183 % yield, 37 % UTS) after 99.6 % reduction, attributed to fine particle distribution in the Al core and residual stresses from dissimilar elastic properties. However, the study did not evaluate high-temperature IMC formation, long-term stability under residual stresses, or fatigue/creep behavior. Future work should address these gaps to ensure industrial applicability,

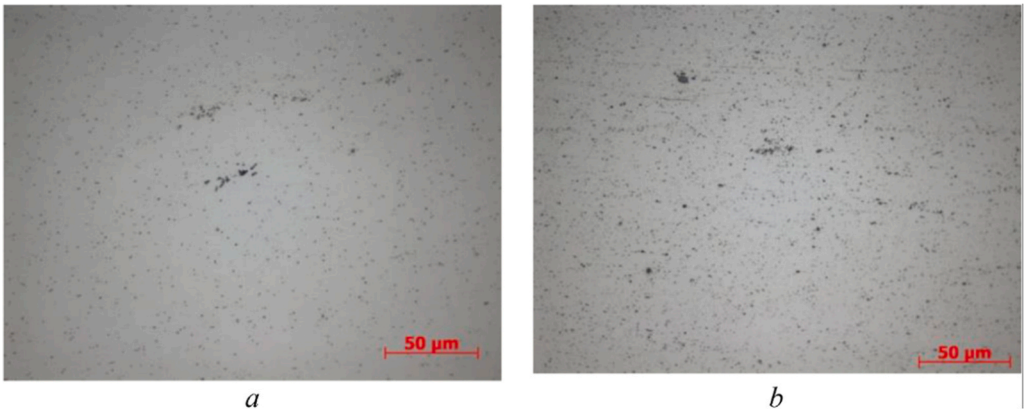

Fig. 55. (a) rod; (b) wire.

particularly under thermal and mechanical cycling conditions. Also, While SPD-processed Al conductors offer superior strength-conductivity balance, challenges remain in scalability, cost-effectiveness, and long-term thermal stability of nanostructures. Additionally, the trade-off between GR and solute scattering (conductivity) may limit performance in extreme environment [139].

To provide a clear and concise comparison of how different alloying elements and processing techniques influence the key properties of aluminum conductors, this summary table presents qualitative effects on EC and TS. Since optimizing aluminum alloys for electrical applications requires balancing these often-competing characteristics, Table 13 guide helps readers quickly assess: (1) which elements improve strength at the expense of conductivity, (2) which treatments can restore desired properties, and (3) where potential compromises exist. The Table 13 can be serves as an efficient reference for material selection and processing decisions in conductor design.

However, selecting the optimal alloy requires balancing electrical performance, mechanical strength, and thermal stability. To facilitate comparison, Table 14 summarizes the key properties of major aluminum conductor alloys, including conventional grades (1350, 6201, 6101, 8030, 8176 Al-Zr-Sc) alloy designed for high-temperature applications. The data covers electrical conductivity, tensile strength, maximum operating temperature, and typical use cases, providing a concise reference for material selection in power T&D systems.

4. Environmental impact and sustainable development

The consideration of environmental impact and sustainable development practices is increasingly important in the use of aluminum for conductors [140]. In the era of heightened environmental awareness and rapidly evolving energy demands, the aluminum industry finds itself at a pivotal juncture, grappling with the dual responsibilities of ensuring material performance while adhering to sustainable practices. Aluminum, is a material of choice in the manufacture of electrical conductors, particularly in overhead power transmission systems [141]. However, the environmental implications of aluminum production and usage warrant a comprehensive exploration, as the industry faces increasing scrutiny regarding the sustainability of its operations [142]. In light of these concerns, the recycling of aluminum has emerged as a pivotal strategy in promoting sustainability. Remarkably, recycling aluminum requires only about 5 % of the energy needed for its extraction from ore[143]. This dramatic reduction in energy input not only curtails greenhouse gas emissions but also mitigates the pressures on raw material extraction, making recycling a vital component of a circular significantly decrease their carbon footprints, aligning with the objectives of various international sustainability frameworks and regional environmental policies. Moreover, advancements in aluminum alloy technology are essential to enhance both performance and sustainability. New alloy compositions can be engineered to achieve improved characteristics such as increased strength, better corrosion resistance, and enhanced thermal performance [144–146]. The high recyclability of aluminum alloys used in conductors ensures that end-of-life materials can be reprocessed with minimal degradation in quality, reducing the need for virgin resources. However, challenges such as contamination from alloying elements and inefficient collection systems hinder optimal recycling rates. Implementing closed-loop recycling systems, along with stricter regulations on scrap sorting and processing, can enhance sustainability. Furthermore, advancements in alloy design to improve conductivity and mechanical properties while minimizing hazardous elements can further reduce environmental impacts across the product lifecycle. These innovations ensure that aluminum conductors can meet the stringent demands of modern energy transmission while maintaining resilience in diverse environmental conditions. The commitment to sustainability extends beyond production and recycling; it encompasses the entire lifecycle of aluminum products. Effective end-of-life management strategies are crucial for minimizing environmental impacts. Designing products with recyclability in mind ensures that materials can be easily retrieved and repurposed at the end of their service life [145,147]. Stakeholders, including manufacturers, policymakers, and consumers, must foster collaboration to develop and implement more efficient recycling systems, increase awareness about the value of recycled aluminum, and advocate for policies that support sustainable practices in the industry. Furthermore, the aluminum sector must address the broader implications of its operations on local communities and ecosystems. Engaging with stakeholders and adopting transparent practices can help mitigate the social impacts of aluminum production, fostering better relationships with communities affected by mining activities. Employing responsible and ethical sourcing practices can enhance the industry's sustainability credentials, building trust and goodwill. As the global community increasingly confronts the challenges of climate change, resource depletion, and environmental degradation, the aluminum industry must evolve to navigate these complexities responsibly. This means not only adopting innovative technologies and processes but also embracing a holistic view of sustainability that encompasses economic vitality and social responsibility. By prioritizing environmentally sound practices and demonstrating a commitment to stewardship, the aluminum sector can not only improve its ecological footprint but also secure its long-term viability in a competitive landscape.

Table 13
Effects of alloying elements and treatments on conductivity and tensile strength of aluminum alloys.

Alloying Element / Treatment	Effect on Conductivity	Effect on Tensile Strength	Key Implications
Pure Aluminum (99.9 %)	Very High	Low	Baseline for high-conductivity applications
Copper	Significant Decrease	Large Increase	Favored for high-strength applications
Magnesium	Slight Decrease	Moderate Increase	Balanced properties for general use
Silicon	Moderate Decrease	Large Increase	Improves castability and durability
Iron	Minor Decrease	Slight Increase	Cost-effective GR
Zirconium	Negligible Impact	Moderate Increase	Thermal stability enhancer
Cold Working	Slight Decrease	Significant Increase	Immediate strength improvement
Annealing	Restores Conductivity	Reduces Strength	Reverses work hardening effects
Precipitation Hardening	Moderate Decrease	Very Large Increase	Maximum strength achievable

5. Future considerations

Future research must prioritize the strategic development and refinement of aluminum alloys to fundamentally optimize the critical balance between MS and EC. Leveraging cutting-edge advancements in nanotechnology and material science offers a transformative pathway to engineer novel alloy compositions and microstructures capable of decoupling these traditionally competing properties. Concurrently, pioneering more efficient manufacturing methodologies—including advanced thermomechanical processing, precision HTs, and SPD techniques—is essential to further enhance conductor performance. Environmental imperatives demand rigorous integration, necessitating a focus on sustainable material sourcing, energy-efficient production, and comprehensive lifecycle assessment to minimize ecological footprint, with dedicated investigation into optimized recycling protocols. Furthermore, the proliferation of renewable energy sources and smart grid technologies mandates critical assessment of aluminum conductor integration within these evolving frameworks. Finally, to ensure grid resilience amidst escalating power demands, continuous research into

Table 14
Comparative properties of major aluminum alloys for EC, (% IACS), MS, operating temperature limits, and standard applications.

Alloy	Composition (wt %)	Conductivity (% IACS)	Tensile Strength (MPa)	Operating Temp. (°C)	Standard Applications	Key Advantages	Relevant Standards
1350	≥ 99.5 % Al	61–62 %	60–100	Up to 90	Overhead power lines, busbars	High conductivity, corrosion resistance	ASTM B230/B231, IEC 61089
6201	Al−0.6Mg−0.8Si	52–54 %	240–300 (T6)	Up to 150	AAAC conductors, transmission lines	High strength-to-conductivity ratio	ASTM B399, IEC 62004
6101	Al−0.5Mg−0.6Si	55–57 %	150–200 (T6)	Up to 120	Busbars, electrical enclosures	Balanced formability/ conductivity	ASTM B317/ B317M
8030	Al−0.5Fe−0.2Cu	59–60 %	110–150	Up to 90	Building wiring (e.g., NM cables)	Creep resistance, compact stranding	ASTM B800
8176	Al−0.5Fe	60–61 %	80–120	Up to 90	Flexible cables, automotive wiring	Fine-stranded, high flexibility	ASTM B801
Al-Zr-Sc	Al−0.1Zr−0.05Sc	55–58 %	180–250 (annealed)	Up to 250	High-temp. conductors (aerospace)	Thermal stability, recrystallization resistance	ASTM B941

conductor behavior under emergent operational extremes—such as sustained high-temperature regimes and ultra-high current densities—remains paramount.

Carbon fiber composite core conductors offer superior strength, lightweight, and corrosion resistance for high-capacity transmission but face challenges in bending performance and defect detection. Future development lies in multi-strand core designs for flexibility, embedded fiber-optic sensing for defect monitoring, and eco-friendly thermoplastic composites for sustainable solutions [148]. Also, The development of high-performance aluminum matrix composites for transmission conductors faces several critical challenges: (1) inhomogeneous dispersion of CNTs/graphene due to agglomeration, addressed through ball milling, ultrasonication, and functionalization [149]; (2) weak interfacial bonding of pristine CNTs/graphene with Al, improved by chemical functionalization to introduce reactive groups [150]; (3) high production costs of nanomaterials, potentially mitigated by sustainable synthesis from biowastes; (4) formation of brittle $TiAl_3$ intermetallic in Al-TiN composites, suppressed through Si addition or two-step sintering [151]. Also, novel superhydrophobic nanostructured Al conductors, fabricated via anodization, demonstrate exceptional anti-icing properties (ice adhesion as low as 3.82 kPa) and improved electrical performance (corona inception voltage up to 27.86 kV). The honeycomb-like nanoporous structure outperforms reticular designs in water repellency, ice resistance, and power transmission efficiency. While lab results are promising, field validation under actual transmission line conditions remains essential for practical implementation [152].

6. Conclusion

This review has provided a detailed exploration of the mechanical, physical, and thermal properties of aluminum and its alloys used in electrical conductors. Aluminum's inherent advantages – high EC, light weight, and corrosion resistance – solidify its position as an ideal material for power T&D systems. However, the persistent challenge lies in optimizing the critical balance between enhancing mechanical properties and maintaining high EC. As demonstrated, the incorporation of alloying elements and sophisticated HT processes offers pathways to improved strength, but often necessitates compromises in conductivity. Sustainability emerges as another vital theme, where lifecycle analysis of aluminum production and its exceptional recyclability present significant advantages in aligning with global environmental goals and the circular economy. The review underscores the paramount importance of understanding the intricate trade-offs involved in alloy design and the critical role of precise chemical composition control and advanced manufacturing processes in achieving optimal conductor performance. Moving forward, this synthesis of current knowledge clearly mandates focused future research and development:

Advanced Alloy Design: Exploring novel alloying strategies (micro-alloying, RE elements) and nano-reinforcements to decouple the strength-conductivity trade-off more effectively.

Precision Processing: Investigating the impact of emerging manufacturing techniques (e.g., SPD, additive manufacturing for specialized components, optimized continuous casting) on microstructure control and property enhancement.

Surface Engineering: Researching advanced surface treatments and coatings to further enhance corrosion resistance, reduce oxidation, and improve contact behavior, especially in harsh environments.

AI-Driven Optimization: Leveraging machine learning and artificial intelligence for accelerated discovery of optimal alloy compositions and processing parameters for specific application requirements.

Sustainable Manufacturing: Optimizing production processes for lower energy consumption, reduced emissions, and maximizing the use of recycled aluminum content will be crucial for meeting environmental regulations and ESG goals.

Cost-Effectiveness: Innovations leading to conductors with a better overall performance-to-cost ratio (factoring in lifetime, losses, maintenance, and installation) will drive broader adoption, particularly in developing grid infrastructure and renewable energy integration projects.

In conclusion, this comprehensive review not only synthesizes the current state of knowledge but also provides a clear roadmap for advancing aluminum conductor technology. By addressing the identified research challenges and leveraging the opportunities, the industry can develop more efficient, reliable, and sustainable electrical conductors essential for the future energy landscape.

CRediT authorship contribution statement

Pooya Parvizi: validation, formal analysis, data curation, writing – review & editing, visualization, supervision, funding acquisition, writing – original draft. **Milad Jalilian**: conceptualization, validation, formal analysis, data curation, visualization, supervision, funding acquisition, writing – original draft, and writing – review & editing. **Pedram Sorouri Mirazizi**: investigation, resources, writing – review & editing, project administration, and funding acquisition. **Mohammad Reza Zangeneh**: validation, formal analysis, investigation, resources, data curation, supervision, and funding acquisition, writing – review & editing. **Alireza Mohammadi Amidi**: conceptualization, methodology, resources, data curation, investigation, funding acquisition, writing – review & editing

Ethical approval

This review does not raise any ethics issues.

Supplementary information

Not Applicable.

Declaration of Competing Interest

The authors declare that they have no known competing financial interests or personal relationships that could have appeared to influence the work reported in this paper.

Acknowledgments

Not Applicable.

References

[1] P. Parvizi, et al., High temperature low sag conductors: a brief review on strategies used to prevent destruction, and maintenance considerations, Trans. Indian Natl. Acad. Eng. (2025) 1–22.
[2] Q. Mao, et al., Optimizing strength and electrical conductivity of 6201 aluminum alloy wire through rotary swaging and aging processes, J. Mater. Process. Technol. (2024) 118497.
[3] O'Boyle, M., C. Baker, and M. Solomon, Supporting Advanced Conductor Deployment: Barriers and Policy Solutions. Energy Innovation and GridLab. https://energyinnovation. org/wpcontent/uploads/2024/04/Supporting-Advanced-Conductor-Deployment-Barriers-and-Policy-Solutions. pdf, 2024.
[4] S.B. Sidelnikov, et al., Modeling and investigation of combined processes of casting, rolling, and extrusion to produce electrical wire from alloys Al-Zr system, Int. J. Lightweight Mater. Manuf. (2024).
[5] Kiessling, F., et al., Overhead power lines: planning, design, construction. 2014: Springer.
[6] Rossiter, P.L., The electrical resistivity of metals and alloys. Vol. 6. 1991: Cambridge university press.
[7] X. Sauvage, et al., Optimization of electrical conductivity and strength combination by structure design at the nanoscale in Al–Mg–Si alloys, Acta Mater. 98 (2015) 355–366.
[8] R.Z. Valiev, M.Y. Murashkin, I. Sabirov, A nanostructural design to produce high-strength al alloys with enhanced electrical conductivity, Scr. Mater. 76 (2014) 13–16.
[9] Y. Li, R. Wang, Z. Yang, Optimal scheduling of isolated microgrids using automated reinforcement learning-based multi-period forecasting, IEEE Trans. Sustain. Energy 13 (1) (2021) 159–169.
[10] F. Czerwinski, Aluminum alloys for electrical engineering: a review, J. Mater. Sci. (2024) 1–46.
[11] Y. Wang, et al., Conductive al alloys: the contradiction between strength and electrical conductivity, Adv. Eng. Mater. 23 (5) (2021) 2001249.
[12] Y. Liu, S. Xiong, Research progress on thermal conductivity of High-Pressure Die-Cast aluminum alloys, Metals 14 (4) (2024) 370.
[13] Thrash, F., Transmission conductors–A review of the design and selection criteria. Tech. Support Artic. Southwire Company.(http//www. southwire. com/support/TransmissionConductoraReviewOfTheDesignandSelectionCrite ria. htm (accessed 9/8/2014), 2014.
[14] S. Karabay, I. Uzman, Inoculation of transition elements by addition of AlB2 and AlB12 to decrease detrimental effect on the conductivity of 99.6% aluminium in CCL for manufacturing of conductor, J. Mater. Process. Technol. 160 (2) (2005) 174–182.
[15] T. Kishore, S. Singal, Optimal economic planning of power transmission lines: a review, Renew. Sustain. Energy Rev. 39 (2014) 949–974.
[16] A. Alawar, E.J. Bosze, S.R. Nutt, A composite core conductor for low sag at high temperatures, IEEE Trans. Power Deliv. 20 (3) (2005) 2193–2199.
[17] S. Karabay, Modification of AA-6201 alloy for manufacturing of high conductivity and extra high conductivity wires with property of high tensile stress after artificial aging heat treatment for all-aluminium alloy conductors, Mater. Des. 27 (10) (2006) 821–832.
[18] V.M. Bespalov, et al., Influence of the parameters of combined processing and drawing on the structure and properties of conductor Semi-finished products from aluminum alloys with additives of rare earth and transition metals, Met. Mater. Int. 30 (3) (2024) 773–799.
[19] H. Li, et al., Effect of rolling temperature on the microstructure and mechanical properties of 6201 al alloy, Mater. Test. 61 (5) (2019) 455–458.
[20] P. Rocha, et al., Influence of 1350 and 6201 aluminum alloys on the fatigue life of overhead conductors–A finite element analysis, Tribology Int. 186 (2023) 108661.
[21] A. Allamki, et al., Precipitation hardening of the electrical conductor aluminum alloy 6201, Metals 13 (6) (2023) 1111.
[22] J.A. Araújo, et al., Overhead conductors. in Fretting Wear and Fretting Fatigue, Elsevier, 2023, pp. 565–597.
[23] Al Aqil, M.A., Increasing Overhead Line Power Rating by Optimising Conductor Electro-Mechanical Performance. 2021, University of Manchester.
[24] M. Jalilian, J.-R. Riba, P. Parvizi, Aluminum conductor Steel-Supported conductors for the sustainable growth of power line capacity: a review and discussion, Materials 17 (18) (2024) 4536.
[25] C. Ujah, A. Popoola, O. Popoola, Review on materials applied in electric transmission conductors, J. Mater. Sci. (2022) 1–18.
[26] H. Rhee, et al., Mechanical properties of novel aluminum metal matrix metallic composites: application to overhead conductors, Mater. Des. 88 (2015) 16–21.
[27] K. Ma, et al., Mechanical behavior and strengthening mechanisms in ultrafine grain precipitation-strengthened aluminum alloy, Acta Mater. 62 (2014) 141–155.
[28] M.Y. Murashkin, et al., Enhanced mechanical properties and electrical conductivity in ultrafine-grained al alloy processed via ECAP-PC, J. Mater. Sci. 48 (13) (2013) 4501–4509.
[29] H.-c Liao, H.-t Xu, Y.-y Hu, Effect of RE addition on solidification process and high-temperature strength of al– 12% si– 4% cu– 1.6% mn heat-resistant alloy, Trans. Nonferrous Met. Soc. China 29 (6) (2019) 1117–1126.
[30] T. Wróbel, J. Szajnar, Modification of pure Al and AlSi2 alloy primary structure with use of electromagnetic stirring method, Arch. Metall. Mater. 58 (2013).
[31] R.Z. Valiev, et al., Grain refinement and mechanical behavior of the al alloy, subjected to the new SPD technique, Mater. Trans. 50 (1) (2009) 87–91.
[32] M. Cabibbo, Microstructure strengthening mechanisms in different equal channel angular pressed aluminum alloys, Materials Science Engineering A 560 (2013) 413–432.
[33] J. Hou, et al., Breaking the trade-off relation of strength and electrical conductivity in pure al wire by controlling texture and grain boundary, J. Alloy. Compd. 769 (2018) 96–109.
[34] K. Durczewski, Z. Gajek, J. Mucha, Influence of electron–phonon interaction and crystal field on thermal and electrical resistivity in rare earth intermetallics, Eur. Phys. J. B Condens. Matter Complex Syst. 93 (5) (2020) 1–18.
[35] J. Hou, et al., Origin of abnormal strength-electrical conductivity relation for an Al–Fe alloy wire, Materialia 7 (2019) 100403.
[36] H. Seyedrezai, et al., Study of the early stages of clustering in Al–Mg–Si alloys using the electrical resistivity measurements, Materials Science Engineering A 525 (1-2) (2009) 186–191.
[37] S.N. Khangholi, et al., Effect of ag and cu addition on the strength and electrical conductivity of Al-Mg-Si alloys using conventional and modified thermomechanical treatments, J. Alloy. Compd. 914 (2022) 165242.
[38] V. Tcherdyntsev, et al., Phase composition and microhardness of rapidly quenched Al–Fe alloys after high pressure torsion deformation, Materials Science Engineering A 375 (2004) 888–893.
[39] D.-b CHEN, et al., Effects of impurity elements on conductivity of the electric circular aluminum rod, Light Alloy Fabr. Technol. 6 (2009).
[40] C. Liu, et al., Enhancing electrical conductivity and strength in al alloys by modification of conventional thermo-mechanical process, Mater. Des. 87 (2015) 1–5.
[41] Y. Birol, Aluminothermic reduction of boron oxide for the manufacture of Al–B alloys, Mater. Chem. Phys. 136 (2-3) (2012) 963–966.
[42] A. Zhang, Y. Li, Thermal conductivity of aluminum alloys—a review, Materials 16 (8) (2023) 2972.
[43] K.F. Lunn, D. Apelian, Thermal and electrical conductivity of aluminum alloys: fundamentals, structure-property relationships, and pathways to enhance conductivity, Materials Science Engineering A (2024) 147766.
[44] F. Czerwinski, Aluminum alloys for electrical engineering: a review, J. Mater. Sci. 59 (32) (2024) 14847–14892.
[45] B. Smyrak, Analysis of the quality of aluminum overhead conductors after 30 years of operation, Eng. Fail. Anal. 154 (2023) 107600.
[46] Thrash, R., Overhead conductor manual. 2007: Southwire Company.
[47] S. Beryozkina, Evaluation study of potential use of advanced conductors in transmission line projects, Energies 12 (5) (2019) 822.
[48] Kaufman, J.G., Introduction to aluminum alloys and tempers. 2000: ASM international.
[49] K.O. Cooke, Introductory chapter: structural aluminum alloys and composites, Alum. Alloy. Compos. (2020) 1–14.
[50] T. Koizumi, M. Kuroda, Grain size effects in aluminum processed by severe plastic deformation, Materials Science Engineering A 710 (2018) 300–308.
[51] R. Sanders Jr, P. Hollinshead, E. Simielli, Industrial development of non-heat treatable aluminum alloys, Mater. Forum (2004).
[52] T.S.V. Vilela, et al., Application and comparative study of the master curve methodology for predicting fatigue life in overhead conductor, J. Braz. Soc. Mech. Sci. Eng. 46 (3) (2024) 152.
[53] Kaufman, J.G., Properties of aluminum alloys: fatigue data and the effects of temperature, product form, and processing. 2008: ASM International.
[54] Papailiou, K.O., Overhead lines. 2017: Springer.
[55] Davis, J.R., Aluminum and aluminum alloys. 1993: ASM international.
[56] J.R., E.A. STARKE, Heat-treatable aluminum alloys, Alum. Alloy. Contemp. Res. Appl. Contemp. Res. Appl. 31 (2012) 35–63.
[57] F.U. Flores, et al., Development of high-strength and high-electrical-conductivity aluminum alloys for power transmission conductors. in TMS Annual Meeting & Exhibition, Springer, 2018.
[58] I. Albizu, et al., Aspects to take into account in the application of mechanical calculation to high-temperature low-sag conductors, IET Gener. Transm. Distrib. 4 (5) (2010) 631–640.
[59] J.-R. Riba, et al., Uprating of transmission lines by means of HTLS conductors for a sustainable growth: challenges, opportunities, and research needs, Renew. Sustain. Energy Rev. 134 (2020) 110334.
[60] A. Taslimov, F. Rakhimov, F. Rakhimov, Economic interval analysis of loads for selection of cross-section surfaces of electrical transmission lines. in E3S Web of Conferences, EDP Sciences, 2023.
[61] Ali, S., Soil to Foil: Aluminum and the Quest for Industrial Sustainability. 2023: Columbia University Press.
[62] Q. Shao, et al., Development of thermal-resistant Al–Zr based conductor alloys via microalloying with sc and manipulating thermomechanical processing, J. Mater. Res. Technol. 25 (2023) 7528–7545.

[63] J. Hou, et al., Mechanisms behind the macro-and microscopic behaviors of the electric heated Al–Mg–Si alloy wires, Materials Science Engineering A 849 (2022) 143490.
[64] M. Hassanipour, et al., Characterization of aluminum conductors steel reinforced in overhead transmission lines. in TMS Annual Meeting & Exhibition, Springer, 2023.
[65] R. Dubey, Indian INSTITUTE OF TECHNOLOGY MADRAS CHENNAI, Ballist. Impact Response thermoMech. Process. Al Alloy (6082 (2023).
[66] W. Shen, et al., Al-Mn alloys for electrical applications: a review, J. Alloy. Metall. Syst. (2) (2023) 100008.
[67] J. Zhang, et al., Comparative study of sc and er addition on microstructure, mechanical properties, and electrical conductivity of Al-0.2 Zr-based alloy cables, Mater. Charact. 145 (2018) 126–134.
[68] R.-z Chao, et al., Effect of zr and sc on mechanical properties and electrical conductivities of al wires, Trans. Nonferrous Met. Soc. China 24 (10) (2014) 3164–3169.
[69] X. Xu, et al., Effects of various Mg/Si ratios on microstructure and performance property of Al-Mg-Si alloy cables, Mater. Charact. 119 (2016) 114–119.
[70] Y. Zhang, et al., The difference of la and ce as additives of electrical conductivity aluminum alloys, Mater. Charact. 158 (2019) 109963.
[71] Q. Zhao, et al., Influences of fe, si and homogenization on electrical conductivity and mechanical properties of dilute Al–Mg–Si alloy, J. Alloy. Compd. 666 (2016) 50–57.
[72] H. Tecer, et al., Effect of aging on conductivity of heat resistant overhead line conductors. in Materials Science Forum, Trans Tech Publ, 2013.
[73] K. Majchrowicz, et al., Enhanced strength and electrical conductivity of ultrafine-grained Al-Mg-Si alloy processed by hydrostatic extrusion, Mater. Charact. 135 (2018) 104–114.
[74] X. Cui, et al., Effects of grain refinement and boron treatment on electrical conductivity and mechanical properties of AA1070 aluminum, Mater. Des. 86 (2015) 397–403.
[75] X. Cui, et al., The improvement of boron treatment efficiency and electrical conductivity of AA1070Al achieved by trace ti assistant, J. Alloy. Compd. 735 (2018) 62–67.
[76] X. Cui, et al., Study on the improvement of electrical conductivity and mechanical properties of low alloying electrical aluminum alloys, Composites Part B Engineering 110 (2017) 381–387.
[77] P. Koprowski, et al., The effect of low content additives on strength, resistivity and microstructural changes in wire drawing of 1xxx series aluminium alloys for electrical purposes, Mater. Today Commun. (2020) 101039.
[78] S.N. Khangholi, et al., Investigation on electrical conductivity and hardness of 6xxx aluminum conductor alloys with different si levels. in MATEC Web of Conferences, EDP Sciences, 2020.
[79] G. Langelandsvik, et al., Effects of iron precipitation and novel metal screw extrusion on electrical conductivity and properties of AA1370 aluminium, Materials Science Engineering B 254 (2020) 114505.
[80] S. Jiang, R. Wang, Grain size-dependent Mg/Si ratio effect on the microstructure and mechanical/electrical properties of Al-Mg-Si-Sc alloys, J. Mater. Sci. Technol. 35 (7) (2019) 1354–1363.
[81] X. Cui, et al., The improvement of electrical conductivity of hypoeutectic Al-Si alloys achieved by composite melt treatment, J. Alloy. Compd. 788 (2019) 1322–1328.
[82] M. Murashkin, et al., Enhanced mechanical properties and electrical conductivity in ultrafine-grained al 6101 alloy processed via ECAP-conform, Metals 5 (4) (2015) 2148–2164.
[83] L. Pan, et al., Effect of fe on microstructure and properties of 8xxx aluminum conductor alloys, J. Mater. Eng. Perform. 25 (12) (2016) 5201–5208.
[84] W. Yuan, Z. Liang, Effect of zr addition on properties of Al–Mg–Si aluminum alloy used for all aluminum alloy conductor, Mater. Des. 32 (8-9) (2011) 4195–4200.
[85] Q. Zhao, et al., The synergistic effect of Al–B–C master alloy to improve conductivity and strength of 1070 alloy, J. Alloy. Compd. 639 (2015) 478–482.
[86] M. Hassanabadi, et al., Grain refinement of commercial EC grade 1370 aluminium alloy for electrical applications. in Light Metals 2019, Springer, 2019, pp. 1015–1023.
[87] T. Knych, M. Piwowarska-Uliasz, P. Uliasz, Aluminium alloys with zirconium additions, in the range from 0.05 to 0.32%, intended for applications in the overhead electrical power engineering, Arch. Metall. Mater. 59 (2014).
[88] L. Pan, et al., Effects of minor cu and mg additions on microstructure and material properties of 8xxx aluminum conductor alloys, J. Mater. Res. 32 (6) (2017) 1094.
[89] H. Chen, et al., Development of Al-Fe-(Cu) series alloys for aluminum cables and the related annealing behaviors. in Materials Science Forum, Trans Tech Publ, 2018.
[90] N. Zhao, et al., Optimized combination of strength and electrical conductivity of Al-Mg-Si alloy processed by ECAP with Two-Step temperature, Materials 13 (7) (2020) 1511.
[91] W. Feng, et al., Effect of trace elements la, ti and homogenization on electrical properties of pure aluminum, Rare Met. Mater. Eng. 47 (11) (2018) 3257–3263.
[92] Q. Zhao, et al., Optimizing microstructures of dilute Al–Fe–Si alloys designed with enhanced electrical conductivity and tensile strength, J. Alloy. Compd. 650 (2015) 768–776.
[93] M. Wang, et al., High strength high electrical conductivity ultrafine-grained Al–Y alloy processed via cold drawing, Materials Science Engineering A 772 (2020) 138824.
[94] J. Fu, et al., Influence of zr addition on precipitation evolution and performance of Al-Mg-Si alloy conductor, Mater. Charact. 159 (2020) 110021.
[95] J. Hou, et al., Effects of annealing treatment on the microstructure evolution and the strength degradation behavior of the commercially pure al conductor, Materials Science Engineering A 707 (2017) 511–517.
[96] Q. Wang, et al., Microstructure and texture evolution of cold rolled 1070 al alloy during the subsequent annealing treatment, Results Phys. 13 (2019) 102178.
[97] W.-P. Li, Y.-L. Zhang, J. Mao, Enhanced strength and electrical conductivity of Al–0.3 ce alloy simultaneously with ti (C, N) nanoparticle addition, Rare Met. (7) (2020) 1.
[98] H. Liao, et al., Effect of ce addition on castability, mechanical properties and electric conductivity of Al–0.3 Si–0.2 mg alloy, Int. J. Cast. Met. Res. 28 (4) (2015) 213–220.
[99] W. Yuna, et al., Effect of homogenization temperature on microstructure and conductivity of Al-Mg-Si-Ce alloy, J. Mater. Eng. Perform. 25 (7) (2016) 2720–2726.
[100] M.Y. Murashkin, et al., MICROSTRUCTURE, STRENGTH, ELECTRICAL CONDUCTIVITY AND HEAT RESISTANCE OF AN Al-Mg-Zr ALLOY AFTER ECAP-CONFORM AND COLD DRAWING, Rev. Adv. Mater. Sci. (2016) **47**.
[101] A. Morozova, et al., Effect of si and zr on the microstructure and properties of Al-Fe-Si-Zr alloys, Metals 7 (11) (2017) 495.
[102] A. Kalinenko, et al., Effect of rolling temperature and subsequent annealing on electrical conductivity and strength of an aluminum alloy. in AIP Conference Proceedings, AIP Publishing LLC, 2018.
[103] W. Guo, et al., Effects of er additions on the microstructure, mechanical properties, and electrical conductivity of the Al-0.4 Fe-0.05 si alloy, Adv. Eng. Mater. (2020) 2000955.
[104] A.E. Medvedev, et al., Enhancement of mechanical and electrical properties of Al-RE alloys by optimizing rare-earth concentration and thermo-mechanical treatment, J. Alloy. Compd. 745 (2018) 696–704.
[105] A. Pozdniakov, et al., Effect of zr on the microstructure, recrystallization behavior, mechanical properties and electrical conductivity of the novel Al-Er-Y alloy, J. Alloy. Compd. 765 (2018) 1–6.
[106] R.Y. Barkov, et al., Effects of thermomechanical treatment on the microstructure, precipitation strengthening, internal friction, and thermal stability of Al-Er-Yb-Sc alloys with good electrical conductivity, J. Alloy. Compd. 855 (2020) 9.
[107] A. Mamala, et al., New Al-Ag alloys for electrical conductors with increased current carrying capacity, Arch. Metall. Mater. 61 (4) (2016) 1875–1880.
[108] X. Ji, et al., Microstructures and properties of Al–Mg–SI alloy overhead conductor by horizontal continuous casting and continuous extrusion forming process, Materials Science Engineering A 649 (2016) 128–134.
[109] X.-y Zhang, et al., Microstructure and properties of Al–0.70 Fe–0.24 cu alloy conductor prepared by horizontal continuous casting and subsequent continuous extrusion forming, Trans. Nonferrous Met. Soc. China 25 (6) (2015) 1763–1769.
[110] H.C. Khanh, L.T. Phap, Manufacturing Thermal-resistant aluminum alloy wire for overhead line conductor, VNUHCM J. Eng. Technol. 6 (SI3) (2023) 26–33.
[111] K.C. Huynh, Effects of the heat treatment on the mechanical properties of 6201 aluminium alloy wire, Vietnam J. Sci. Technol. 57 (3A) (2019) 11.
[112] W. Kang, et al., Effects of homogenization treatments on the microstructure evolution, microhardness and electrical conductivity of dilute Al-Sc-Zr-Er alloys, J. Alloy. Compd. 704 (2017) 683–692.
[113] H. Liao, et al., Mechanisms for Ce-induced remarkable improvement of conductivity in al alloys, J. Mater. Res. 32 (3) (2017) 566.
[114] X. Luo, et al., Microstructural evolution and service performance of cold-drawn pure aluminum conductor wires, J. Mater. Sci. Technol. 33 (9) (2017) 1039–1043.
[115] Y. Yang, et al., Improving the combination of electrical conductivity and tensile strength of al 1070 by rotary swaging deformation, Results Phys. 13 (2019) 102236.
[116] V. Chuvil'deev, et al., Thermal stability of the structure and mechanical properties of Fine-Grained aluminum conductor alloys Al–Mg–Zr–Sc (Yb), Russ. Metall. (Met.) 2020 (9) (2020) 987–998.
[117] L.-x Cui, et al., Precipitation of metastable phases and its effect on electrical resistivity of Al-0.96 Mg2Si alloy during aging, Trans. Nonferrous Met. Soc. China 24 (7) (2014) 2266–2274.
[118] J. Zhang, et al., Influence of deformation and annealing on electrical conductivity, mechanical properties and texture of Al-Mg-Si alloy cables, Materials Science Engineering A 710 (2018) 27–37.
[119] S. Nikzad Khangholi, Improvement of mechanical strength and electrical conductivity in 6xxx series aluminum conductor alloys, Univ. é du Québec à Chicoutimi (2021).
[120] X. Li, et al., Influence of mg and si content and heat treatment on electrical conductivity and hardness of AA6101 al alloy, J. Mater. Sci. 58 (20) (2023) 8478–8488.
[121] D. Han, et al., Effect of Al/Cu weight fraction on the mechanical and electrical properties of Al-Cu conductors for overhead transmission lines, Arch. Metall. Mater. (2020) **65**.
[122] J. Hou, et al., Nano-scale precipitates: the key to high strength and high conductivity in al alloy wire, Mater. Des. 132 (2017) 148–157.
[123] R. Li, et al., Strengthening mechanism and yield strength prediction of cold-drawn commercially pure aluminum wire. in IOP Conference Series: Materials Science and Engineering, IOP Publishing, 2018.
[124] J. Ye, et al., Effect of zr content on the precipitation and dynamic softening behavior in Al–Fe–Zr alloys, Mater. Charact. 162 (2020) 110181.
[125] A. Allamki, et al., Improved tensile strength and electrical conductivity of the electrical conductor aluminum alloy 6201. in ASME International Mechanical Engineering Congress and Exposition, American Society of Mechanical Engineers, 2021.

[126] B. Smyrak, et al., Research of chemical composition influence on the mechanical and electrical properties of Al-Mg-Si wires. in Key Engineering Materials, Trans Tech Publ, 2016.
[127] A.T. Ertürk, E.A. Güven, S. Karabay, Determination of zr inoculation effect on improving thermal resistivity of EC grade aluminum, Trans. Indian Inst. Met. 68 (4) (2015) 535–541.
[128] W. Jiang, et al., Enhanced mechanical properties of 6082 aluminum alloy via SiC addition combined with squeeze casting, J. Mater. Sci. Technol. 88 (2021) 119–131.
[129] N. Alshwawreh, et al., Electrical resistivity and tensile strength relationship in heat-treated all aluminum alloy wire conductors, Materials 14 (19) (2021) 5738.
[130] T. Orlova, et al., Effect of annealing on microstructure, strength and electrical conductivity of the pre-aged and HPT-processed Al-0.4 zr alloy, J. Alloy. Compd. 784 (2019) 41–48.
[131] L. Chen, et al., Effects of processing paths on microstructure evolution and properties of High-Strength and High-Conductivity Al-Mg-Si alloys, Materials Science Engineering A (2025) 148606.
[132] M.Y. Murashkin, et al., Mechanical and electrical properties of an ultrafine grained Al–8.5 wt% RE (RE= 5.4 wt% Ce, 3.1 wt% La) alloy processed by severe plastic deformation, Mater. Des. 90 (2016) 433–442.
[133] E. Bobruk, et al., Aging behavior and properties of ultrafine-grained aluminum alloys of Al-Mg-Si system, Rev. Adv. Mater. Sci. 31 (2012) 109–115.
[134] Y. Wang, L. Zhu, J. Mao, High-Strength conductive Al-0.5 Mg-1.0 si alloys modified by ce and cu, J. Mater. Eng. Perform. 32 (3) (2023) 1357–1368.
[135] A. Pozdniakov, R.Y. Barkov, Microstructure and mechanical properties of novel Al-Y-Sc alloys with high thermal stability and electrical conductivity, J. Mater. Sci. Technol. 36 (2020) 1–6.
[136] H. Jiang, et al., The influence of rare earth element lanthanum on the microstructures and properties of as-cast 8176 (Al-0.5 Fe) aluminum alloy, J. Alloy. Compd. 859 (2021) 157804.
[137] Y.N. Mansurov, J. Rakhmonov, A. Aksyonov, Modified aluminum alloys of Al–Zr system for power transmission lines of Uzbekistan, NonFerr. Met. 2 (2020) 51.
[138] F.S. Amiri, et al., Fabrication of a novel high-strength and high-conductivity copper-clad aluminum composite wire, CIRP J. Manuf. Sci. Technol. 41 (2023) 144–159.
[139] M.Y. Murashkin, N.A. Enikeev, X. Sauvage, Potency of severe plastic deformation processes for optimizing combinations of strength and electrical conductivity of lightweight Al-based conductor alloys, Mater. Trans. 64 (8) (2023) 1833–1843.
[140] D. Brough, H. Jouhara, The aluminium industry: a review on state-of-the-art technologies, environmental impacts and possibilities for waste heat recovery, Int. J. Thermofluids 1 (2020) 100007.
[141] R. Yanniello, P. Pollak, J. Rooks, Technical and economic considerations of aluminum conductors. in Conference Record of 2007 Annual Pulp and Paper Industry Technical Conference, IEEE, 2007.
[142] KACKER, A., Copper or Aluminium cable conductors, broadly compared in a life cycle perspective.
[143] Y. Yang, et al., Supply potential, carbon emission reduction, energy conservation, and sustainable pathways for aluminum recycling in China, Sustain. Prod. Consum. 50 (2024) 239–252.
[144] S. Al-Alimi, et al., Recycling aluminium for sustainable development: a review of different processing technologies in Green manufacturing, Results Eng. (2024) 102566.
[145] Green, J.A., Aluminum recycling and processing for energy conservation and sustainability. 2007: ASM International.
[146] Schlesinger, M.E., Aluminum recycling. 2006: CRC press.
[147] G. Liu, D.B. Müller, Addressing sustainability in the aluminum industry: a critical review of life cycle assessments, J. Clean. Prod. 35 (2012) 108–117.
[148] Y. Wang, et al., Research progress of overhead conductors with carbon fiber composite core, J. Comput. Methods Sci. Eng. (2024), 14727978241295538.
[149] F. Ferreira, et al., Dodecylamine functionalization of carbon nanotubes to improve dispersion, thermal and mechanical properties of polyethylene based nanocomposites, Appl. Surf. Sci. 410 (2017) 267–277.
[150] P. Shao, et al., Can CO2 molecule adsorb effectively on Al-doped boron nitride single walled nanotube? Appl. Surf. Sci. 285 (2013) 350–356.
[151] N. Thiyaneshwaran, et al., Dynamic compression behavior of Ti/TiAl3/Al metal intermetallic laminates, J. Mater. Eng. Perform. 31 (10) (2022) 8483–8496.
[152] X. Dai, et al., Influence of different anodised nanoporous structures on the anti-icing and electrical properties of transmission al lines, High. Volt. 10 (1) (2025) 167–177.